Neutrophil Elastase and Myeloid-Related Protein-8/-14 as Executors and Regulators of Tissue Damage in Autoimmune Bullous Diseases

DISSERTATION

In Fulfilment of the Requirements for the Degree “Dr. rer. nat.”

of The Faculty of Mathematics and Natural Sciences

University of Kiel

(Christian-Albrechts-Universität zu Kiel)

Submitted by

Reza Akbarzadeh

Kiel-Germany, 2015

First referee:	Prof. Dr. Thomas Roeder
Second referee:	Prof. Dr. Frank Petersen
Date of the oral examination:	23.02.2015
Approved for publication:	23.02.2015

Signed: Prof. Dr. Wolfgang J. Duschl, Dean

To my wife, my son,

and my parents

TABLE OF CONTENTS

ABBREVIATIONS

A	**a**cceptor
A1AT	**a**lpha**1**-**a**nti**t**rypsin
AIBD	**a**uto**i**mmune **b**ullous **d**iseases
AID	**a**uto**i**mmune **d**isease
amCOLVII	**a**nti-**m**urine type **VII col**lagen IgG
amCOLXVII	**a**nti-**m**urine type **XVII col**lagen IgG
AUC	**a**rea **u**nder the **c**urve
BMZ	**b**asement **m**embrane **z**one
BM	**b**one **m**arrow
bp	**b**ase **p**air
BP	**b**ullous **p**emphigoid
BSA	**b**ovine **s**erum **a**lbumin
TAMRA	carboxymethylrhodamine
C3	**c**omplement component **3**
CIA	**c**ollagen-**i**nduced **a**rthritis
COLVII	**col**lagen **VII**
$\mathbf{C_t}$	**c**ycle **t**hreshold
D	**d**onor
D/A	**d**onor to **a**cceptor ratio
DAMP	**d**amage-**a**ssociated **m**olecular **p**attern
DEJ	**d**ermal-**e**pidermal **j**unction

DMSO	**d**i**m**ethyl **s**ulf**o**xide
EBA	**e**pidermolysis **b**ullosa **a**cquisita
ECM	**e**xtra**c**ellular **m**atrix
EDTA	**e**thylene**d**iamine**t**etraacetic **a**cid
EGFP	**e**nhanced **g**reen **f**luorescent **p**rotein
ELISA	**e**nzyme **l**inked **i**mmuno**s**orbent **a**ssay
FACS	**f**luorescence-**a**ctivated **c**ell **s**orting
FCS	**f**etal **c**alf **s**erum
FRET	**f**oerster or **f**luorescence **r**esonance **e**nergy **t**ransfer
G-CSF	**g**ranulocyte **c**olony-**s**timulating **f**actor
h	**h**our
hNE	**h**uman **n**eutrophil **e**lastase
H&E	**h**ematoxylin **and e**osin
HBSS	**H**ank's **b**uffered **s**alt **s**olution
HEPES	**h**ydroxy**e**thyl **p**iperazine **e**thane**s**ulfonic acid
IC	**i**mmune **c**omplex
IM	**i**maging **m**edium
IVIG	**i**ntra**v**enous **i**mmuno**g**lobulin
kDa	**k**ilo **D**alton
KO	**k**nock**o**ut
LUT	**l**ook **u**p **t**able
mBSA	**m**ethylated **b**ovine **s**erum **a**lbumin
min	**m**inute

MMP-9	**m**atrix **m**etallo**p**roteinase-9
MPM	**m**ulti-**p**hoton **m**icroscopy
MRP	**m**yeloid **r**elated **p**rotein
NE	**n**eutrophil **e**lastase
NEmo-2	**n**eutrophil **e**lastase **mo**nitoring**-2**
NC	**n**on-**c**ollagenous
PAGE	**p**oly**a**crylamide **g**el **e**lectrophoresis
PBS	**p**hosphate **b**uffered **s**aline
PMN	**p**oly**m**orpho**n**uclear leukocyte
RA	**r**heumatoid **a**rthritis
RLU	**r**elative **l**ight **u**nits
ROS	**r**eactive **o**xygen **s**pecies
RAGE	**r**eceptor for **a**dvanced **g**lycation **e**nd product
ROI	**r**egion **o**f **i**nterest
RT	**r**oom **t**emperature
RT-PCR	**r**everse **t**ranscriptase-**p**olymerase **c**hain **r**eaction
s.c.	**s**ub**c**utaneously
SDS	**s**odium **d**odecyl **s**ulphate
sec	**s**econd
SLE	**s**ystemic **l**upus **e**rythematosus
TLR	**t**oll-**l**ike **r**eceptor
WT	**w**ild **t**ype

1. INTRODUCTION

1.1. The structure of the skin

The skin is a multifunctional organ which protects the body from pathogens and components from the environment, including the protection against external physical, chemical, and biologic attacks, the control of thermoregulation and water homostasis of the body. It is continuous with mucous membranes and basically consists of the epidermis, dermis, and subcutaneous tissue which constitutes the three main layers of the skin[1,2] (Figure 1).

The epidermis, which is the outer layer of the skin, contains squamous and stratified epithelium and mainly consists of keratinocytes[2]. According to keratinocyte position and morphology, the epidermis can be divided into four layers including the cornified or horny cell layer (stratum corneum), the granular cell layer (stratum granulosum), the squamous cell layer (stratum spinosum), and the basal cell layer (stratum germinativum)[2–4]. The dermis as middle layer of the skin, is an integrated system of fibrous, filamentous, and connective tissues as well as nerve and vascular networks[2,5]. The outer zone, the papillary stratum is a thin layer below the epidermis and the basement membrane and is composed of epidermally derived macrophages, fibroblasts, and mast cells[2,5]. The inner zone of the dermis, the reticular stratum, is rich in elastic fibers and collagen[2]. The primary materials of the dermal matrix are collagens which are the stress-resistant component of the skin and considered as a fibrous family of proteins with genetically distinct types[2]. The major collagens of the dermis are type I, IV and VII collagens which can be found in the basement membrane zone (BMZ)[2]. Collagen type VII (COLVII) is the major structural component of anchoring fibrils produced by keratinocytes[2,3]. The dermis and epidermis interact with each other in shaping a dermal-epidermal junction (DEJ) which maintains the structure of both tissues[2].

The interface between the epidermis and dermis (DEJ) is characterized by mainly basal keratinocytes[2,6]. Basal cell plasma membrane, lamina lucida, lamina densa, and the sub-lamina densa fibrous part are the most important component of the BMZ[7]. The basal cell plasma membrane is constituted of the keratinocyte and attachment molecules or hemidesmosomes[7]. The lamina lucida includes mainly laminin, whereas the lamina densa, as the central part of the basal membrane is composed of collagen IV[8]. Type VII collagen forms the anchoring fibrils of the fibrillar

zone which is a connection between the lamina densa and the anchoring plaques of the papillary dermis[9,10]. The DEJ provides the integrity of the skin by attaching the dermis to epidermis and also support the epidermis[11]. The basement membrane is connected to the underlying connective tissue and provides the stability of the skin structure. Therefore, in addition to the desmosomes as cell-cell junctions in the epidermis and also numerous fibers and hemidesmosomes anchoring fibrils as cell-matrix contacts in the dermis, the basement membrane is an essential component for the integrity of the skin.

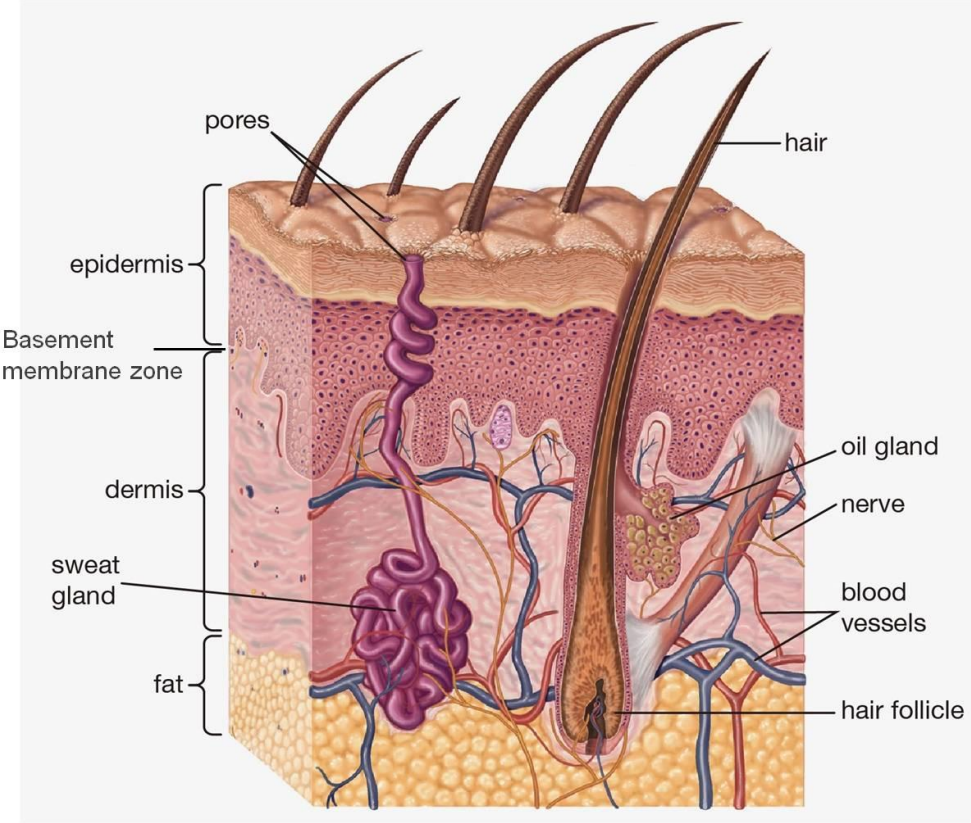

Figure 1 Schematic cross-section of the skin and panniculus (Ref.[12], modified). The three main layers of the skin epidermis, dermis and hypodermis as well as hair follicles, glands, blood vessels and nerves in the dermal layer are shown. The basement membrane is located as a thin layer between the epidermis and dermis.

1.2. Autoimmune bullous diseases

The immune system consists of specific organs, tissues, cells and molecules, which protect the body against pathogenic organisms or substances. This system is categorized into two major sections, the 'innate' immunity and the 'adaptive' immunity[13]. The innate immune system is a fast acting mechanism which includes, beside others, the complement pathway, antimicrobial peptides, and phagocytes. The main components of the innate immune system are anatomic, humoral (complement system), and cellular barriers (neutrophils, dendritic cells, macrophages, and etc.)[13]. The innate immune response is activated immediately after infection and controls rapidly the replication of the infecting pathogen. By contrast, the adaptive immune system is considered as a second line defense mechanism which secures host survival if invading pathogens succeed in escaping innate host defense. The term 'adaptive' refers to the ability of the system for shaping the response to adapt to the microbial challenge; it is also called 'acquired' or 'specific immunity'. This immune system consists of antibodies and lymphocytes, specifically attackting the invading pathogens and retains a "memory" of them for speeding up future responses. The adaptive system requires some time to develop its response and react slower than the innate system[13].

To protect the body effectively against disease, the immune system must recognize and respond to invading microbial pathogens (non-self). Furthermore, to avoid the unwanted reactions against to the healthy self components, the immune system must identify and ignore host structures, a phenomenon called 'self-tolerance'. Self tolerance is controlled by various immune tolerance mechanisms. However, genetic and enviromental factors can break self-tolerance which can result in autoimmunity and consequent autoimmune disease (AID)[14]. Several AIDs[15] have been identified so far with systemic or local manifestations which can affect different regions of the body, including skin.

Autoimmunity may be a concequence of a loss of central as well as peripheral tolerance. A loss of central tolerance can be due to an immune dysregulation in the thymus including abnormal negative selection in neonatal thymus, involving autoimmune regulator proteins, regulatory T cells, and antigen expression by medullar thymic epithelial cells. Loss of immune tolerance outside the thymus can be related to different immune dysregulations involving regulatory T cells, regulatory B

cells, memory T cells, MHC class II, antigen-presenting cells, and cytokines[16,17]. However, this type of tolerance disruption can develop only in genetically susceptible individuals[18–21].

Autoimmune bullous diseases (AIBDs) represent a rare and heterogeneous group of skin and mucous membrane disorders characterized by various diverging clinical manifestations with some overlapping features, and by their potential lethality[22]. AIBDs are believed to be aberrant immunological reactions to self-antigens which are related to pathogenic autoantibodies against different adhesion and structural molecules of the epidermis and dermal-epidermal BMZ[23,24]. The integrity of the epidermis is maintained by a strong cell adhesion between keratinocytes at the epidermal BMZ[25–28]. Desmosomes and hemidesmosomes are two major cell adhesion structures which are relevant for adhesion between keratinocytes as well as between the epidermis and dermis[28]. In the epidermal BMZ, many molecules located in the uppermost dermis are important for the integrity of the skin. While BP230 is found in the intracellular attachment plaques in hemidesmosomes, BP180 is involved in the connection between keratinocytes and extracellular matrices at the epidermal BMZ[28]. Laminin, type IV collagen and COLVII are among the most important extracellular matrix (ECM) proteins within the BMZ[28]. Pathogenic genetic mutations within genes encoding those molecules lead to inherited skin blistering diseases, demonstrating their essential role in maintaining the normal structure of the skin[27].

Depending on the site of autoantibodies binding, AIBDs have been defined as pemphigus, pemphigoids, dermatitis herpetiformis, and epidermolysis bullosa acquisita (EBA)[29–31]. The presence of autoantibodies is associated with a loss of skin adhesion which is clinically characterized by the formation of blisters or erosions[31]. Patients with AIBDs have reactive autoantibodies to the skin adhesion and structural proteins, which induce separation between epidermal keratinocytes or at the BMZ[32]. Based on clinical, histopathological and immunological features, AIBDs are classified to those with loss of adhesion within the epidermis like pemphigus, and those with blister within or underneath the BMZ, such as pemphigoids and EBA which termed subepidermal AIBD[29–31]. This thesis focuses on two AIBDs, EBA and bullous pemphigoid (BP).

Autoantibodies are hallmarks of AIDs and are used as specific markers for disease diagnoses[28]. Although in many autoimmune disorders, especially in several rheumatic diseases, the relevant autoantigens are not clear, the pathogenic role of autoantibodies in most AIBDs has been clearly demonstrated in several disease models[28,33,34]. Furthermore, it has been shown in human disease as well as animal models that each AIBD results in blisters by a different pathway[28]. Therefore, different inflammatory processes are involved in the development of skin lesions in various subepidermal AIBDs[28].

Patients suffering from AIBDs are routinely treated with systemic corticosteroids alone or in combination with other immunosuppressive drugs which are effective therapeuticals[28,35]. However, treatment with these drugs is frequently associated with various serious side effects such as hypertension, systemic infections, osteoporosis, diabetes mellitus, obesity, etc. which are significantly associated with increased mortality of patients[28,36,37]. Therefore, more medical efforts are needed for more secure and effective therapeutic approaches for AIBDs.

1.2.1. Bullous Pemphigoid

1.2.1.1. Definition, prevalence, and symptoms

Bullous Pemphigoid (BP), a chronic blistering skin eruption, was first described in 1953 as a subepidermal bullous dermatosis seen in the elderly[38]. As the most common autoimmune subepidermal skin blistering disease[39,40], BP is characterized immunohistologically by DEJ separation, infiltration of inflammatory cells in the upper dermis, and presence of autoantibodies against hemidesmosomal proteins BP180 (also called BPAG2 or COLVII) and BP230 (BPAG1)[39,41]. These autoantibodies and complement components deposit along the BMZ and are pathogenic by triggering an inflammatory cascade that leads to tissue damage and subepidermal blister formation[42–44]. The DEJ separation is accompanied by an extensive inflammatory mononuclear and eosinophilic cellular infiltrate and destruction of ECM components[45,46]. BP patients suffer from the lesions that predominantly affect the inner parts of the limbs and the trunk, while mucous membranes, and face and neck regions are usually not affected[47].

1.2.1.2. Autoantigens BP230 and BP180 in BP

As aforementioned, patients suffering from BP display circulating autoantibodies targeting two major hemidesmosomal proteins BP230 and BP180 (COLVII). These proteins contain structural components of hemidesmosomes promoting the adhesion of basal keratinocytes cytoskeleton to the underlying BMZ and structures within the papillary dermis[48] (Figure 2). Keratin intermediate filaments are connected to hemidesmosomal proteins such as α6β4 integrins and BP180. The intracellular fragments of these proteins are attached to the BP230 and plectin, two elements of hemidesmosomal plaque, and their extracellular domains extend into the BMZ[48]. BP230 contribute in the correlation of hemidesmosomes with keratin intermediate filaments and contains a central coil-coiled domain region flanked by two globular end domains[41,48–50] (Figure 2A, B). By contrast, BP180 is a transmembrane glycoprotein with its amino-terminal located in the hemidesmosomal plaque and its carboxy-terminal projecting into the basal lamina[48,51]. The extracellular portion of BP180 is composed of 15 interrupted collagen domains separated by noncollagen sequences and form a collagen-like trimeric structure[48,52,53]. The largest noncollagenous NC16A domain of BP180 in the N-terminal region localizes within the lamina lucida under the hemidesmosome and the C-terminal part is conneted to the anchoring filaments at the interface between the lamina lucida and the lamina densa[48,54,55] (Figure 2A). Although the extracellular region of NC16A domain is the immunodominant part in BP[56], IgG antibodies against epitopes outside the NC16A domain are also elevated in most patients[57–59]. Reactivity of antibodies against the C-terminal epitopes could be associated with mucosal involvement and severe skin disease, whereas the intracellular domain is targeted at an early clinical stage[58,60,61]. In addition to IgG reactivity, IgA and IgE anti-BP180 antibodies are present in serum samples of most patients[62–65]. Thus, transmembrane BP180 antigen is the target for pathogenic autoantibodies in BP[48].

1.2.1.3. Diagnosis and therapeutic approaches for the treatment of BP

Beside a significant impact on the quality of life related to severity of the skin blisters and lesions, BP patients have a considerable increased mortality rate which could be between 20% and 40% in the first year[37,66–68]. Diagnosis of the disease is usually based on a combination of criteria, including positive immunopathological

findings and typical clinical features[69,70]. Direct immunofluorescence microscopy can be used for detecting IgG or complement component 3 (C3) deposition at the DEJ[68]. Serum antibodies against BP180 NC16A and BP230 are detectable with commercially enzyme linked immunosorbent assay (ELISA) systems[68,71–74]. Autoantibodies can be detected in serum samples from all patients by using different recombinant fragments of BP180 and BP230[59,68]. Subepidermal separation and inflammatory infiltration (lymphocytes, neutrophils, and eosinophils) are typical histopathological features of lesional biopsy[68]. Localized and mild form of the disease are mostly treated with topical corticosteroids alone while patients with moderate and wide spread disease receive topical corticosteroids or oral prednisolone at 0.5 mg per kg per day[36,68]. Other drugs such as azathioprine, chlorambucil, dapsone, methotrexate, mycophenolic acid, and tetracyclines can also have a therapeutical effects[68]. In resistant cases, high-dose intravenous immunoglobulin (IVIG), plasmapheresis, immunoadsorption, or rituximab can be combined[68].

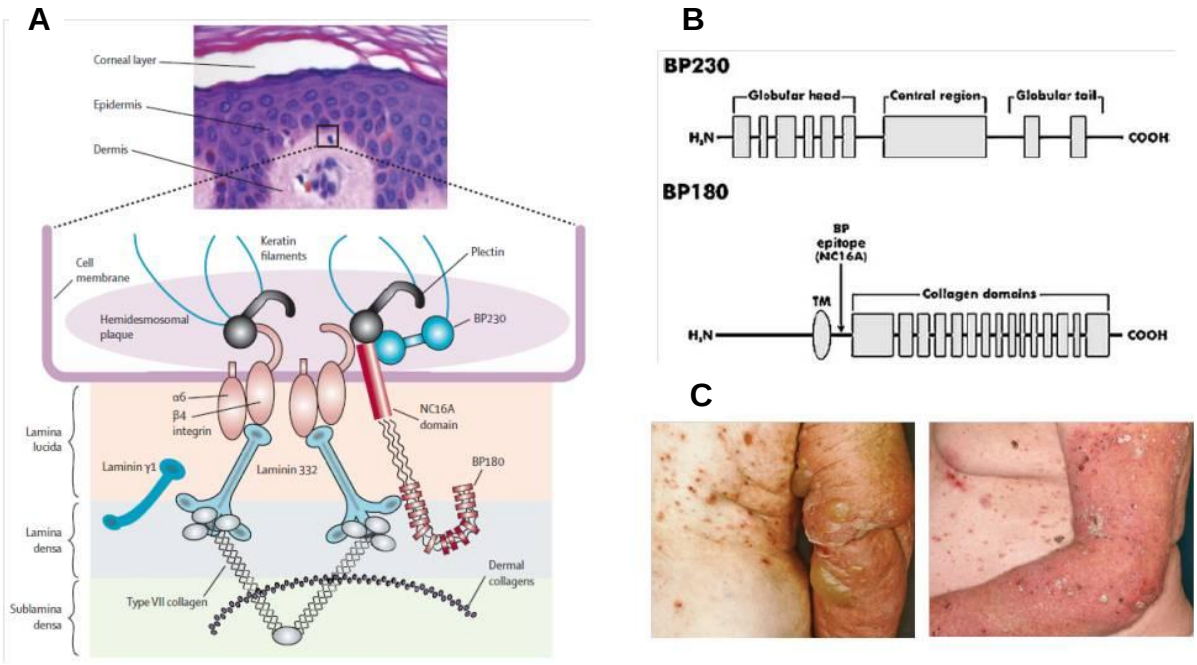

Figure 2 Schematic structure of skin molecules and clinical features in BP (Ref.[48,68], modified). (A) Schematic representation of the DEJ. Keratin filaments are connected to the hemidesmosomal plaque containing plectin and BP230 which BP230 interact with the cytoplasmatic domain of the transmembrane components BP180 and α6β4 integrin. The extracellular domains of these transmembrane structures link the basal cells to the underlying basement membrane by binding

to laminins, which associates with COLVII, the major component of anchoring fibrils of the upper dermis. **(B)** Schematic organization of BP230 and BP180. BP230 is predicted to consist of a central coil-coiled region flanked by two globular end domains, while BP180 has a type II orientation with an extracellular COOH-terminal portion consisting of 15 interrupted collagen domains. The 16th noncollagenous domain localizes next to the cell membrane and harbors the major epitopes targeted by autoantibodies from BP patients. TM, transmembrane domain. **(C)** Clinical and immunopathological characteristics of BP. Tense blisters and erosions on back and right arm and eczematous lesions, erosions, and crusts on left arm and flank of patients with BP.

1.2.2. Epidermolysis bullosa acquisita

1.2.2.1. Definition, prevalence, and symptoms

The term "epidermolysis bullosa acquisita" (EBA) was first described as a characteristic diagnosis of an acquired bullous disease with clinical manifestations similar to inherited epidermolysis bullosa dystrophica[75]. EBA is a rare disease, with an estimated prevalence of 0.2-0.5 new cases/million per year[76–79]. It is a chronic blistering disease of skin and mucous membranes characterized by subepidermal blisters and tissue-bound and circulating autoantibodies to the DEJ[80]. EBA is an organ-specific AID with generally well-characterized clinical, histo- and immunopathological features[80,81]. In general, IgG and complement deposition are located at the DEJ of EBA patient skin. According to the clinical presentation, EBA is a heterogenous disease and its clinical spectrum is still being defined[81]. However, two main categories have been distinguished that include the noninflammatory (classical or mechanobullous) and the inflammatory form[79]. The non-inflammatory form of EBA presents as a mechanobullous features with skin fragility, blisters, erosions, and milia formation[79]. Blisters, erosions, and scars occur over the back of the hands, knuckles, elbows, knees, sacral area, and toes[81]. The inflammatory form of EBA is marked by bullous eruption involving the trunk, extremities and skin folds usually accompanied by pruritus[81]. Skin fragility is not eminent in this form and scarring and milia formation are rare[81]. However, EBA patients may present an inflammatory phenotype which have overlap with non-inflammatory features[82,83].

1.2.2.2. Autoantigens collagen type VII in EBA

COLVII is the main constituent of anchoring fibrils at the DEJ[9]. It is an ECM protein and is one major target of autoantibodies in AIBDs[29]. COLVII consists of three identical α chains where each chain is composed of a central collagenous region of 145 kDa, flanked by a 145 kDa (NC1) and 34 kDa (NC2) non-collagenous domain at the amino and carboxy-terminal[84,85]. Inherited or targeted disruptions in COLVII gene which result in subepidermal blisters indicate the essential role of this protein in maintaining cell-matrix adhesion in the skin[86–89]. Pathogenesis of EBA involves the production of autoantibodies directed against the 145-kDa non-collagenous amino-terminal (NC-1) domain of COLVII, a major component of anchoring fibrils in the BMZ of skin and mucosa[80]. Antibodies bind most likely at the DEJ which induces a cascade of proinflammatory pathways including the activation of the complement system and Fc receptors[90]. Inflammatory cells such as neutrophils release different mediators including cytokines, proteases (Elastase, matrix metalloproteinase-9 (MMP-9)), and reactive oxygen species (ROS) which could be responsible for amplification of local inflammation and finally tissue damage[90] (Figure 3).

1.2.2.3. Diagnosis and therapeutic approaches for the treatment of EBA

EBA is generally diagnosed by clinical presentation and detection of circulating as well as tissue-bound antibodies directed against COLVII[79]. In unclear cases of disease, additional tests such analysis by transmission electron microscopy or antigen mapping could be performed[79]. Clinical presentation includes hematoxylin and eosin (H&E) staining and direct immunofluorescence microscopy of lesional skin[79]. IgG and/or IgA deposition at basement membrane could be observed in almost all EBA patient and is detectable in at least 93% of all cases[79]. Circulating anti-COLVII IgG can also be detected by different ELISA systems that provides additional information[79,91–93]. Detection of autoantibodies directed against COLVII can also be specifically performed by immunofluorescence microscopy[93] or by Western blotting[94].

Concerning to the treatment of EBA, controlled clinical studies are missing due to the low prevalence of the disease. Thus, current recommendations for treatment are only based on the clinical expertise by clinicians specialized in AIBD[79,95,96]. Moreover,

the disease severity as well as clinical phenotype has to be considered for treatment of EBA[79]. Various therapeutic procedures have identified by increased understanding of EBA pathogenesis. The use of systemic corticosteroids is the most common pharmaceutical treatment of EBA patients[97] which has also been approved in experimentally induced EBA[98]. Due to several side effects, different treatment procedures should be considered before systemic corticosteroid treatment is used[79]. Methotrexate[99], azathioprine[99], cyclosporine[95,100–102] and colchicine[103–109], IVIG[110,111], rituximab[112–114], dapsone[103], and cyclophosphamide[115] are several alternative drugs for EBA treatment with high efficacy. Currently, colchicine due to beneficial effects and fewer adverse events is highly recommended as first line treatment for EBA treatment[79].

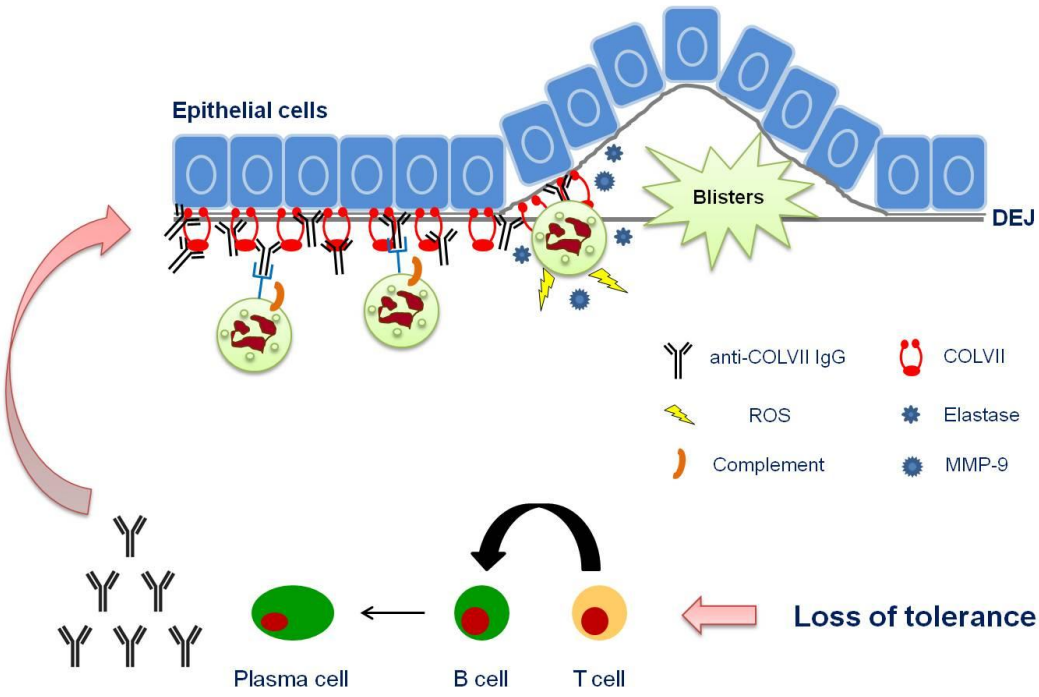

Figure 3 Schematic figure of the pathological mechanisms in EBA (Ref.[90,116], modified). The pathogenesis of EBA is characterized by three phases, loss of tolerance, production of autoantibodies, and tissue damage. Disruption of tolerance to structural proteins of the skin initiates the pathogenesis of EBA. In the next step, the interaction of T and B lymphocytes leads to the production of autoantibodies targeting COLVII in the skin. Finally, binding the autoantibodies to their targets activate an inflammatory cascade including activation of complement and recruitment of leucocytes. Activated neutrophils release toxic mediators as well as proteases which cause blister formation and tissue damage.

1.2.3. Experimental models of EBA and BP

Animal models are essential tools to understand the causes and pathogenic mechanisms of diseases and are required to develop new treatments for AIDs. From a technical point of view, animal models are helpful instruments to study EBA and BP pathogenesis as they enable an identification of pathological processes including cellular and molecular pathways, disease-relevant genetic as well as environmental factors. Several experimental systems such as *in vivo* and *ex vivo* models are currently available to study the pathogenesis of EBA and BP. Antibody transfer models using rabbit or human IgGs against COLVII and type XVII collagen (COLXVII) have been established in mice for both diseases[43,117–119]. Moreover, both, autoimmune response against COLVII and the active subepidermal blistering disease can be reproduced by immunizing mice with autologous COLVII[120].

To reproduce the blistering phenotype, purified IgG antibodies against murine COLVII are injected repeatedly into mice[90,117–119]. Moreover, antibody transfer from EBA patients or from rabbits immunized against murine[117] or human[118] COLVII[119] results in a blister formation in mice. Several inbred mouse strains including C57BL/6, BALB/c, and nude mice as well as mice of the SKH-1 outbred stock are susceptible to blister development by the transfer of antibodies against COLVII[90,117–119]. Total IgG (20 to 500 µg/g body weight/injection) induces blistering in mice 2-4 days after the first administration which depends on their reactivity to the DEJ[90]. Disease severity increases during the observation period and a full disease phenotype is usually observed 5-6 days after the first administration[90]. The onset and severity of the disease are related to the dose of IgG injected and the levels of COLVII-specific antibodies in the serum of mice[117]. In mouse models of BP, administration of anti-murine BP180 IgG induces subepidermal blister formation with a correlation between severity of the disease and the levels of anti-BP180 antibodies in the serum of mice[43,121].

1.3. Neutrophils in autoimmune skin diseases

Neutrophil granulocytes (also called polymorphonuclear leukocytes or PMNs) are the most abundant type of leukocytes in humans and essential for the innate immune response against invading pathogens[122]. Neutrophils are able to kill microorganisms immediately without dependency on previous exposure to the pathogen[13]. These cells are highly motile and form a first line of defense against invaders[123]. Beside their protective function in clearing extracellular pathogens, neutrophils have to be considered also as tissue distructing cells[124,125]. In AIBDs, neutrophils can be considered as an important component of effector and regulatory pathways[124]. In the concept of effector function, they play a significant role as executors of tissue damage, e.g. by the release of serine proteases[126]. On the other hand, neutrophils are regulators in inflammation which communicate with other immune cells by cell-cell contacts or secretion of mediators[124].

1.3.1. Neutrophils as executors of tissue damage

Neutrophils are equipped with granules which contain toxic materials against pathogens, but also to promote damage in the host[127]. Four different granule compartments (primary/azurophilic, secondary/specific, tertiary/gelatinase granules, and secretory vesicles) are recognized in neutrophils and classified according to their content of antimicrobial enzymes and peptides, as well as specific membrane receptors[127]. Granule contents are released into the extracellular space or into the phagosome by a process termed neutrophil degranulation which results in degradation of the invading microbes or of ECM components[128]. Furthermore, neutrophils are an important source of toxic oxygen species under inflammatory conditions and cause endothelial dysfunction and tissue injury[129]. Neutrophil serine proteases are implicated in various non-infectious inflammatory mechanisms[130]. It has been shown that inhibition of these proteases could reduce neutrophil infiltration and neutrophil-mediated injury in different models of inflammation, such as collagen-induced arthritis, endotoxin-induced acute lung injury, and ischaemia and reperfusion injury[131–133]. Although the destructive activity of these proteases has been in the main focus so far, it becomes more and more clear that these enzymes may have also an important regulatory role in the local inflammatory response[130]. For example,

extracellular neutrophil serine proteases are contributed in proteolytic modification of cytokines and chemokines and activation of specific cellular receptors[130].

Neutrophils are present in lesional skin in inflammatory EBA patients and BP patients as well as in experimentally EBA or BP diseased mice[43,68,134,135]. A direct relationship between disease severity and number of infiltrating neutrophils has been reported[136]. The depletion of neutrophils protects mice from developing disease in the antibody transfer model of EBA[137], and, in addition, also from experimental BP[136]. A comparable effect was observed when recruitment of neutrophils from the circulation to the skin was prevented[137,138]. These findings indicate that neutrophils play an essential role in the effector phase of the pathogenesis. After recruitment of neutrophils into the skin, they are activated by the immobilized IC via FcγR leading to the generation of ROS and the release of granule constituents including elastase, all of which have been proven to be essential factors for autoantibody mediated tissue damage[117,137,139]. This tissue damage process depends strictly on the binding of autoantibodies to Fc-receptors[140], indicating a pathogenic role of these receptors in neutrophil activation. By using a modified *ex vivo* model of EBA, it has been shown that neutrophils are not only necessary but also sufficient to cause the tissue damage[141].

Neutrophil elastase (NE) together with further serine proteinases, such as proteinase 3 and cathepsin G[142] are encoded by highly homologous genes in human and mice. The neutrophil granule-associated serine protease genes are tightly regulated and expressed only during the promyelocytic stage of neutrophil maturation[143] and proteins are stored in their mature active form in cytoplasmic azurophilic granules of naïve neutrophils[144,145]. Active NE is released upon activation of neutrophils. The term elastase originates from the ability of the enzyme to release soluble peptides from insoluble elastin, which was used as one of the first substrates to characterize the activities of an enzyme[128]. NE has a large substrate repertoire with the capacity to degrade most components of the ECM, including elastin, collagens and fibronectin[146]. This enzyme regulate the release of toll-like receptore (TLR)4-induced CXCL8[147,148]. NE could also be detected in the lesional skin in mouse models of BP. NE-deficient mice do not develop experimental BP despite normal IgG and C3 deposition could be found at the basal membrane zone[149] and NE inhibitors blocked disease development in the animals. Reconstitution of NE-deficient mice with intradermal injection of wild type neutrophils results in recovering

susceptibility to experimental BP[149], indicating a significant role of neutrophils in disease pathogenesis. This protease has been detected in BP blister fluid and within lesional/perilesional skin sites on BP patients[150]. Moreover, an *ex vivo* model also suggest that elastase is essential for granulocyte-mediated proteolysis resulting in dermal-epidermal separation in EBA and BP patients' skin[139].

Taken together, these data suggest neutrophils as the major effector cells executing the tissue damage mediated by pathogenic antibodies. Therefore, delineation of the molecular mechanisms how neutrophils cause tissue damage and visualization of NE *in vivo* will help to understand pathogenesis of the AIBDs such as EBA and provide a novel therapeutic avenue specifically targeting the terminal phase of the disease.

Given an important role of NE in many neutrophil mediated diseases, monitoring the NE activity could be a helpful research tool. The NE proteolytic activity can be detected by semiquantitative assays like zymography using elastin as a substrate[151,152]. Enzyme activity detection is also possible by using fluorophore-labelled elastin, in which solubilisation of elastin results in release of the fluorophore and subsequent increase in fluorescence intensity correlating with NE activity. Development of chromophoric and fluorescent NE substrates enables faster and quantitative measurements. Some substrates such as NMeOSuc-AAPV-pNA (4-nitroanilide)[153] and its fluorescent variant (4-methyl-7-coumarylamide)[154] are used in research and diagnostic purposes to determine soluble NE activity which is efficiently hydrolysed by human NE. However, the short tetrapeptide substrate sequence does not extend into the P' site of the enzyme active centre which negatively affects the substrate specificity. As a consequence, the substrate is also cleaved by proteinase 3, but the the hydrolysis speed is much faster by human NE[155]. Due to a lower substrate specificity of the mouse variants of the enzymes, differential determination of both protease activities is difficult[156]. In order to increase the specificity of the NE substrates, some attempts were performed to screen potential substrate sequences which include S'-P' subsite interaction[146,155]. Such a substrate sequence has been identified in both mouse and human leukemogenic PML-RARα protein, which allows sensitive and specific detection of mouse and human NE[157].

However, all of the methods described so far are limited to the detection of protease activities in supernatants and provide no information about their role in

complex systems like living organism. To close this gap, much effort has been made to develop new imaging technique which enables the detection of biological processes in intact tissues or even living animals. Fluorescence imaging has become a powerful technique to visualize biology in its native physiological settings in a living subject[158–161]. Proteolytic degradation of peptides and detecting peptidase activity in living cells can be monitored by using peptides containing a foerster or fluorescence resonance energy transfer (FRET) fluorophore pair. FRET, a potent technique for studying molecular interactions inside living cells, is extensively used in biomedical and biological research, including cell biology, medical diagnostics, optical imaging and drug discovery. FRET is a physical phenomenon of energy transfer whereby energy created by fluorescence excitation of one molecule as a donor is transferred to an adjacent molecule as an acceptor[162]. This will be possible only when the donor/acceptor (D/A) fluorophore pair are close to each other (<100 Å) and in a favorable orientation. Due to such a short distance, the principle of energy transfer does not occur by emission of a photon that is captured by the acceptor fluorophore, but merely electromagnetic energy transfer as a consequence of dipole moments. The efficiency of FRET depends highly on distance and decays with distance, as formulated in Foerster's law[163]. Because of its sensitivity to distance, which is comparable to the size of biomolecules or the distances of molecular interactions, FRET has become suitable for studying the dynamics and interactions of biological molecules, for the detection of conformational changes in a protein (when the distance between donor and acceptor changes) or protein degradation[164,165] (when the donor and acceptor fluorophore are separated as a result of substrate cleavage), as well as for monitoring cellular events *in vivo*[166–168]. This event can be imaged by multiphoton microscopy which becomes a powerful technique for monitoring the cellular dynamics in tissues.

Due to distance-dependent nature of FRET interaction, spatial separation of two fluorophores as a consequence of protease activity can be easily detected as this will result in increased emission from the donor fluorophore at the expense of emission from the acceptor fluorophore[162] (Figure 4). This strategy has been used with peptides containing a fluorescein group as donor and a tetramethylrhodamine group as acceptor. The donor and the receptor are separated by six amino acids, in which energy transfer from donor to acceptor occurred with intact peptides but was lost when the peptides were separated as the result of degradation[169]. By using two

fluorophores and their stoichiometry in the reporter, a ratiometric read-out of FRET (D/A emission ratio) can be achieved by detection of donor fluorescence and sensitized emission of the acceptor, which is excited by receiving energy from the donor[170,171]. Since the cleavage of the reporters is irreversible, a dynamic read-out can not be identified by the protease reporters. However, due to amplification of the signal by functioning as a substrate, the sensitivity for detection of protease activity is sufficiently high. This is in contrast to activity-based probes, which act as a suicide inhibitor and react covalently with an enzyme, leading to an enzyme to reporter ratio of 1:1[172].

According to the detection of NE at the cell surface of activated neutrophils, direct detection and quantification of membrane-bound activity might help to investigate the role of NE in inflammation. In addition, spatial information of protease activity as well as information about a local accumulation of the signal can be achieved by using this approach.

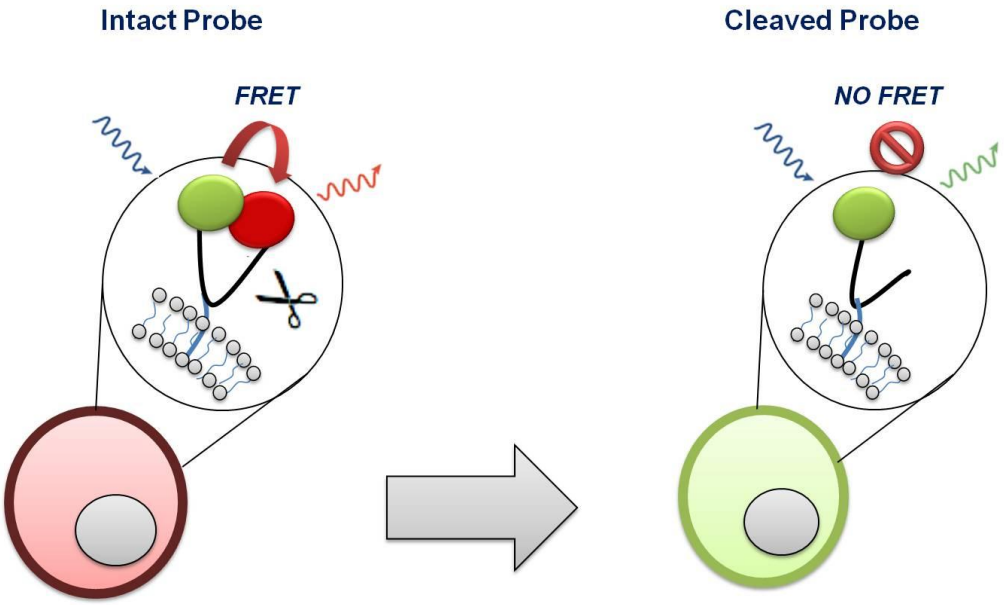

Figure 4 Principle of the FRET protease sensor (Ref.[165], modified). Donor and acceptor fluorophore molecules are designed with spectral overlap on a peptide substrate sequence. Close proximity of the fluorophores results in FRET process and acceptor fluorescence will be emitted at the expense of donor fluorescence. Cleavage of the peptide backbone results in separation of donor and acceptor fluorophores, thereby preventing FRET and increased emission from the donor with loss of acceptor fluorescence.

1.3.2. The regulatory role of neutrophils

Although the essential role of neutrophis in AIBDs as executors of tissue damage by releasing proteases and other toxic metabolites has clearly been shown, the regulatory role of neutrophils is less investigated. Since innate immunity is essential in host defence, molecules targeting innate immune mechanisms are effective in the most relevant autoinflammatory diseases[173–175]. In addition to the regulatory function of neutrophils facilitated by classical mediators such as cytokine regulation, chemokine production, activation of complement and adhesion molecules, and their respective receptors[176,177], a novel group of molecules has been suggested as important proinflammatory factors of innate immunity. These molecules are summarized as "endokines", "alarmins", or damage-associated molecular patterns (DAMPs), as they are activated or released under cell stress conditions[178]. Myeloid related proteins (MRPs) are involved in general modes of functioning like regulation of the protein kinases[179], antimicrobial activity[180–183], and a regulatory role in inflammatory reactions[184–187]. Among these molecules, phagocytic MRPs, especially MRP-8 (S100A8) and MRP-14 (S100A9), are the most abundant proteins expressed by myeloid cells, which represent ~45% of neutrophil and ~1% of monocyte cytosolic proteins[186,188–191]. MRP-8/-14 proteins are two calcium-binding factors which belong to the S100 family and are characterized by two calcium binding EF-hand motifs connected by a central hinge region. The EF-hand contains a calcium binding loop flanked by α-helices resulting in a helix-loop-helix motif[192]. All S100 proteins have tendency to form homodimers, however, the preferred form for human MRP-8 and MRP-14 is the MRP-8/MRP-14 heterodimer under physiological conditions[193,194], although in the mouse, there are some reports indicate that MRP-8 and MRP-14 may exist also as monomers[195–197]. Nevertheless, the function of human and mouse MRP-14 proteins are considered homologous[196–198].

The MRP-8/-14 complex has several pro-inflammatory properties, such as the activation of monocytes[199], the amplification of cytokine production[200], and the regulation of migration of myeloid derived suppressor cells[201]. MRP-8/-14 complexes are also able to amplify inflammatory responses by induction of leukocyte trafficking, enhancing transendothelial migration and production of ROS through activation of NADPH oxidase[202]. They serve as a ligand for the receptor for advanced glycation end products (RAGE)[203] as well as the lipopolysaccharide receptor complex consisting of TLR4, MD2 and CD14[194,199,203,204] and thereby enhance inflammatory

responses in infection and autoimmunity[199,205,206]. MRP-8 is the active part of complex, which specifically binds to TLR4 initiating the recruitment of the adaptor protein myeloid differentiation primary response gene 88 (MyD88), activation of MAP kinases ERK1/2, p38, and protein kinase C (PKC)[194,199,204] (Figure 5). MRP-8 and -14 are assumed to be crucial determinants in the initiation and development of inflammatory processes, especially regarding their role in neutrophil recruitment and cellular activation.

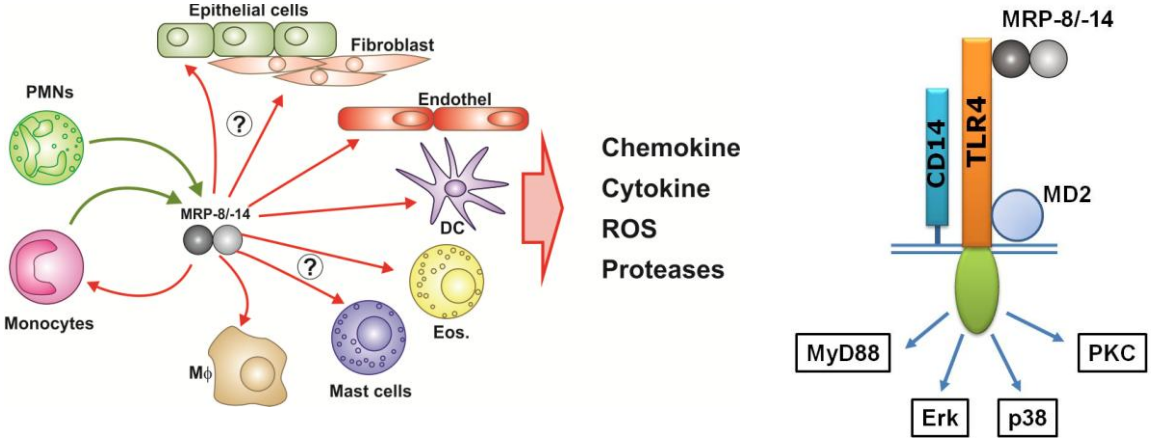

Figure 5 Targets and binding of MRP-8/-14 proteins. MRP-8/-14 promotes proinflammatory responses on various cell types (left panel) through a CD14-independent binding to TLR4 (right panel). As an amplificator of inflammatory processes, they may be involved in a number of chronic inflammatory diseases such as rheumatoid arthritis (RA), psoriasis, or systemic lupus erythematosus (SLE).

1.4. Hypothesis and aims of the study

As provided by several lines of evidence, neutrophils have been identified as the most essential cells in the effector phase of AIBD. Although the involvement of many players such as complement factors, neutrophil proteases and ROS have been recognized in this scenario, the mechanisms how neutrophils regulate and execute the disease still remains unclear. According to my hypothesis, neutrophils contribute to the effector phase by two ways, indirectly by the secretion of MRP-8/-14 proteins leading to amplification and maintenance of the inflammatory loop as well as directly by the release of tissue-destructing elastase (Figure 6).

MRP-8/-14 proteins are highly expressed in activated and circulating myeloid cells and are secreted upon stimulation[207]. Increased local and systemic protein expression has been correlated to various chronic inflammatory diseases[190,205,207]. However, the functional role of these proteins in chronic inflammation is still a matter of debate. While some studies have implicated a role for MRP-8/-14 in experimental inflammatory arthritis models[205,208] and in human autoimmune-mediated diseases including RA[190,205], other studies have failed to confirm these results[209]. Currently, no data exists on the expression and potential function of MRP-8/-14 in AIBD. Different to the latter proteins, the essential pathogenic function of neutrophil elastase in human and experimental AIBD has been well documented. However, until now the role of this enzyme in disease has been shown only indirectly, either by determination of protease activity in cell extracts and supernatants, by inhibitor studies, or by histological localization of the protein in the diseased tissue. Nonetheless, to understand the pathophysiological mode of action of neutrophil elastase in disease, a direct approach allowing their quantification and localization of the enzyme activity at its site of action *in vitro* and *in vivo* is required. By combined studies in humans as well in different models of AIBD, the following questions will be addressed:

1. Are levels of MRP-8/-14 proteins elevated in human and experimental AIBD?
2. Do MRP-8/-14 proteins contribute to the pathology of AIBD?
3. Can MRP-8/-14 proteins affect elastase-mediated tissue damage?
4. How can neutrophil elastase mediate tissue damage in presence of protecting proteases inhibitors?

5. At which site of inflammation is neutrophil activation and elastase activity observed *in vivo*?

By answering these questions, I hope to identify novel therapeutical targets which could help to develop new strategies in the treatment of AIBD.

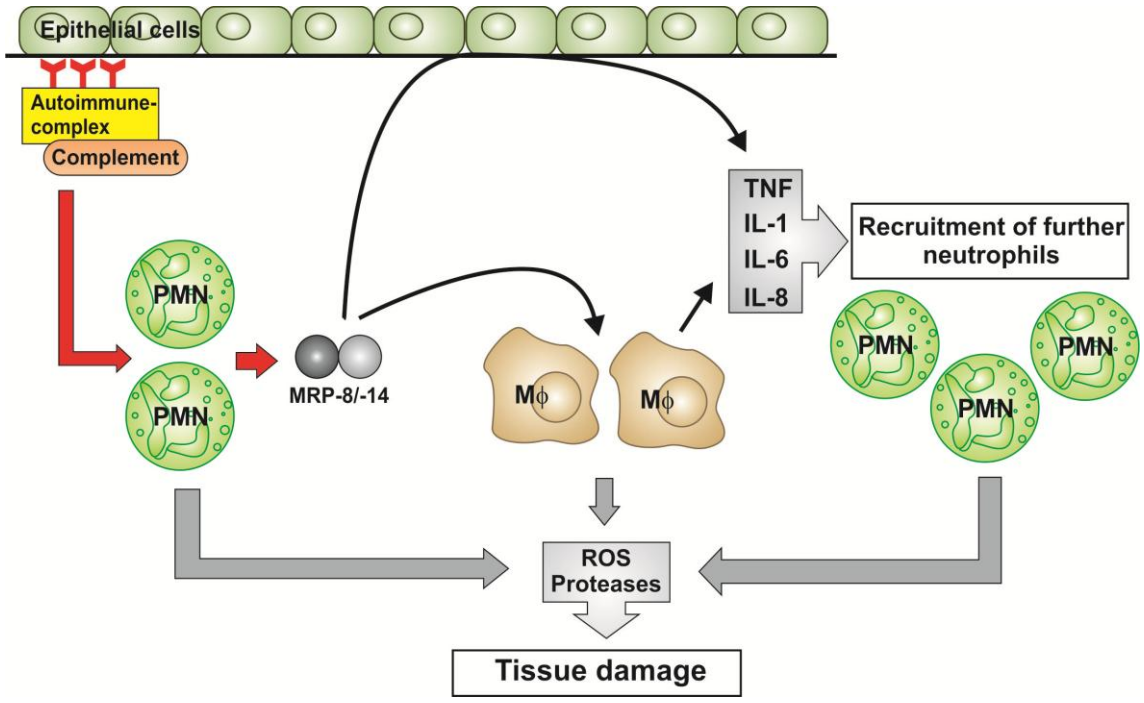

Figure 6 Hypothetical direct and indirect role of MRP-8/-14 in the amplification and chronification of inflammatory response in autoimmune skin disease EBA and BP. Neutrophils are activated by immune complex and complement factors release tissue-destructing elastase and MRP-8/-14. The latter proteins amplify the inflammatory cascade by activation of macrophages (MØ) or barrier cells which release further proinflammatory cytokines and chemokines leading to the recruitment and activation of additional neutrophils enhancing and maintaining the inflammatory response.

2. MATERIALS AND METHODS

2.1. Materials

2.1.1. Antibodies

Specificity	Isotype	Clone	Conjugate	Manufacture	Application
Donkey α-rabbit IgG	IgG	Polyclonal	DyLight 649	Biolegend	IHC
Goat α mouse IgG	IgG	Polyclonal	Alexa Fluor 488	Invitrogen	IHC
Goat α-mouse IgG	IgG	Polyclonal	Alexa Fluor 680	Invitrogen	IHC
Goat α-rabbit IgG	IgG	Polyclonal	Alexa Fluor 488	Invitrogen	WB
Goat α-rabbit IgG	IgG	Polyclonal	IRDye800	Rockland	WB
Isotype mouse IgG1	IgG1, κ	MOPC-21	-	Biolegend	IHC
Isotype mouse IgG1	IgG1, κ	DAK-GO1	APC	Dako	FACS
Isotype mouse IgG1	IgG1, κ	DAK-GO1	FITC	Dako	FACS
Isotype mouse IgG2a	IgG2a, κ	DAK-GO5	PE	Dako	FACS
Isotype mouse IgG2b	IgG2b, κ	DAK-GO9	FITC	Dako	FACS
Isotype rabbit IgG	IgG	Polyclonal	-	University of Lübeck	*in vivo*
Isotype rabbit IgG	IgG	Polyclonal	Alexa Fluor 488	University of Lübeck	*in vivo*
Isotype rat IgG2a	IgG2a, κ	RTK2758	-	Biolegend	IHC
Isotype rat IgG2b,	IgG2b, κ	RTK4530	-	Biolegend	IHC
Mouse α-human CD3	IgG1	UCHT1	APC	Dako	FACS
Mouse α-human CD14	IgG2a, κ	M5E2	PE	BD Pharmingen	FACS
Mouse α-human CD16	IgG1, κ	DJ130c	FITC	Dako	FACS
Mouse α-human MRP8/14	IgG1	27E10	-	Acris Antibodies	IHC, WB

Specificity (continued)	Isotype	Clone	Conjugate	Manufacture	Application
Mouse α-human MRP8/14	IgG1	27E10	-	Acris Antibodies	IHC, WB
Rabbit α-mouse COL VII	IgG	Polyclonal	-	University of Lübeck	*in vivo*
Rabbit α-mouse COL VII	IgG	Polyclonal	DyLight 649	University of Lübeck	*in vivo*
Rabbit α-mouse COL XVII	IgG	Polyclonal	-	University of Lübeck	*in vivo*
Rabbit α-mouse MRP8	IgG	Polyclonal	-	University of Münster	IHC, WB
Rabbit α-mouse MRP8	IgG	Polyclonal	Cy3	antibodies-online	IHC
Rabbit α-mouse MRP8	IgG	Polyclonal	Cy5.5	University of Münster	IHC
Rabbit α-mouse MRP14	IgG	Polyclonal	-	University of Münster	IHC, WB
Rabbit α-mouse MRP14	IgG	Polyclonal	Cy3	antibodies-online	IHC
Rabbit α-mouse MRP14	IgG	Polyclonal	Cy5.5	University of Münster	IHC
Rabbit α-rat ERK 1	IgG	Polyclonal	-	Santa Cruz	WB
Rat α-mouse Ly-6G	IgG2a, κ	1A8	PE-Cy7	BD Pharmingen	FACS
Rat α-mouse Ly-6G/Ly-6C	IgG2b	NIMP-R14	-	Santa Cruz	IHC
Rat α-mouse C3	IgG2a	RMC11H9	-	Cedarlane	IHC

APC: **a**llo**p**hy**c**ocyanin; CD: **c**luster of **d**ifferentiation; COL: Collagen; Cy: **cy**anine; ELISA: **e**nzyme-**l**inked **i**mmuno**s**orbent **a**ssay; ERK: **e**xtracellular signal-**r**egulated **k**inase; FACS: **f**luorescence-**a**ctivated **c**ell **s**orting; FITC: **f**luorescein **i**so**t**hio**c**yanate; IHC: **i**mmuno**h**isto**c**hemistry; Ly: lymphocyte antigen; MRP: **m**yeloid **r**elated **p**rotein; PE: **p**hyco**e**rythrin; WB: **w**estern **b**lot

2.1.2. Reagents

Chemicals/Reagents	Manufacture
Acetone	Merck, Darmstadt, Germany
Ammonium persulfate (APS)	Serva, Heidelberg, Germany
Aqua dest *(Aqua ad iniectabilia)*	B. Braun, Melsungen, Germany
BOC-Ala-Pro-Nva-4-chloro-SBzl, substrate buffer	Bachem, Bubendorlf, Switzerland
Bovine serum albumin (BSA), low endotoxin	PAA Laboratories, Pasching, Austria
Citric acid	Merck, Darmstadt, Germany
DABCO	Roth, Karlsruhe, Germany
Desoxynukleotide (dNTPs)	Roth, Karlsruhe, Germany
Dimethyl sulfoxide (DMSO)	Serva, Heidelberg, Germany
Ellman´s Reagent (5,5´-dithiobis (2-nitrobenzoic acid))	Sigma-Aldrich, Steinheim, Germany
Ethylenediaminetetraacetic acid (EDTA)	Merck, Darmstadt, Germany
Fetal calf serum (FCS)	PAN-Biotech, Aidenbach, Germany
Fluoromount-G mounting buffer	SouthernBiotech, Birmingham, AL, USA
Formaldehyd, 35 %	Merck, Darmstadt, Germany
Glycerol	Sigma-Aldrich, Steinheim, Germany
Glycin	Biomol, Hamburg, Germany
Granulocyte colony-stimulating factor (G-CSF)	Peprotech, Hamburg, Germany
Goat serum	PAN-Biotech, Aidenbach, Germany
Hank's Balanced Salt Solution (HBSS), 10x	PAN-Biotech, Aidenbach, Germany
Hydrogen peroxide	Merck, Darmstadt, Germany
Hydroxyethyl piperazine ethanesulfonic acid (HEPES)	Merck, Darmstadt, Germany
Ketamin, 10%	WDT, Garbsen, Germany
Lipidated FRET-probe for neutrophil elastase (NEmo-2)	Cell Biology and Biophysics Unit, EMBL, Heidelberg, Germany
Low-range Amersham Rainbow Marker	GE Healthcare Europe, Freiburg, Germany
Luminol (5-amino-2,3-dihydro-1,4-phthalazindione)	Sigma-Aldrich, Steinheim, Germany
Magnesium chloride hydrate (MgCl2.6H2O)	Merck, Darmstadt, Germany
Methanol	Merck, Darmstadt, Germany

Chemicals/Reagents (continued)	**Manufacture**
Nonidet P-40	Sigma-Aldrich, Steinheim, Germany
Ponceau S	Sigma-Aldrich, Steinheim, Germany
Pancoll human (density 1,077 g/mL)	PAN Biotech, Aidenbach, Germany
Paraformaldehyde	Sigma-Aldrich, Steinheim, Germany
Paraplast Plus (Paraffin)	Roth, Karlsruhe, Germany
Plasmasteril	Fresenius, Oberursel, Germany
ProLong Gold antifade reagent with DAPI	Invitrogen, Eugene, OR, USA
Tetramethylbenzidine, TMB	Sigma-Aldrich, Steinheim, Germany
Penicillin	PAA Laboratories, Pasching, Austria
Plasmasteril	Fresenius Kabi, Bad Homburg, Germany
Recombinant mouse collagen VII	University of Lübeck , Germany
RNA*later* RNA Stabilization Reagent	Qiagen, Hilden, Germany
Roti-ImmunoBlock	Roth, Karlsruhe, Germany
Roti®-Load 1 protein loading buffer, reducing	Roth, Karlsruhe, Germany
Rotiphorese® Gel 30	Roth, Karlsruhe, Germany
RPMI 1640, modified	Biochrom, Berlin, Germany
*S*odium Chlorid (NaCl)	Merck, Darmstadt, Germany
Sodium dodecyl sulfate (SDS)	ICN Biomedicals, Meckenheim, Germany
Sodium fluoride (NaF)	Sigma-Aldrich, Steinheim, Germany
Sodium orthovanadate (Na_3VO_4)	Sigma-Aldrich, Steinheim, Germany
Sulfuric acid (H_2SO_4)	Merck, Darmstadt, Germany
Tetramethyl-ethylenediamine (TEMED)	SERVA Electrophoresis, Heidelberg, Germany
Triton X-100	Sigma-Aldrich, Steinheim, Germany
Tris	Roth, Karlsruhe, Germany
Tween 20	Sigma-Aldrich, Steinheim, Germany
Xylazin (RompunR), 2%	Bayer, Leverkusen, Germany

2.1.3. Enzymes, inhibitors, stimuli

Substance	Manufacture
A-1-Antitrypsin from human plasma	Sigma-Aldrich, D-Steinheim, Germany
Collagenase type IV	Worthington Biochemical Cooperation, Lakewood, NJ, USA
Complete Protease Inhibitor Cocktail Tablets	Roche Diagnostics, D-Mannheim, Germany
Elastase, Human Neutrophil	Calbiochem, D-Darmstadt, Germany
Murine collagen Type VII (mCOLVII)	University of Lübeck , Germany

2.1.4. Consumable materials

Consumable material	Manufacture
15 mL- und 50 mL-Tubes	Sarstedt, D-Numbrecht
Embedding cassette (Histosette)	Sanowa, D-Leiman (G. Kisker)
Embedding medium, Tissue-Tek O.C.T.™ Compound	Sakura Finetek, D-Staufen
Embedding molds, Tissue-Tek Intermediate Cryomold	Sakura Finetek, D-Staufen
Falcon cell strainer (70 micron)	BD Falcon, Franklin Lakes, NJ, USA
FEATHER® microtome blade A35 and C35	pfm medical, D- Koln
Gel tubes, BD Microtainer SST™ Tubes	BD, Franklin Lakes, NJ, USA
Glass bottom culture dishes, No. 1.5 coverglass	MatTek Corporation, Ashland, MA, USA
Immobilon-P Membrane, PVDF, 0.45 µm	Carl Roth, Karlsruhe, Germany
LightCycler 480 Multiwell Plate	Roche, Penzberg, Germany
LightCycler 480 Multiwell Sealing Foil	Roche, Penzberg, Germany
Microlance sterile needles; 26G, 27G, 30G	BD, Drogheda, Ireland
µ-Slide VI 0.4 uncoated microscopy chamber	Ibidi BioDiagnostics, Munich, Germany
µ-Slide 8 well ibiTreat microscopy chamber	Ibidi BioDiagnostics, Munich, Germany
PAP PEN	Kisker Biotech, Germany
Polystyrene FACS tube with lid	BD Falcon, Franklin Lakes, NJ, USA
Plastipak sterile syringe (1 ml)	BD, Madrid, Spain
Thermo nunc ImmunoPlate for ELISA	Thermo Fisher Scientific; Denmark

2.1.5. Devices

Device	Manufacture
Confocal microscope Leica (SP5)	Leica, Wetzlar, Germany
Electrophoresis power supply	Consort, Turnhout, Belgium
ELISA Reader Tecan Sunrise	Tecan, Crailsheim, Germany
Fluorescent microscope Olympus IX81	Olympus, Hamburg, Germany
Incubator, 37°C, with CO2	Thermo Scientific, Langenselbold, Germany
Incubator, 37°C, without CO2	Thermo Scientific, Langenselbold, Germany
Incubator, 65°C	Memmert, Dschwabach, Germany
LightCycler® 480 Real-Time PCR system	Roche, Penzberg, Germany
Light microscope	Zeiss, Gottingen, Germany
Light microscope Olympus BX41 (Camera: Nikon DSRi1)	Olympus, Hamburg, Germany
LSR II Flow Cytometer	BD Bioscience, NJ, USA
Microcentrifuge with high speed	Hettich, Tuttlingen, Germany
Microm STP 120 Spin Tissue Processor	Thermo Scientific, Langenselbold, Germany
Microplate Luminometer LB 96V	Berthold Technologies, Bad Wildbad, Germany
NanoDrop spectrophotometer	PeqLab, Erlangen, Germany
Odyssey infrared imaging system	LICOR, Bad Homburg, Germany
Paraffin-Microtome SM 2000R	Leica, Nussloch, Germany
Protein gel electrophoresis system	Bio-Rad, Munick, Germany
SDS ABI 7900 system	Applied Biosystems, Darmstadt, Germany
Shandon Cytospin Cytocentrifuge	Thermo Electron, Astmoor, Runcorn, Cheshire, UK
Shaker Type 3015	GFL, Burgwedel, Germany
Shaker Type KL2	Edmund Buhler, Hechingen, Germany
Thermal Cycler MJ Mini	Bio-Rad, Munchen, Germany
Tissue homogenizer and vessels	IKA-Werke, Staufen, germany
TriM Scope multi-photon microscope	LaVision BioTec, Bielefeld, Germany
Vacuum pump ME2	Vacuubrand, Wertheim, Germany
Water bath Typ 12B	Julabo, Seelbach, Germany
xCELLigence system	Roche, Penzberg, Germany
XLPlanN 25×1.05 WMP Objective	Olympus, Hamburg, Germany

2.1.6. Primer sequences

Primer	Sequence	Amplicon size (bp)
B2M, forward	5′- TTC TGG TGC TTG TCT CAC -3′	104
B2M, reverse	5′- CAG TAT GTT CGG CTT CCC ATT -3′	
Mrp-8, forward	5′- CCT TTG TCA GCT CCG TCT TC -3′	80
Mrp-8, reverse	5′- CAA GGC CTT CTC CAG TTC AG -3′	
Mrp-14, forward	5′- CAC CCT GAG CAA GAA GGA AT-3′	95
Mrp-14, reverse	5′- TGT CAT TTA TGA GGG CTT CAT T-3′	

All primers were manufactured and supplied by Metabion international, Martinsried, Germany.

2.1.7. Reagent kits

Reagent Kit	Manufacture
GenElute™ Direct mRNA Miniprep Kit	Sigma-Aldrich, MO, USA
First Strand cDNA Synthesis Kit	Thermo Fisher Scientific, MA, USA
Light Cycler480 SYBR Green I Master Mix	Roche, Mannheim, Germany

2.1.8. Human blood and serum samples

This study enrolled 30 consecutive patients (20 patients with BP and 10 patients with EBA) as well as 20 sex/age matched healthy control individuals who admitted to Department of Dermatology, Universitätsklinikum Schleswig-Holstein in Lübeck. Approval for these studies was obtained from the Institutional Review board at the University of Lübeck (Lübeck, Germany; Az. 12-202A) according to the Declaration of Helsinki. All volunteers gave written informed consent.

2.1.9. Mouse strains

Mrp-14-deficient mice (*Mrp-14*$^{-/-}$) and their C57BL/6 wild type controls were provided by Thomas Vogl, Department of Immunology, University of Münster (Germany). *Mrp-14*$^{-/-}$ mice were generated as described previously[210] by targeted gene disruption which 760 bp of the genomic sequence containing exon 2 and the adjacent intron region was replaced with the pMC1-derived neomycin-poly(A) expression cassette. This mutation results in deletion of the initial start codon. *Mrp-14*$^{-/-}$ mice are phenotypically normal and since MRP-8 and MRP-9 proteins form a hetrodimer, expression of both proteins are absent in mice lacking a functional *Mrp-14* gene.

Lys-eGFP mice were provided by Dr. Mario Pieper from general animal facility of University of Lübeck (Germany). *Lys-eGFP* mice were generated as described previously[211] by deleting a fragment containing the coding part of exon 1 (including the start codon) as well as parts of intron 1 and inserting EGFP-Lox-Tk-neo Lox cassette. This was achieved by knocking the enhanced *green fluorescent protein (eGFP)* gene into the murine lysozyme M (*lys*) locus and using a targeting vector, which contains a neomycin resistant (*neo*) gene flanked by LoxP sites and ‘‘splinked’’ ends, to increase the frequency of homologous recombination. As a result, a mouse line was generated in which eGFP was expressed specifically in the myelomonocytic lineage.

Neutrophil elastase-deficient (NE$^{-/-}$) mice were provided by Prof. Dr. Enno Schmidt from Department of Dermatology at University of Lübeck. NE$^{-/-}$ mice were generated as previously described[212,213]. Gene inactivation was achieved by deletion of restriction enzyme sites in exon one (ATG start codon disruption) and exon two (frameshift mutation upstream of catalytic active site).

For each set of experiments, all animals (male and female) were selected at the age of 10-16 weeks and housed under specified pathogen free conditions during breeding and experiments. Average body weights of the mice were measured and all injections, immunizations and bleedings were performed on anaesthetized mice. All animal studies have been reviewed and approved by the Animal Research Ethics Board of the Ministry of Environment, Kiel, Germany.

2.2. Methods

2.2.1. Induction of systemic antibody transfer model of EBA

To induce experimental EBA, mice were immunized according to a slightly modified protocol published elswhere[117]. Rabbit IgG against murine COLVII were transferred into mice, which induced a subepidermal blistering disease closely reproducing clinical, histological and immunopathological features seen in patients with EBA. IgG from sera of sensitized New Zealand white rabbits with recombinant forms of the glutathione *S*-transferase (GST)-tagged NC1 domain of murine COLVII were purified by protein affinity chromatography using protein G and then steril filtrated. The mice were subcutaneously injected at intervals of 2 days (Figure 7). Mice were treated s.c. with 0.5 mg IgG/g body weight/injection on days 0, 2, 4, 6, 8, and 10. Mice in the control groups received identical antibody concentrations of untreated rabbits (irrelevant IgG). Each experiment consisted of four groups as follow:

1. *Mrp-14*$^{-/-}$ mice + irrelevant rabbit IgG (isotype) (4 mice)
2. *Mrp-14*$^{-/-}$ mice + amCOLVII (12 mice)
3. Wild type mice + irrelevant rabbit IgG (isotype) (4 mice)
4. Wild type mice + amCOLVII (10 mice)

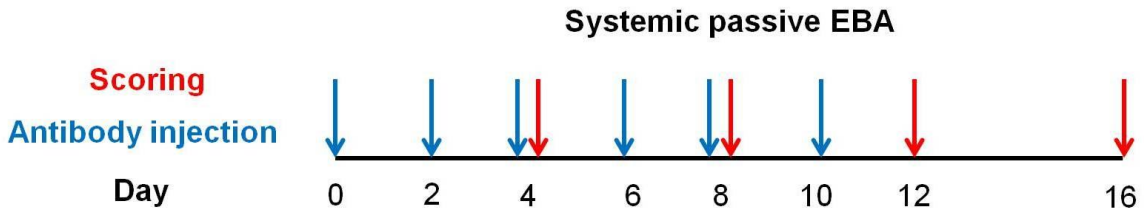

Figure 7 Protocol of the induction of experimental systemic EBA. EBA was induced in wild type (C57BL/6) as well as *Mrp-14*$^{-/-}$ mice by transfer of rabbit IgG against mouse COLVII. Purified rabbit pathogenic IgG or normal rabbit control IgG was injected subcutaneously (systemic antibody transfer model of EBA).

A clinical examination of the animals under anesthesia (freshly prepared 2 µg/g body weight xylazine and 94 µg/g body weight ketamine) was performed on days 4, 8, 12 and 16. Furthermore, on day 0 and 8, blood samples were collected by puncture of the tail vein (gel tubes; collected blood volume 25-50 µl). On day 16, the experiment was terminated and the animals were sacrificed by cervical dislocation under anesthesia. At this time point, blood (400-500 µl) was collected from the heart to determine the serum levels of MRP-8/-14 proteins. Moreover, skin samples from different regions of the body were collected for histological examination and for further analysis. The blood samples were first stored on ice and then centrifuged at 13.000xg for 2 min to prepare serum. The serum was then aliquoted and stored at -20°C.

Termination criteria which resulted in removal of an animal from the experiment were defined as large and open skin infections, long-legged transition of animals, and more than 20% weight loss in all experimental groups.

2.2.2. Induction of local antibody transfer model of BP

The induction of a local experimental BP was carried out with a rabbit anti-mCOLXVII antibody which was locally administrated into the ears of the mice. Rabbit anti-mouse COLXVII IgG from sera of sensitized rabbits with recombinant fragments of murine COLXVIIA (aa497-573 of murine COLXVII) tagged with a glutathione-S-transferase (GST) were purified by protein affinity chromatography using protein G and then steril filtrated[214]. On day 0 of the experiment, mice were anesthetized (freshly prepared 2 µg xylazine and 94 µg ketamine per g body weight, respectively) and antibodies were intradermally injected into the base of one ear (Figure 8). As a control, the second ear was treated with IgG of non-immunized rabbit. Each injection volume was 40 µL (2 mg antibody).

All subsequent steps were performed on anesthetized animals. On days 1 and 2, a clinical examination with regard to the percentage of infestation was performed at the ear skin of the animals and additionally documented by photographs. The assessment of the disease state was performed in comparison to the control ear treated with the irrelevant antibody. On day 0, 25-50 µl blood samples were taken by puncture of the tail vein. After an observation period of 48 hours (h), the experiment

was terminated and the animals were sacrificed by cervical dislocation. At this time point, a further blood sample was taken by puncture of the heart (400-500 µl collected blood volume) and the skin samples were collected for further histological analysis. The termination criteria refered to those described in section 2.2.1. Each experiment consisted of two groups as follow:

1. *Mrp-14*$^{-/-}$ mice (16 mice)
   + Irrelevant rabbit IgG (isotype, left ear)
   + amCOL17 (right ear)
2. Wild type mice (10 mice)
   + Irrelevant rabbit IgG (isotype, left ear)
   + amCOL17 (right ear)

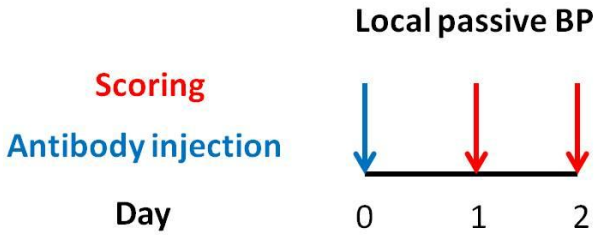

Figure 8 Protocol of the induction of experimental local BP. BP was induced in wild type (C57BL/6) as well as *Mrp-14*$^{-/-}$ mice by transfer of rabbit IgG against mouse COLXVII. Purified rabbit pathogenic IgG or normal rabbit control IgG was injected intradermally into the ear (local antibody transfer model of BP).

2.2.3. Quantification of clinical symptoms

The clinical disease severity was determined using the scoring system described elsewhere[117,215] . Briefly, the disease severity was expressed as percent of total body surface area. The affected skin was defined as the skin with alopecia, erosion, redness, or peeling of the epidermis (blistering). Then the percentage of the affected skin was determined in relation to the total surface in individual parts of body. To calculate the overall infestation of an animal, the individual parts of the body were

assigned to their percentage of the total size of the animal which then multiplied by the percentage of infestation of the body parts (= clinical severity). This value includes the size of each body regions and their relative percentage infestation in the calculation. In order to minimize subjective assessment of the errors, the group affiliation of the animals was blinded by a second person. Accordingly, the calculation of clinical severity is written as a formula as follows:

Clinical severity = $A * 0.025 + B * 0.025 + C * 0.005 + D * 0.005 + E * 0.05 + F * 0.09 + G * 0.1 + H * 0.4 + I * 0.05 + J * 0.05 + K * 0.1 + L * 0.1$

A to *L* indicate the percentage of infestation in the left ear (*A*), right ear (*B*) left eye (*C*), right eye (*D*), snout (*E*) head / neck (*F*), tail (*G*), hull (*H*), left front leg (*I*), right front leg (*J*), the left hind leg (*K*) and right hind leg (*L*).

2.2.4. Histological methods

For preparation histological samples, the skin tissue was shaved and freed from fatty tissue prior to embedding. H&E staining was performed by Department of Clinical and Experimental Pathology (Research Center Borstel).

2.2.4.1. Paraffin tissue sections

Tissues were embedded in paraffin according to established protocols[216]. Collected tissues were fixed immediately in 4% paraformaldehyde for 24 h at 4°C, then placed in embedding cassettes (Histosettes) in 4% formalin followed by automatic embedding in paraffin overnight using a tissue processor (Autotechnikon). Samples were dehydrated by a reducing series of alcohols (70%> 80%> 90%> 96%> 3 x 100% ethanol for 1 h each), then transferred to xylol as intermedium (twice, 1 h each) and finally saturated with liquid paraffin (60°C) (twice for 2 h each). The final samples were casted at the casting station in Paraplast Plus and attached to paraffin blocks on the embedding cassettes.

Procedures for creating paraffin sections of 3 micron thickness were performed by using a microtome SM 2000R with A35-disposable blades. Paraffin blocks were cooled down on ice before cutting. After slicing, sections were straightened in a 20°C water bath and then transferred on microscope slides followed by smoothing in a 45°C water bath before they were dried on a 37°C hot plate.

2.2.4.2. Cryogenic tissue sections

To prepare frozen sections, embedding molds were filled with O.C.T embedding compound and skin samples were then placed vertically without air bubbles. The embedded samples were frozen in liquid nitrogen and stored at -80°C[216]. The cryo-blocks were cut on a frozen Cryo-Mikrotom CM 3000 with CM-C35 disposable blades in sections of 5 micron thickness and stored until use at -80°C.

2.2.5. Immunohistochemical staining

2.2.5.1. IgG and complement factor C3 deposition

Immobilized IgG and complement factor C3 were simultaneously detected in tissue samples by immunofluorescence staining of frozen sections using a method described by Sitaru et al[117] with slight modifications. Briefly, sections were thawed at room temperature (RT), dried, and blocked with 1x Roti-ImmunoBlock solution (1:10 in phosphate buffered saline; PBS) to minimize nonspecific background staining for 30 min at RT. Thereafter, the sections were placed in a humid chamber and incubated with rat anti-mouse C3 antibody (5 µg/ml) for 30 min at RT in the dark. After two washing steps with PBS on a shaker (10 min each, RT, dark), specimen were incubated with the secondary antibodies AlexaFluor488-conjugated goat anti-rat IgG (10 µg/ml) and DyLight649-conjugated donkey anti-rabbit IgG (5 µg/ml) for 30 min at RT in the dark. After washing, residual liquid was removed from the slides and ProLong Gold antifade reagent supplemented with 4',6-diamidino-2-phenylindole (DAPI) was added to the samples and specimen were mounted with coverslipes. The stained sections were stored before and after microscopic evaluation at -20°C.

2.2.5.2. Detection of neutrophils and MRP-8/-14

Neutrophil Marker (NIMP-R14) was used for detection of neutrophils of mouse origin by immunofluorescence. For this purpose, frozen mouse skin cryosections were thawed at RT, dried, and fixed by ice-cold aceton for 10 min. The staining procedure was carried out as described in the section 2.2.5.1, except that rat anti-mouse NIMP-R14 antibody (0.5 µg/ml) was used as a detecting antibody. Alternatively, MRP-8/-14 proteins were detected by Cy5.5-conjugated rabbit anti mouse MRP-8 or MRP-14 IgG (1.97 and 1.87 µg/ml, respectively).

2.2.6. Molecular biological methods

In this study, the gene expression levels of *Mrp-8/-14* were confirmed by quantitative reverse transcriptase-polymerase chain reaction (RT-PCR).

2.2.6.1. Isolation of mRNA from mouse skin samples

After collecting the skin samples derived from diseased and healthy control mice, specimen were directly transferred to RNA Stabilization Reagent (RNA*later*) and stored at 4°C. The mRNA isolation was performed by using the GenElute™ Direct mRNA Miniprep Kit according to the recommendations of the manufactures. For lyses and homogenization of tissues, lysis solution containing proteinase K (1 ml) was added to an appropriate tube and the skin samples were solubilized immediately until no visible pieces remain. Lysates were subsequently incubated at 65°C for 10 min to inactivate nucleases and other proteins. To prepare mRNA for binding, 64 µl of the 5M NaCl solution was added to the respective skin tissue lysate. Oligo(dT) beads were mixed thoroughly and 25 µl of the beads solution was added to each lysate and thoroughly mixed. After hybridization of mRNA with the oligo(dT) beads for 10 min at RT, complexes were pelleted by centrifuging for 5 min at maximum speed in a microfuge. The supernatants were carefully discarded. Afterwards, the pellets were resuspended in 350 µl of washing solution. Suspensions were transfered into a GenElute spin filter-collection tube assembly and samples were spun for 1-2 min at maximum speed in a microfuge. Flowthroughs were discarded and washing was repeated two times with 350 µl of low salt wash solution. For elution, spin filters were

transfered into fresh collection tubes and 50 µl of preheated elution solution (65°C) were pipetted onto the spin filters. Tubes were incubated for 2-5 min at 65°C and spun for 1-2 min. The flow-throughs containing of the purified mRNA were collected and residual mRNA was removed from the beads by a repeated elution step. RNA samples were stored at -80°C.

2.2.6.2. Measurement of RNA quantity

DNA, RNA, and protein concentrations were determined by the NanoDrop spectrophotometer. Nuclease-free water was used for cleaning before and after measurements and the initialization of the device and the device software. For the calibration function of the zero point and also verification, the elution buffer from the GenElute™ Direct mRNA Miniprep Kit was used. Respective mRNA eluates were combined and concentrations and quality of mRNA were spectrophotometrically estimated by measuring absorbance at 260 and 280 nm.

2.2.6.3. cDNA synthesis from isolated mRNA

The cDNA synthesis was performed by using First Strand cDNA Synthesis Kit as recommended by the manufactures. All components of the kit and mRNA samples were kept on ice. Poly(A)$^+$ mRNA (10 ng), Oligo(dT)$_{18}$ Primer (1 µl/sample), and DEPC-treated water (to 11 µl) were added into a sterile, nuclease-free tube on ice in the indicated order. Tubes were mixed gently, centrifuged briefly and incubated at 65°C for 5 min. After cooling down on ice, 5X Reaction Buffer (4 µl), RiboLock RNase Inhibitor (20 u/µl; 1 µl), 10 mM dNTP Mix (2 µl), and M-MuLV Reverse Transcriptase (20 u/µl; 2 µl) were added into each tube in the indicated order. Tubes were then incubated for 60 min at 37°C and the reaction was terminated by heating at 70°C for 5 min. Reversed transcribed cDNA samples were stored at -20°C.

2.2.6.4. Analysis of MRP-8/-14 gene expression by Real time RT-PCR

Quantitative RT-PCR was performed by using the Light cycler® 480 SYBR Green I Master Kit according to recommendation of the manufactures. These analyses were performed as previously described[217] with some modifications using mouse-specific primer pairs (2.1.6). All reagents were kept on ice. PCR-grade water (2 µl/sample), SYBR Mix (2×5 µl/sample), and Primer Mix (10 µM; 1 µl/sample) were added into a sterile, nuclease-free tube on ice in the indicated order and mixed carefully. Then, PCR-Mix (8 µl) was added into each well of the LightCycler® 480 Multiwell Plate and the cDNA template (2 µl) was added to each target gene well. Standard cDNA was diluted 1:1, 1:10, 1:100; $1:10^3$, $1:10^4$ and added into the plate. The Multiwell plate was sealed, centrifuged at 1500 × *g* for 5 s, and transfered into the plate holder of the LightCycler 480 Real-Time PCR system. LightCycler experimental protocol was setup as follows: denaturation program at 95°C for 10 min, amplification program for 45 cycles at 95°C for 10 s, 64°C for 5 s, and 72°C for 10 s, and melting curve program at 95°C for 10 s and at 65°C for 10 s. Data were analyzed using the comparative cycle threshold (C_t) and target gene C_t values were normalized to the corresponding C_t values of a houskeeping gene (*B2M*).

2.2.7. Protein separation and analysis

2.2.7.1. ELISA analysis

MRP-8 and MRP-14 concentrations were determined in serum samples of patients and mice by ELISA. Murine blood samples were collected by Microtainer Gel Tubes and allowed to clot for a minimum of 30 min. Samples were centrifuged for 90 s at 13.000 g. Sera from human (section 2.1.8) and mice were analyzed by Dr. Thomas Vogl, Department of Immunology, University of Münster (Germany) by ELISA as described[199,218].

2.2.7.2. SDS-PAGE

In sodium dodecyl sulphate (SDS) polyacrylamide gel electrophoresis (PAGE) proteins are separated according to their polypeptide length which allows estimating their molecular weight. Proteins were separated on a discontinuous gel system consisting of stacking and separating gel using a method of Laemmli[219] with modification. The stacking gel contains a lower pH (pH 6.8) and a lower acrylamide concentration (5%) as compared to the running gel (15%, pH 8.8), allowing the proteins to be concentrated into a tight band in a lane before entering the running gel. After polymerization, gels were mounted in a Mini-protean II apparatus and equal amounts of protein extracts (10 µg) as well as low molecular weight protein marker were subjected in protein loading buffer (Roti-Load 6x, reducing) to the lanes. Gels were run in electrophoresis buffer (25 mM Tris, 200 mM Glycin, and 3.5 mM SDS) for 30 min (30 V, 35 mA, 15 W) and 1.5 h (400 V, 35 mA, 15 W) using a Consort electrophoresis power supply.

SDS polyacrylamide gels	**Stacking Gel (5%)**	**Running Gel (15%)**
Tris-Base (125 mM, pH = 6.8)	1.9 ml	9.4 ml
Rotiphorese Gel 30 (30%)	2.5 ml	12.5 ml
Distilled water (Milli Q)	10.1 ml	2.2 ml
SDS (0.1%)	150 µl	250 µl
Ammonium persulfate (APS, 10%)	100 µl	150 µl
TEMED (0.2%)	30 µl	12.5 µl

SDS: **s**odium **d**odecyl **s**ulfate; TEMED: **te**tra**m**ethyl-**e**thylene**d**iamine

2.2.7.3. Western blot and immunodetection

Following electrophoretic separation, proteins were transferred to a PVDF membrane by electroblotting (1.5 h, 100 V, 250 mA, 15 W) in blotting buffer (25 mM Tris, 150 mM Glycin, and methanol 100% (20% v/v)) for 30 min. After transfer, membranes were incubated in blocking buffer (1:10 Roti-ImmunoBlock in MilliQ; pH 7.4) and washed 4×5 min in rinsing buffer (PBS-Tween 20; pH 7.4). Membranes

were incubated for 1h with the primary antibodies rabbit anti mouse MRP-8 (2 µg/ml), rabbit anti mouse MRP-14 (1.9 µg/ml), or rabbit anti-rat ERK 1 (0.4 µg/ml), respectively, all dissolved in blocking buffer. After repeated washing, membranes were incubated with IRDye800-conjugated goat anti-rabbit IgG (0.2 µg/ml) and finally washed 4×5 min in rinsing buffer. Protein bands were visualiyzed by scanning with an Odyssey infrared imaging system and and relative density of protein bands was analyzed using Odyssey software 1.2.

2.2.8. Cell culture, isolation, and activation

2.2.8.1. Jurkat T cell culture

Jurkat cells are lymphoid cells derived from an acute T-cell leukemia which do not express NE[220]. These cells were grown in RPMI 1640 medium supplemented with 10% FCS and maintained at 37°C with 5% CO_2. Cells were cultured in a density of 0.05×10^6 cells/ml with a medium change twice a week. Total cell number as well as their viability was determined with trypan blue staining.

2.2.8.2. Isolation and differentiation of PMNs

Human neutrophils were isolated from citrated blood from healthy donors by dextran sedimentation (Plasmasteril) followed by pancoll density centrifugation[48]. Briefly, citrated peripheral blood was diluted with 1 volume PBS-D and Plasmasteril (1 volume of blood) was added. To remove erythrocytes, cell pellets were allowed to settle for 30 min and leukocyte rich supernatants were transfered onto the Pancoll solution and centrifuged at 850 g for 24 min at RT. Cell pellets were dissolved in 5 ml cold Aqua dest for 40 s and erythrocyte lysis was stoped by adding 5 ml 2xPBS. Cells were washed and centrifuged two times at 200g for 10 min at 4°C and suspended in CL-medium (RPMI 1640 buffered with 25 mM HEPES without phenol red) before use. Total cell number as well as their viability was determined with trypan blue staining. Viability of isolated human neutrophils exceeded 98% in all experiments.

Murine neutrophils were differentiated *in vitro* from bone marrow (BM) cells. Briefly, mice were sacrificed by cervical dislocation. The femurs and tibias were cut out and after removing muscles, the bones were placed into HBSS-Prep (Ca-Mg-free HBSS supplemented with 20 mM HEPES and 0.5% FCS) to prevent dry-out. After cutting the ends of the bones, the BM was flushed into conical tube with HBSS-Prep using syringe with a 25G needle. Isolated BM was homogenized through an 18 G needle to disaggregate larger BM pieces and preceded through a 70 micron cell strainer. Suspensions were sedimented at 400xg for 5 min and resuspended in 10 ml of erythrocyte lysis buffer (155 mM NH_4Cl, 10 mM $KHCO_3$, 0.1 mM EDTA; pH 7.2). After lyes of erythrocytes for 10 min, HBSS-Prep (30 ml) was added and the suspensions were pelleted at 400xg for 5 min. Cells were counted and subsequently cultured in RPMI 1640 medium supplemented with 5% FCS and 10 nM granulocyte colony-stimulating factor (G-CSF) at 37°C with 5% CO_2 for 24 h. Afterwards, the cells was placed on 62% percoll gradient in HBSS-Prep and centrifuged for 30 min at 1000xg. Thereafter, cells at the interface and the upper part of the 62% Percoll fractions were carefully removed and discarded. Neutrophil-containing pellets were transferred to clean tubes, washed with and then resuspended in CL-medium.

2.2.8.3. Purity of neutrophils

Flow cytometry or fluorescence-activated cell sorting (FACS) is a well determined technique in research laboratories as well as clinical medicine and biology. This tool measures optical and fluorescence characteristics of single cells in a stream of fluid that physical properties of certain cell populations, such as size (represented by forward scatter) and internal complexity (represented by side scatter) can be analyzed[221]. Specific antigens or proteins on cell membranes or inside cells can also be analyzed by using conjugated antibodies to fluorescent dyes in which the fluorescent molecules on labeled cells are excited to a higher energy state by passing a light source[221]. When the electrons return to their ground state, the fluorochrome molecules emit light energy at higher wavelengths[221]. Since purified cell populations are frequently used in experimental studies, FACS can be a suitable procedure to purify cell populations of known phenotype. Here, FACS was applied to analyze the purity of human and murine neutrophils for further experiments.

The purity of the PMN preparation was determined by analyzing the forward and side scatters as well as by measuring expression of CD16 and Ly-6G, markers of human and murine PMNs, respectively. Isolated human or murine PMNs were resuspended in fluorescence-activated cell sorting (FACS) buffer (PBS-D without Ca^{2+} and Mg^{2+} + 0.1% BSA). For analysis, human cells (2×10^5 - 10^6 cells/ml) were incubated for 15 min at 4°C with CD16-FITC, CD14-PE, and CD3-APC, while murine PMNs were stained with Ly-6G-PE-Cy7, CD11b-APC, and CD3-FITC. For all these antibodies, corresponsding isotypes were also applied. The cells were centrifuged at 450 g for 5 min at 8°C and washed with FACS buffer. Fluorescence intensities as well as forward and side scatter intensities were quantified by BD LSR II Flow Cytometer and analyzed by FCS Express Flow Cytometry software.

2.2.8.4. Activation of neutrophils by immobilized immune complex

Activation of neutrophils by immobilized immune complex (IC) was performed *in vitro* as described previously with modification[214]. Briefly, immobilized IC was prepared using recombinant murine COLVII and rabbit amCOLVII IgG. Wells of ibiTreat microscopy chambers or 96-well plates were coated with 1 µg recombinant COLVII in 100 µl PBS at 4°C overnight. Following blocking with PBS containing 1% BSA and 0.05% Tween-20, surfaces were covered with 100 µg rabbit amCOLVII in 100 µl PBS containing 1% BSA and 0.05% Tween-20 for 1 h at 37°C and plates were finally washed with CL-medium. Control wells received normal rabbit control IgG instead of rabbit amCOLVII IgG. Neutrophils were applied on IC as well as irrelevant isotype antibody and prepared for measurement of activation parameters.

2.2.8.5. Determination of neutrophil activation measurement

Neutrophil activation is accompanied with several factors such as generation of ROS and release of elastase as well as neutrophil adhesion. ROS production and elastase release are considered as the central of neutrophil defence mechanisms and progression of several inflammatory diseases[129,222]. Beside the importance of neutrophil activation in the host defense, their activation by the immobilized IC after recruitment into the skin also leads to the generation of ROS and the release of

granule constituents including elastase, all of which have been proven to be essential factors for autoantibody-mediated tissue damage[117,137,139]. In addition to release of ROS and elastase, an IC-induced neutrophil adhesion was also observed during activation[214].

Generation of ROS by neutrophils was measured by chemiluminescence assay. In this assay, a probe such as luminol (5-amino-2,3-dihydro-1,4-phthalazindione) reacts with ROS including O2-, OH and hydrogen peroxide in the target fluid which result in production of light photons[223]. Herein, ROS production was determined by measurement of chemiluminescence as described elsewhere[214,224]. Briefly, neutrophils (10^6 cells/ml) in CL-medium supplemented with 60 µg/ml luminol were preincubated for 30 min at 37°C and subsequently distributed in 200 µl aliquots in an intransparent 96 well microtiterplate, coated with IC or with corresponding control proteins as described in section 2.2.8.4. Chemiluminescence was recorded for 60 min and data were expressed as relative light units (RLU) by using Microplate Luminometer and the data was processed with MicroLumatPlus software.

Neutrophil degranulation was also analyzed as another neutrophil activation parameter by measurement of the amount of elastase released as described elsewhere[225]. Briefly, neutrophils activated by immobilized IC were centrifuged for 20 min at RT. Supernatants were added to a 96-well plate containing CL-medium and subsequently a series dilution was performed. Thereafter, substrate solution containing substrate buffer, DMSO, BOC substrate, and Ellman's Reagent was applied and reaction was measured by Tecan Microplate ELISA Reader powered by Magellan data analysis software.

Furthermore, neutrophil adhesion was monitored by phase-contrast microscopy. In parallel, neutrophil adhesion was quantified by real-time impedance measurement by using the xCELLigence system. The xCELLigence system is based on a new method which provides a possibility to investigate the real-time analysis of the adhesion, migration, and invasion proprieties of cells in physiologically relevant conditions[226,227]. The real-time kinetic data enable to characterize more accurately the short-lived cellular events. Cells are cultured in specific plates (E-Plates) on a grid of gold microelectrodes in their base which are connected to a computer system recording the impedance changes during an electrical circuit[226,227]. These changes are converted into cell index value that may be influenced by several parameters,

such as cell number, cell size, cell-substrate, or cell-cell attachment[227–229]. Therefore in present study, the relative change in measured electrical impedance was used to represent cell adhesion, and it was expressed as the arbitrary unit of cell index.

2.2.9. Determination of neutrophil elastase activity by the FRET reporter NEmo-2

2.2.9.1. FRET reporter performance *in vitro*

Activity of NE *in vitro* was determined by the cleavage of FRET reporter and analyzed by confocal microscopy. Laser scanning confocal microscopy is an essential and invaluable instrument in the medical and biological research which enable for imaging three-dimensional reconstructions, single optical sections, multiple wavelength images, and living cell and tissue sequences[230]. The basic principle of a confocal microscope is that the laser light from excitation source as well as emitted fluorescence from sample passes through two pinholes, one placed in front of the light source and one in front of the photodetector[230]. Both pinholes in front of light source and detector as well as the focused point on the sample are all confocal with one another[230]. By contrast to conventional imaging microscopy, this confocal approach prevents the detection of non-confocal fluorescence emissions in focal planes which are away from the region of interest and therefore eliminates the detection of out-of-focus lights[230]. Of note, a multi-dimensional view of living cells is possible by using advanced confocal imaging microscopy[231]. In present study, this system was used to monitor dynamic and cellular processes of the Jurkat T cells as well as neutrophils in an *in vitro* assay.

To detect of NE activity on neutrophils, small-molecule fluorescent ratiometric NE monitoring reporter based on energy transfer was used. The reporter, NE monitoring-2 (NEmo-2), consist of a short human and murine NE specific peptide substrate with a specific cleavage site between the valine residues[146] flanked by ethylenglycol (PEG)-linkers which function as spacers and to increase solubility, a suitable fluorophore is coupled at each end to build a FRET-pair[165] (Figure 9). NEmo-2 reporter has a lipid anchor[164] which enable it to be used as a membrane-targeting NE reporter. The FRET-pair for this lipidated reporter has been designed as red-shifted phlorophores to allow excitation with the 405 nm laser line and to avoid cell damage

by high-energy light[165]. Coumarin 343 and carboxymethylrhodamine (TAMRA) are the fluorophores as donor and acceptor, respectively[164,165]. Coumarin dye has been selected because of less tendency to form nonfluorescing complexes[164]. To prevent diffusion of the intact reporter through the plasma membrane of the cell or its C-terminal part after cleavage, negative charges are included in the substrate sequence by replacing the C-terminal glutamine by two glutamic acid residues[165]. Presence of two fluorophores, instead of a fluorophore and a nonfluorescent quencher, allows for ratiometric readout of reporter cleavage[165]. Upon cleavage of the reporter, the donor fluorophore stays with the lipidated cleavage fragment at the cell surface while the cleavage fragment carying the acceptor fluorophore is lost[165]. To enhance this property and to prevent overall internalisation of the intact reporter as well as the released part upon cleavage, negative charges have been introduced by including two glutamate residues close to the acceptor fluorophore[165] (Table 1).

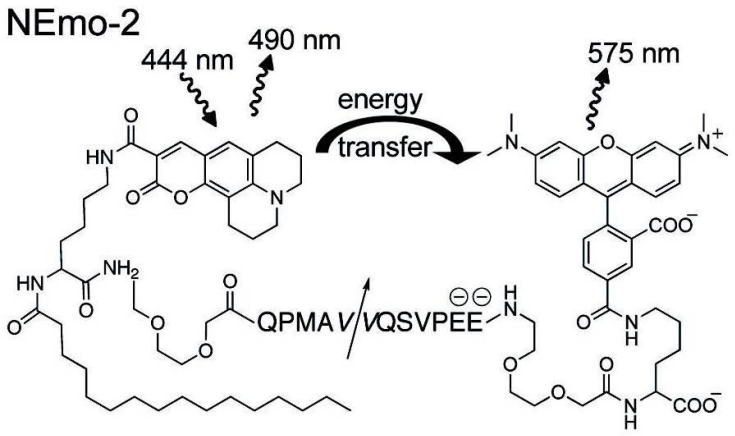

Figure 9 Membrane-targeting lipidated neutrophil elastase (NEmo-2) monitoring fluorescent reporter (According to Ref.[165]). The NE-specific peptidic target sequences are shown by single letter amino acid code. Two negative charges were introduced for NEmo-2 to prevent internalization from the cell membrane. Arrows indicate the cleavage sites.

In the intact reporter, donor and acceptor fluorophores are in proximity which allows an energy transfer upon excitation of the donor to the acceptor. Cleavage of the substrate sequence by the enzyme of interest, here NE, induces separation of the fluorophores, which is detected by an increase of donor fluorescence and loss of FRET (Figure 9). In this study, ratiometric FRET reporters which have previously been developed[165] were used to monitor NE activity in neutrophils.

Table 1 Synthesized lipidated NE FRET reporter.

Name	F1/F2	Donor λ exc/emi (nm)	Accepor λ exc/emi (nm)
NEmo-2	Coumarin 343/TAMRA	450/490	545/575

TAMRA: (5-and 6-)carboxytetramethylrhodamine; F1, F2: **f**luorophores as FRET-pair

2.2.9.2. Acceptor photobleaching

To analyze the FRET efficiency, acceptor photobleaching was used as previously described[232–235]. The basic principle is to measure donor intensity before and after acceptor bleaching, thus providing an internal control by eliminating the occurrence of FRET. In the case of true FRET, an increase in donor fluorescence will result; from the portion of the donor fluorescence that was recovered after acceptor inactivation. The ratio of the donor fluorescence intensity before and after acceptor photobleaching reports the FRET efficiency[232–235]. FRET efficiency is calculated as the ratio of two intensities generated in the same detection channel but from the same sample before and after acceptor bleach. The donor fluorescence will be unquenched after photobleaching of the acceptor. The difference of fluorescence intensity of the donor before and after photobleaching gives a direct indication to the FRET efficiency and can be quantified as follows:

$$FRET_{eff} = (D_{post} - D_{pre}) / D_{post}$$

where D_{post} is the fluorescence intensity of the donor after photobleaching and D_{pre} is the fluorescence intensity of the donor before photobleaching. The FRET efficiency

($FRET_{eff}$) is considered positive when $D_{post} > D_{pre}$. In this regard, the imaging conditions for donor and acceptor fluorescence was defined by seting up the imaging conditions (Donor = coumarin 343, excitation 405 nm, emission 470-510 nm; Acceptor = TAMRA, excitation 561 nm; emission 570-610 nm). Donor detection was performed only by switching off the acceptor detection channel and setting the laser light of the acceptor down to 0%. Acceptor detection was done by setting the donor excitation light down to 0%, turnning off the donor detection channel, turnning on the acceptor detection channel instead and then setting the excitation laser line of the acceptor for adequate excitation light. A region of interest (ROI) was drawn around the area of the cell to bleach. The measurement was started by imaging the donor and acceptor before bleaching, followed by the bleaching of the acceptor and finally imaging the donor and acceptor after bleaching. The imaging conditions before and after bleaching were identical. FRET efficiencies were calculated by provided data[236].

2.2.9.3. NE reporter imaging on Jurkat T cells

For imaging experiments, cells were resuspended in a pH independent imaging medium (IM) (20 mM HEPES, pH 7.4, 115 mM NaCl, 1.2 mM MgCl2, 1.2 mM CaCl2, 1.2 mM K2HPO4, 2 g/l D-glucose) at RT and cell counts were performed. Jurkat T cells (30,000-40,000 cells) were diluted in 100 µl IM at RT and incubated with 2 µM NEmo-2 for 3 min. After addition of 100 µl IM, cell suspensions were spread on glass slides. In some experiments, the cells were incubated with 100 µM alpha1-antitrypsin (A1AT) from human plasma for 15 min at RT prior to addition of the reporter. Reporter cleavage was induced by addition of 1 µl NE (0.5 ng/µl). Slides were mounted with Fluoromount-G and stored at 4°C until analysis.

For direct imaging experiment, cells were plated after incubation with inhibitor and reporter on microscopy Ibidi chambers and were imaged by confocal microscopy in time series of 30 min with 1 image/min. To induce reporter cleavage, 1 µl human NE (hNE; 0.5 ng/µl) was added to the NEmo-2 harboring cells to induce reporter cleavage and incubated for 3 min.

2.2.9.4. Incubation of human or mouse neutrophils with NEmo-2

Human or mouse neutrophils were resuspended in PBS and cell counts were performed. Neutrophils (30,000-40,000 cells) were incubated with 2 µM NEmo-2 in 100 µl IM at RT and for 3 min. IM (100 µl) was added and subsequently cell suspensions were spread on glass slides. In some experiment, the cells were incubated with 10 µM A1AT derived from human plasma for 15 min at RT prior to addition of the reporter. For imaging of neutrophils, cells were allowed to settle on Ibidi microscopy chamber without washing and were imaged by confocal microscopy for a time course of 30 min.

For analyzing of inhibitory effects of CD18 antibodies, 30,000-40,000 mouse BM neutrophils were diluted in 100 µl IM at RT. For inhibition of elastase, 100 µM A1AT from human plasma was incubated for 15 min at RT prior to addition of the reporter. Cells were incubated with 10 µg/ml purified NA/LE rat anti-mouse CD18 or 10 µg/ml purified NA/LE rat IgG1 Isotype Control for 5 min at RT and then incubated with 2 µM NEmo-2 for 3 min. IM (100 µl) was added and the cell solution was spread on ibiTreat microscopy chamber and were imaged by confocal microscopy for a time course of 30 min.

2.2.9.5. Confocal fluorescence microscopy settings and image analysis

Images were acquired on Leica confocal microscopes (SP5) equipped with HCX PL APO Ibd.BL 63x 1.4 oil objective with the following settings: the donor was excited with a 405 nm diode laser and emission was sampled between 470-510 nm. Sensitized emission of the acceptor was sampled between 570-610 nm. The pinhole was set to 150 µm. Images were processed with ImageJ 1.38r software (http://rsb.info.nih.gov/ij/) using background subtraction, smoothing with a median filter, thresholding and calculation of D/A ratio images. Cells were selected as ROI to quantify mean pixel values per cell.

2.2.10. Monitoring of neutrophil elastase enzyme activity by using the FRET sensor NEmo-2 *in vivo*

2.2.10.1. Multi-photon fluorescence microscopy

Assessment of neutrophil elastase activity *in vivo* was performed by analyzing cleavage of NEmo-2 using multi-photon microscopy (MPM). MPM has developed into a powerful and invaluable imaging techniqe in biomedical and biological investigations[237,238]. This optical microscopy tool enables the study of biological function *in vivo* noninvasively such as cellular and subcellular processes in living tissue[237,238]. Basically, MPM is supported by two-photon fluorescence excitation whose adequate combined energy is able to promote a molecular transition from ground state to an excited state[237,238]. This kind of excitation process provides several unique advantages, such as higher spatial and temporal resolution, reduced specimen photodamage, low photon toxicity, and elevated penetration depth[237,238]. In contrast to confocal imaging with a linear ultraviolet or visible light laser excites fluorophores inside the sample, in MPM microscopy, an infrared or near-infrared laser offers pulsed illumination in which the photon density falls off quadratically with distance from the focal plane[237–239]. Therefore, due to the quadratic dependence of two-photon absorption on intensity, sufficient density of photons for simultaneous absorption of two photons by fluorophores is limited to the focal point[237–239]. As a consequence, out-of-focus fluorescence is never generated as excitation and subsequent light detection is localized to a single point[237–239]. This also helps to reduce photobleaching and photon toxicity limited to the focal point. Furthermore, due to less scattering and absorbing of near-infrared light by biological samples, fluorescence can be excited deeper into biological tissues[237,240].

To provide the ability of image analysis *in vivo*, the FRET technique was transferred from the confocal to the MPM. For this purpose, Jurkat T cells or neutrophils were loaded with NEmo-2 as described in sections 2.2.9.4 and 2.2.9.5, respectively. The individual channels > 560 nm and 800 nm for the acceptor and 495-560 nm and 800 nm for the donor were smoothed by smooth time and threshold cutoff. Donor fluorescence and sensitized acceptor emission was imaged and D/A ratio images were calculated. For further analysis, Jurkat and neutrophil cells were analyzed and the ratio was plotted by time.

2.2.10.2. Neutrophil labeling and transfer *in vivo* into an EBA mouse model

Intradermal administration of cells into the mouse ear was performed as described elsewhere[241,242] and used with slight modifications. Briefly, BM neutrophils of Balb/c mice were isolated and differentiated as described in section 2.2.8.2 and subsequently treated with a cell tracker or FRET probe. To monitor neutrophils *in vivo*, a cell tracker (CellTracker Red CMTPX), a fluorescent dye appropriate for monitoring cell movement or location, was used to track the dynamic of the cells. The lyophilized component was dissolved in steril DMSO to a final concentration of 10 mM. Stock solution was diluted to a final working concentration of 5 µM in serum-free medium pre-warmed to 37°C. Neutrophils were harvested by centrifugation and the supernatant was aspirated. The cells were resuspended gently in pre-warmed CellTracker dye working solution and incubated in cell culture medium for 30 min. Neutrophils were centrifuged and the medium was replaced with fresh, pre-warmed medium and incubated for another 30 min at 37°C. Cells were washed with and resuspend in PBS. Neutrophils were labeled with NEmo-2 in the presence of A1AT as described in the section 2.2.8.7.

To analyze the neutrophil kinetics *in vivo*, a local antibody transfer mouse model of EBA was used. Balb/c mice were intraperitoneally anesthetized using a solution of Fentanyl (16 µg/ml), Midazolam (0.4 mg/ml), and Medetomidine (50 µg/ml). Subsequently, hair removal cream was applied on the ears to get rid of the hairs. BM-neutrophils (10×10^6 cells) were taken up in 100 µl sterile imaging buffer and aliquot of 10 µl cell suspension was intradermally injected using an insulin syringe (30-gauge needle) into the ventral side of the mouse ear. Since dermis layer in the ear is susceptible to damage due to thinness, injection procedure was performed by using a dissecting microscope to minimize the area of trauma and consequently the risk of artifacts. Thus, 2 h after injection, local antibody transfer model of EBA was induced by application of affinity purified rabbit α-mouse COLVII IgG labeled with Dylight 594 (7.5 µg) as well as an irrelevant antibody of the same isotype (rabbit IgG) were also intradermally administrated as described above into the different mouse ears.

2.2.10.3. Intravital multi-photon imaging of neutrophil activation

For intravital MPM imaging, Balb/c mice were used for respective experiments to prevent occurrence of a phenomenon so-called 'speckling' (a pattern of dots)[243,244]. Under this condition, in pigmented mice (like C57BL/6 mice) laser light can be absorbed by melanin-containing dermal cells resulting in compromising the image quality as well as inducing heat damage that the later can trigger an inflammatory response characterized by the neutrophil invasion[241]. To achieve the best outcome, ear skin was used for MPM imaging which is commonly preferred[243–248]. Due to accessibility and the minimal requirements of preparation before imaging, mouse ear skin is a matter of choice as the imaging site enables fast preparation and reproducible conditions for generating consistent results[241]. Hair removal was performed to reduce the interference from hairs which is essential to prevent autofluorescence compromising contrast and to prevent the absorption of laser light by hairs obscuring effective illumination of cells and tissue structures[241]. Intravital imaging of ear pinnae of anaesthetized mice was carried out as described elswhere[242,248,249]. Briefly, mice were placed in a lateral recumbent position on a custom made imaging platform in which the ventral side of the ear pinna rested on a coverslip. A strip of Durapore tape was placed lightly over the ear pinna and affixed to the imaging platform to immobilize the tissue. Care was taken to minimize pressure on the ear. Images were captured towards the anterior half of the ear pinna where hair follicles are sparse.

For focal skin tissue damage and to induce sterile injury in a spatially and temporally controlled manner, a laser ablation technique was applied which has been described previously[241,250] with slight modifications. A highly localized injury was induced by a focused two-photon laser pulse at a limited area within the ear dermis for a short period of time. The wavelength of the two-photon laser was set at 740 nm with a pulse length of approximately 200 femtosecond (fs) and laser power of 23.6 mW. A small injury region of 20 x 20 µm for 3 to 5 seconds (sec) was created as indicated by a bright autofluorescent area around the focal point of the beam.

Imaging was performed by using a TriM Scope two-photon microscope equipped with an XLPlanN 25×1.05 WMP Objective. FRET reporter was exited with 920 nm. Emitted light was detected by 4 wavelength separated PMTs (<435 nm, 453-495 nm, 495-560-560 nm and >560 nm). Image processing was done using Imaris Software

(Bitplane, Zurich, Switzerland) using background subtraction, smoothing with a median filter, thresholding and calculation of D/A ratio images. Cells were selected as ROIs to quantify mean pixel values per cell. Of note, to confirm that an operational FRET process is present, the acceptor was directly excited which results in direct fluorescent signal of the acceptor.

2.2.11. Statistical analysis

All data were first tested using the D'Agostino and Pearson normality omnibus tests for presenting a normal distribution. In cases with normal distribution of data, the statistical analysis was performed using the two-side, independent t-test or one-way ANOVA and a post-test Bonferroni's Multiple Comparison Test. The data were presented, unless indicated otherwise, as mean ± SEM. In cases with non-normal distribution of data, the analysis was performed using the Mann-Whitney or Kruskal - Wallis tests and the Dunn's Multiple Comparison test (95 % confidence interval) as post-tests which was stated otherwise in the legend of the figures. Data were analyzed with GraphPad Prism version 5.0. The $p<0.05$ was accepted to indicate statistical significance.

3. RESULTS

In the present study, the role of the neutrophil proteins MRP-8/-14 and neutrophil elastase in the regulation and execution of the effector phase of two autoimmune diseases, EBA and BP, was investigated. While the first part is focused on the analysis of MRP-8/-14 expression in human diseases as well as in murine disease models, the second part addressed the question of a potential functional role of these proteins in the pathogenesis of EBA and BP. Finally, mechanisms of proteolytic tissue damage as a consequence of neutrophil activation were investigated by visualization neutrophil protease activity (elastase) in experimental models of EBA and BP *in vitro* as well as *in vivo*.

3.1. Protein concentration analysis of MRP-8/-14 levels in human serum of the BP patients

MRP-8 and its heterodimeric partner MRP-14 proteins are cytosolic calcium-binding proteins belonging to the S100 family. Although principally located in the cytosol of phagocytes like neutrophils they may function as danger signals outside of the cell. Increased levels of MRP-8/-14 expression are observed in many chronic diseases like cancer, RA, inflammatory and AIDs disorders. The expression of MRP-8/-14 in AIBD has not been investigated so far. Therefore, MRP-8/-14 serum levels were measured in 20 patients with BP, 10 patients with EBA as well as 20 sex/age matched healthy controls. Serum levels of MRP-8/-14 were highly increased in the patients with BP ($p = 0.0003$) and EBA ($p = 0.02$) as compared to healthy individuals (Figure 10). While in healthy individuals median concentration of MRP-8/-14 were found around 2000 ng/ml, significant higher level could be detected in sera of BP patients (median ~7500 ng/ml). EBA patients also expressed elevated level of MRP-8/-14 (median ~2500 ng/ml) although less prominent as compared to the BP group. These results clearly indicate that AIBD patients are characterized by an increased serum level of MRP-8/-14 proteins.

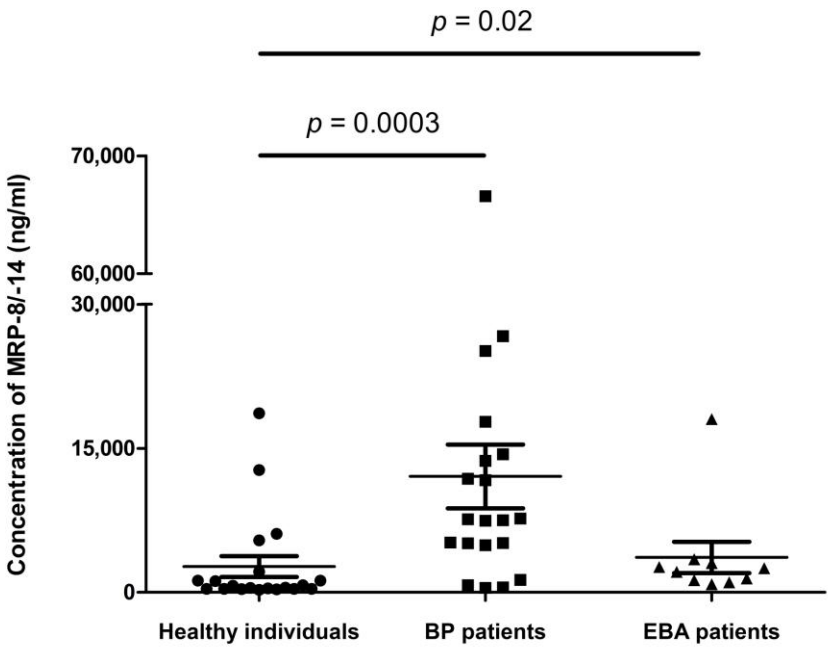

Figure 10 MRP-8 and MRP-14 concentrations in the sera of BP and EBA patients as well as healthy control individuals. Serum levels of BP patients (n=20), EBA patients (n=10), and healthy donors (n=20) were analyzed by ELISA. The data were expressed as medians with interquartile range. Indicated statistically significant differences between the respective patient groups and healthy controls were calculated using the Mann-Whitney test.

3.2. MRP-8/-14 expression in experimental EBA and BP

Based on the findings in human, expression of MRP-8/-14 was analyzed in experimental AIBD. A previous, more generalized study using whole genome expression analysis of inflamed tissue in experimental EBA led to the identification of 33 distinct and differentially expressed gene modules regulated in disease[251]. Among these, both *Mrp-8* and *Mrp-14* belong to the group of the top ten of the highly upregulated genes, with an expression increased more than 60-fold as compared to the healthy controls. To confirm these initial findings, we investigated the gene and protein expression of MRP-8/-14 in both experimental EBA and BP.

3.2.1. Experimental antibody transfer models of EBA and BP in wild type mice

To investigate the role of MRP-8/-14 in experimental EBA and BP, C57BL/6J mouse strain was used for antibody transfer models of EBA and BP. A systemic antibody transfer model of EBA was induced by administration of pathogenic rabbit amCOLVII IgG. After repetitive administration of pathogenic rabbit amCOLVII IgG or IgG from non-immunized rabbit (isotype), all mice were examined on days 4, 8, 12 and 16 for EBA typical skin lesions, and finally the percentage of diseased skin in relation to body surface were calculated as the severity of the disease (Figure 11A). At the end of the experiment (day 16), skin lesions on the mice skin were examined. Four days after antibody administration, local inflammation was developed on the different parts of the mice skin that had received the pathogenic antibody (Figure 11A). This inflammatory response was manifested in the form of redness, scabs and peeling of the epidermis (Figure 11B). Injection of pathogenic antibody induced about 20% of affected skin on the surface of the mice body.

Due to the low pathogenicity of our anti-mCOLXVII antibody, animals did not develop disease sympotom in the systemic antibody transfer model of BP even after administration of high antibody doses. To circumvent this, a local antibody transfer model of BP was used as already described before[252]. In this model, the pathogenic antibody was injected intradermally in the ear base once resulting in a local inflammatory response and blistering in the area of the injection site within 24 h observed. To establish the local antibody transfer model of BP, the pathogenecity of the pathogenic amCOL17 IgG was first determined *in vivo*. Ears of C57BL/6J wild type mice were intradermally injected with different doses of the antibody, including 0.125, 0.25, 0.5, 1, and 2 mg, respectively. After administration of antibodies, all mice were examined for BP typical skin lesions, and finally the percentage of diseased skin in relation to body surface was calcuated as the severity of the disease. After 24 and 48 h, skin lesions on the ear were examined. Just 24 h after antibody administration, local inflammation was developed on the ears that had received the pathogenic antibody (Figure 11A). The two highest dosages of antibody (1 and 2 mg/ear) lead to the induction of clinical symptoms of the disease in the wild type mouse ears (Figure 11B). This inflammatory response was manifested in the form of redness, scabs and peeling of the epidermis (Figure 11B). Injection of 1 mg and 2 mg antibody induced about 5% and 30% of affected skin on the surface of the ear,

respectively. Therefore, a dose of 2 mg/ear was selected for the following experiment.

To determine the histopathology of the diseases in the skin induced by pathogenic antibodies, lesional skin tissues were used further analysis. Therefore, H&E Staining was used to monitore the changes in the tissue sections. All animals treated with pathogenic IgGs showed inflammation of the skin by infiltration of inflammatory cells like neutrophils in the dermis, thickening of the epidermis, and blister formation (Figure 11C). Moreover, blister formation by splitting the epidermis from the dermis could be observed.

Furthermore, since neutrophils are the major producers of MRP-8/-14 proteins, neutrophil recruitment was examined as a potential mechanism by which their MRP-8/-14 proteins may amplify inflammation and tissue damage in the skin. Therefore, we then determined the neutrophils in the affected skin in experimental EBA and BP. The neutrophils in the skin was determined using immunofluorescent staining with monoclonal antibody NIMP-R14[253], a neutrophil-specific marker. Figure 11D shows representative images from each treatment group. There were an increased number of NIMP positive cells in all wild type animals treated with amCOL VII or XVII IgG when compared to the control groups treated with irrelevant isotype antibody. This histologic analysis revealed that the neutrophils are present in the diseased part of skin in pathogenic wild type mice. The number of neutrophils was substantially increased relative to healthy part of the skin in control mice.

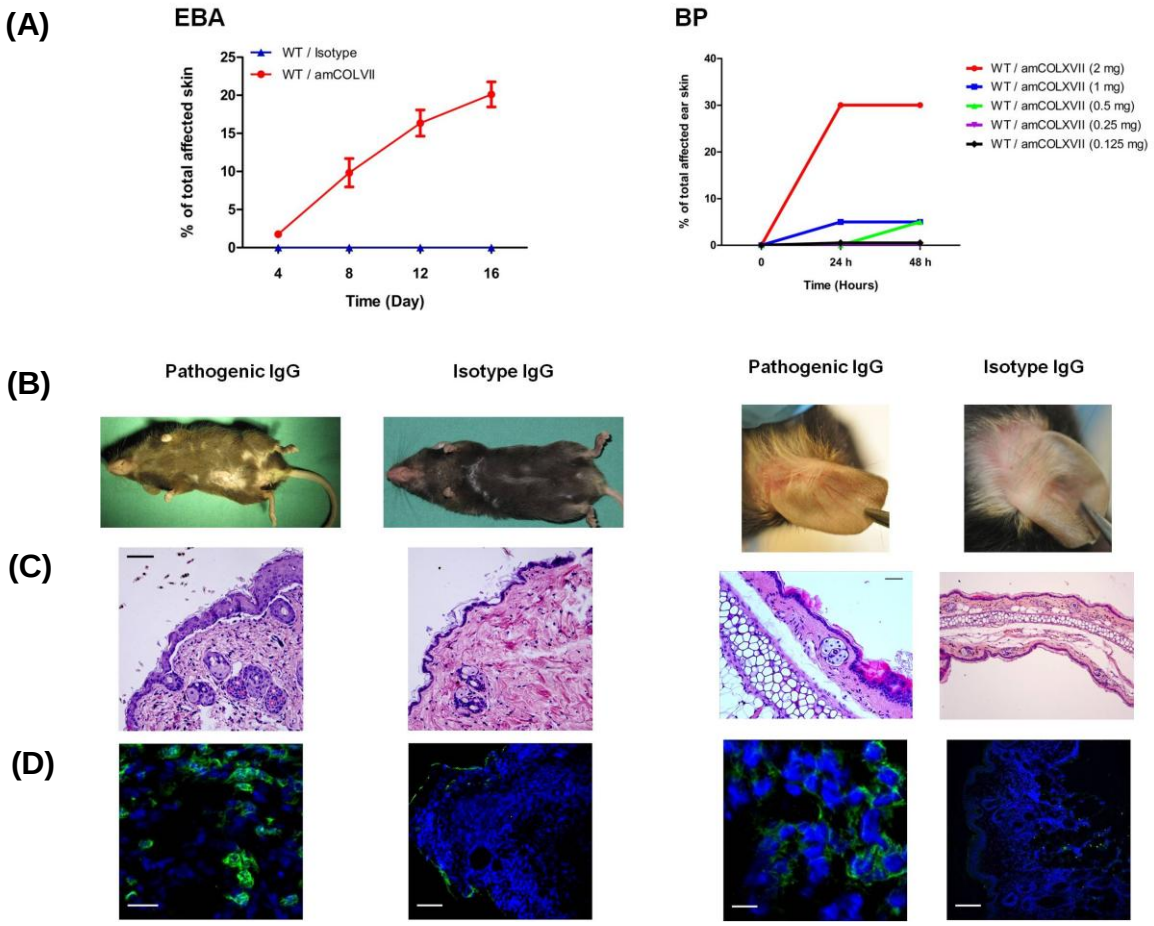

Figure 11 Experimental systemic EBA and local BP in wild type mice. Mice were treated with pathogenic rabbit amCOLVII or COLXVII IgG for experimental EBA and BP as well as rabbit isotype antibody for control group. For systemic model of EBA, antibody was injected on day 0, 2, 4, 6, 8 and 10 and mice were scored on days 4, 8, 12 and 16 for clinical symptoms (skin lesions). For local model of BP, antibody was injected intradermally once only and mice ears were scored 48 h after antibody injection for ear skin lesions. **(A)** Disease development in systemic EBA as well as local BP model animals by injection of amCOLVII IgG and amCOLXVII IgG, respectively. In BP model, a dose of 2 mg/ear was selected for the following experiment. **(B)** Mice phenotypes were photographically documented and representative images were mapped. **(C)** Infiltration of inflammatory cells and dermal-epidermal separation was determined by histology (H&E staining) of mice skin in EBA and BP models at day 16 (systemic experimental EBA) or day 2 (local experimental BP) in sections of skin treated with pathogenic antibodies. Scale bar: 500 µm. **(D)** NIMP immunofluorescent staining of skin tissue was performed for diseased as well as control groups. Cryosections (5 µm) of skin tissue were incubated with neutrophil marker (NIMP-R14) and subsequently with secondary antibody (Alexa Fluor® 488 Goat anti-mouse IgG). NIMP positive neutrophils (green areas) were detected in all pathogenic amCOL VII (upper) and XVII (lower) treatment groups, but not in irrelevant isotype treatment animals. Scale bar: controls, 50 µm; pathogenic EBA, 10 µm; pathogenic BP, 5 µm.

3.2.2. Quantitative *Mrp-8/-14* gene expression in EBA and BP

Gene expression of *Mrp-8* and *Mrp-14* in the affected skin of experimenal EBA and BP as well as control skin from healthy mice was quantified by quantitative RT-PCR. The expression of these two genes was normalized to the mean expression of the housekeeping gene *b2M*. In experimenal EBA, *Mrp-8* and *Mrp-14* genes were upregulated by 64-fold and 101-fold, respectively, as compared to controls (Figure 12A). A comparable effect was seen in BP where *Mrp-8* and *Mrp-14* expression in diseased mice exceeds those of healthy controls by 23-fold and 18-fold, respectively (Figure 11B).

In the next step, it was investigated whether the upregulation of the gene expression of *Mrp-8/-14* reflect the situation at the protein level in mice suffering from experimental EBA and BP.

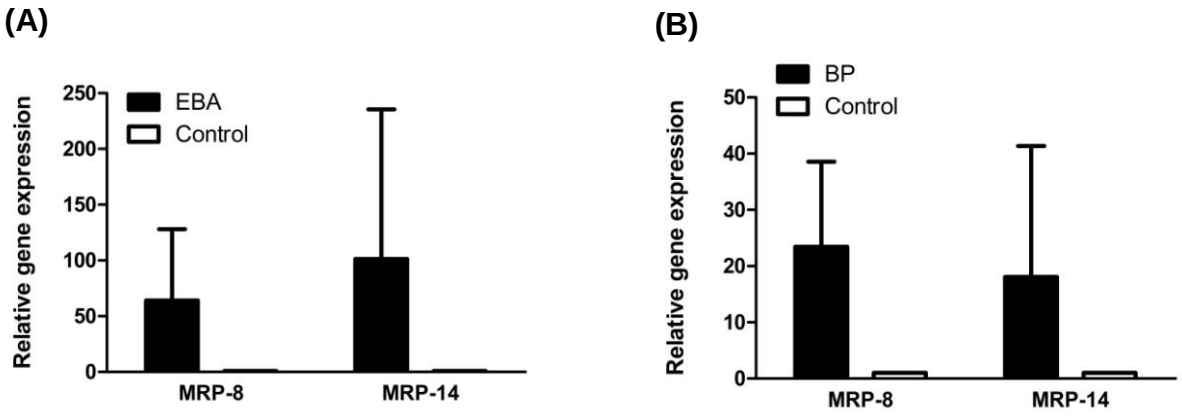

Figure 12 Upregulation of *Mrp-8* and *Mrp-14* genes in experimental EBA and BP. Gene expression of *Mrp-8* and *Mrp-14* detected by using RT-PCR in EBA **(A)** BP **(B)**. The gene expressions were presented as relative value where the gene expression in healthy individuals was set as one. *Mrp-8* and *Mrp-14* genes were upregulated in the diseased skin by 64-fold and 101-fold in EBA as well as 23-fold and 18-fold in BP as compared to the healthy control. Results of one experiment containing 3 mice/group are expressed as mean±SD.

3.2.3. Expression of MRP-8/-14 proteins in experimental EBA and BP *in vivo*

To determine whether the upregulation of the MRP-8 and MRP-14 also exist on protein level in the inflamed skin, the protein expression was determined by immunofluorescence staining. Samples of lesional skin of anti-mCOLVII-treated diseased mice as well as skin of healthy mice treated by irrelevant antibodies of the same isotype derived from the experiment shown in section 3.2.1 were taken on day 16 and cryosections were prepared. Immunofluorescence staining of specimen revealed that MRP-8/-14 proteins were found in the diseased skin but absent in the healthy control skin (Figure 13A). The results showed that protein expression of MRP-8 and MRP-14 was predominantly and abundantly found within the inflammatory cellular mass and stained polymorphonuclear cells in the affected skin compared with healthy control skin.

Furthermore, to quantify the protein levels of MRP-8/-14 proteins in the skin lesions, SDS-PAGE electrophoresis and western blot analysis was performed to analyze the semi-quantitative changes of these protein levels in the affected skin comparing with healthy control skin. Equal protein loading was controlled by using ERK 1 as a reference protein. Reliable assessment of the changes in target protein expression levels requires the measurement of both the target protein and the loading control protein in their linear dynamic ranges. In this regard, MRP-8/-14 expression levels were normalized to the expression of extracellular-signal-related kinase 1 (ERK 1, p44). The results indicate that these proteins are not expressed in the healthy skin but expressed by diseased skin samples in experimental EBA and BP diseases (Figure 13B).

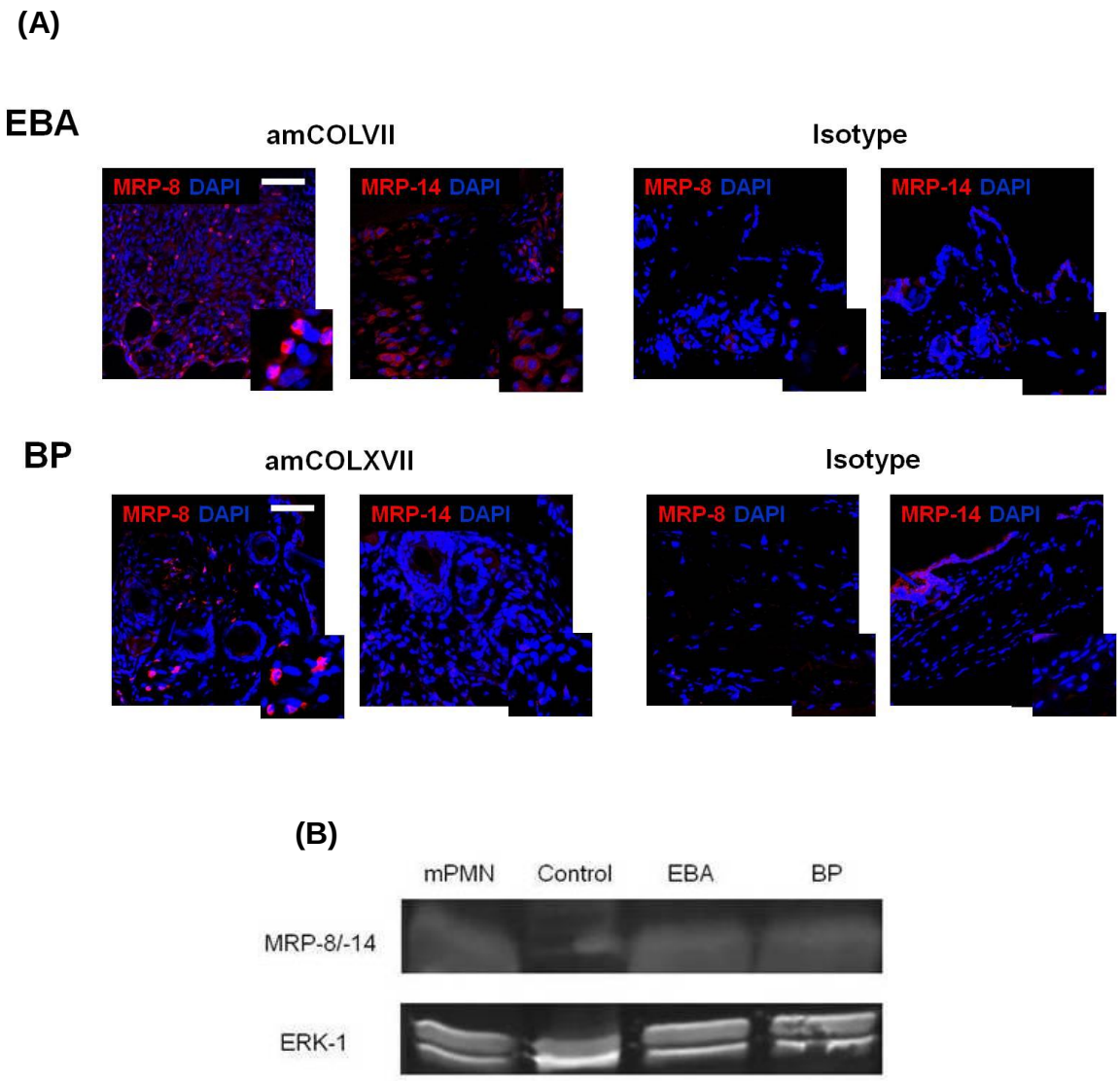

Figure 13 Expression of MRP-8 and MRP-14 proteins in skin tissue in experimental EBA and BP. (A) Cryosections (5 µm) of skin tissues from wild type mice treated with rabbit amCOLVII and amCOLXVII as well as normal rabbit IgG were were incubated with MRP-8 and MRP-14 rabbit anti mouse conjugated to Cy5.5 and analyzed by confocal microscopy. MRP-8/-14 positive proteins (red areas) were detected in all pathogenic amCOL VII (left) and XVII (right) treatment groups, but not in irrelevant isotype treatment animals. Both expression of MRP-8 and MRP-14 were highly expressed in the affected skin comparing with healthy control skin. Expression of MRP-14 was weaker than MRP-8 especially in BP model. **(B)** MRP-8 and MRP-14 protein levels in EBA and BP diseased skin as well as control animals were examined using Western blot. Equal quantities of protein (5 µg) were loaded in each lane. amCOL: anti mouse collagen. Scale bar: 100 µm.

3.3 Experimental EBA and BP in *Mrp-14*-deficient mice

According to the results shown above, MRP-8/-14 was found to be elevated on transcription and protein level in AIBD patients as well as in experimental models of the diseases. Consequently, in the next step the functional role of these proteins in AIBD was investigated by using *Mrp-14* deficient mice in experimental AIBD.

3.3.1. Experimental EBA in MRP-14 deficient mice

MRP-8 and MRP-14 form a heterodimeric complex in the cytosol of monocyte and neutrophil cell types circulating in peripheral blood. Since MRP-8 and MRP-14 expression levels were upregulated significantly in the diseased skin, the next series of experiments were designed to determine the presence of MRP-8 and MRP-14 in serum of diseased mice. The serum levels of heterodimeric complex of MRP-8 and MRP-14 were detected by ELISA. While in diseased wild type mice protein complexes were clearly present, they were undetectable in *Mrp-14* knockout mice (Figure 14). These data provide direct evidence that in *Mrp-14* knockout mice, no functional MRP-8/-14 heterodimers are expressed.

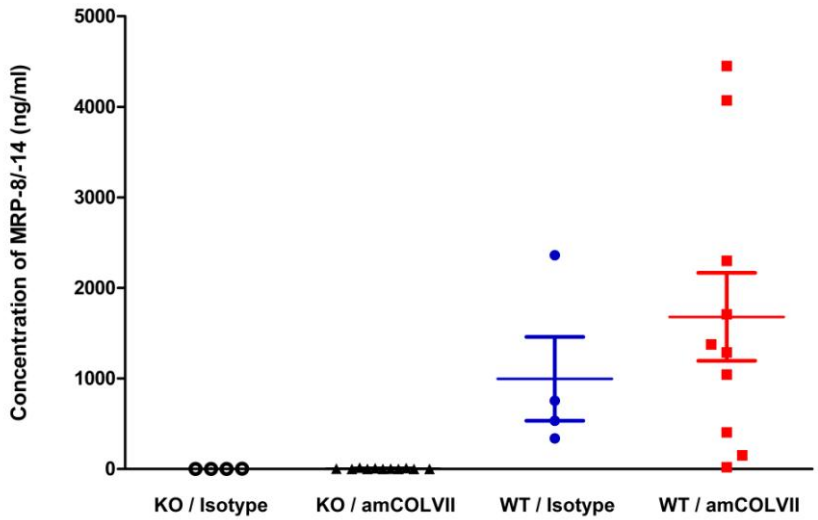

Figure 14 Serum levels of MRP-8 and MRP-14 proteins in experimental EBA. Experimental EBA was induced in wild type (WT) and Mrp-14 knockout (KO) mice and MRP-8 and MRP-14 concentrations in the sera were quantified at the end of the experiment (day 16) by ELISA. Data of one representative experiment is shown.

Since MRP-8 and MRP-14 are not functional in *Mrp-14*$^{-/-}$ mice, the role of MRP-8/-14 proteins was investigated in experimental EBA, where C57BL/6J-*Mrp-14*$^{-/-}$ mouse strain was compared with its corresponding wild type control (C57BL/6J) in a systemic antibody transfer model of EBA described in section 3.2.1. As shown in Figure 15A, MRP-14-deficient as well as wild type controls started to develop the clinical symptoms of EBA on day 8 after the first injection of the pathogenic antibody injection and the disease severity increased over time, with the strongest effect seen at day 16 (Figure 15A, B). Mice which received irrelevant antibodies did not develop disease. According to my initial hypothesis, I expected that *Mrp-14*-deficient mice should show a less severe skin disease as compared to the wild. However, in contrast to my hypothesis, no significant difference in disease severity between knockout and wild type mice was observed (Fig. 15A). This was confirmed after integration of the data derived from mice which had received pathogenic IgG (Figure 15C). In accordance with these findings, a more detailed analysis of the affected skin regions performed at day 16 revealed no significant difference between knockout mice and wild type control animals (Figure 15D). Although the distribution of skin lesions over the body differs slightly in their intensity between knock out and their wild type controls in individual body regions, due to the high variations within the groups, no significant difference could be identified. Animals with deficiency in *Mrp*-14 are not protected from EBA and disease activity is comparable to that of wild type control animals when the entire observation period and the whole body surface are considered.

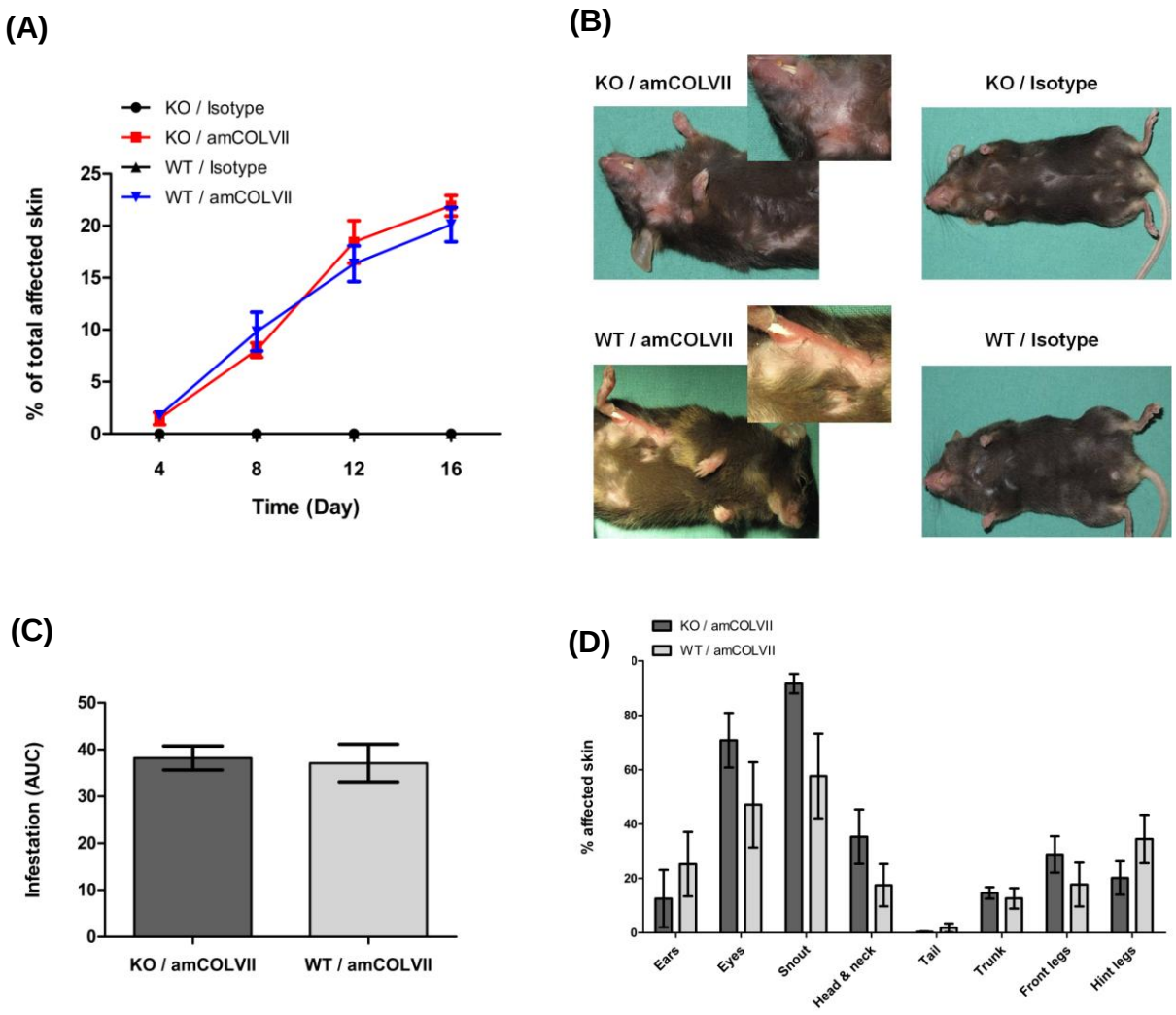

Figure 15 Experimental EBA in *Mrp-14*-deficient and wild type mice. Mice were treated with pathogenic rabbit amCOLVII IgG or irrelevant rabbit IgG control on day 0, 2, 4, 6, 8 and 10 and were scored on days 4, 8, 12 and 16 for clinical symptoms (skin lesions). **(A)** The disease development was represented as the percentage of the affected skin on the body surface over the entire observation period. **(B)** On the last day of the experiment (day 16), the phenotype of the mice was photographically documented and representative images of each group were mapped. **(C)** Data of disease activities derived from mice which had received pathogenic antibodied were integrated and presented as area under the curve (AUC). **(D)** Comparision of the infestation of individual body regions at day 16 between knockout and wild type animals treated with pathogenic antibodies. The data represent two independent experiments with 18 mice (12 and 6 mice for pathogenic and isotype IgG-injected group) in each experiment. amCOL: anti-murine collagen, KO: knockout, WT: wild type.

3.3.2. Experimental local antibody transfer model of BP in mice with MRP-14 protein deficiency

To investigate the role of MRP-8/-14 proteins in experimental local BP, pathogenic amCOL17 IgG as well as irrelevant rabbit IgG (isotype) were intradermally injected into the base of right and left ear of C57BL/6J-*Mrp-14*$^{-/-}$, respectively as described in section 3.2.1. Same procedure was performed for the corresponding wild type animals. According to our initial hypothesis, a less severe skin disease as compared to the wild types was expected in *Mrp-14*-deficient mice in the local antibody transfer model of BP. Disease symptoms became visible 24h after administration of pathogenic IgG and increased further during the next 24h (Fig 16A, B). No lesions have been observed on the ears of mice which had received irrelevant isotype antibody. However, similar to EBA mouse model, no significant differences between knockout and wild type mice could be observed at any time point (Fig. 16B). These findings were confirmed after integration of the data over the time (Figure 16C). Taken together, these data clearly show that animals with deficiency in MRP-14 protein are neither protected to BP nor to EBA.

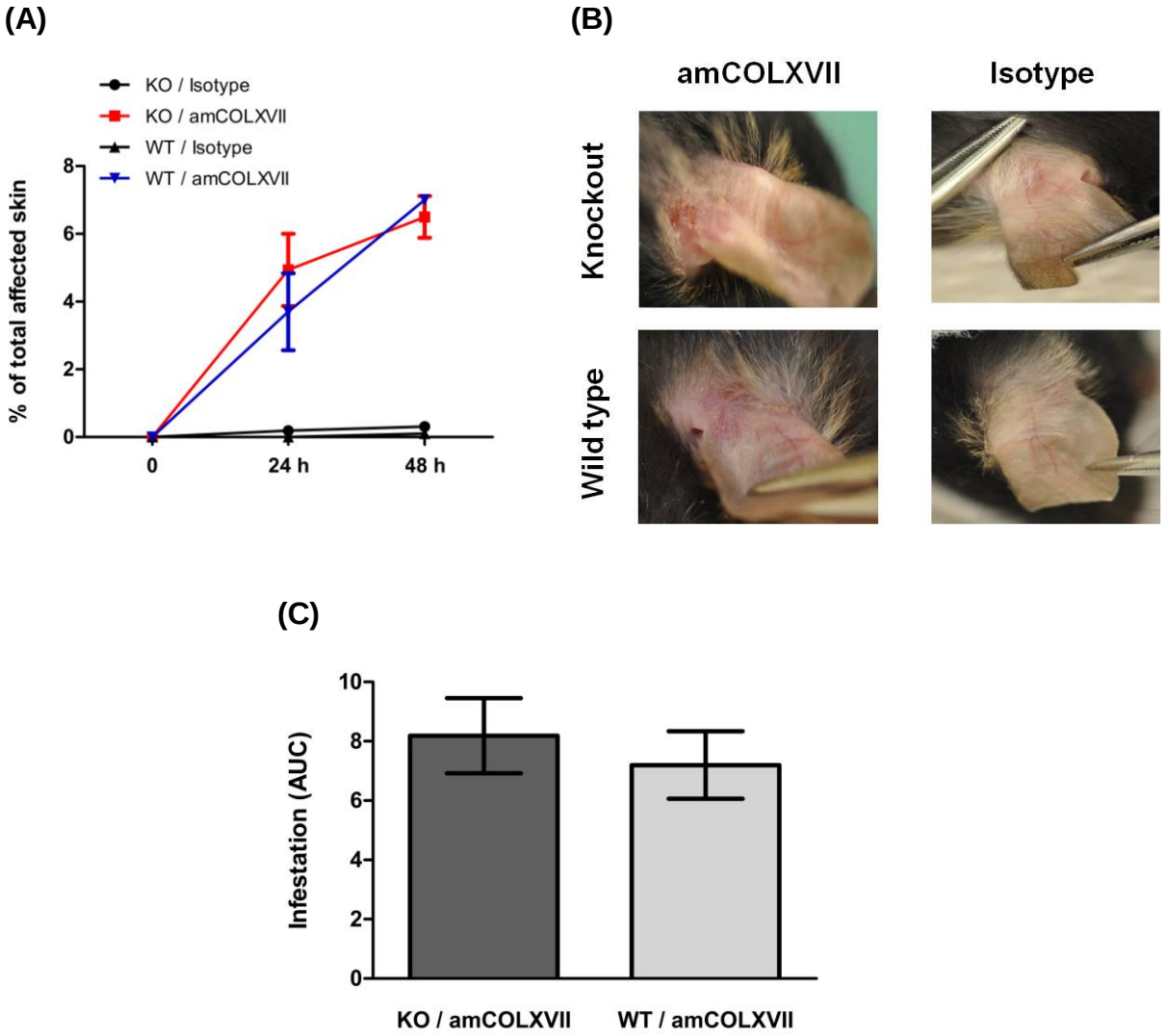

Figure 16 Experimental local antibody transfer model of BP in *Mrp-14*-deficient mice and corresponding wild types. *Mrp-14*-deficient mice as well as wildtype animals received 2 mg amCOLVII IgG into the right ears and 2 mg isotype antibody into the left ear which a representative inflammatory symptoms and lesions were found on the skin with scabs, redness, and peeling of the epidermis. Ears were examined 24 (day 1) and 48 h (day 2) for skin lesions. The disease development was represented as the percentage of the affected skin on the body surface over the entire observation period. **(A)** The percentage of the disease infestation on the ear surface was represented. **(B)** On the last day of the experiment (day 2), the phenotype of the mice was photographically documented and representative images of each group were mapped. **(C)** Data of disease activities derived from mice which had received pathogenic antibodied were integrated and presented as area under the curve (AUC). The data represent two independent experiments with 26 mice (13 and 5 mice for pathogenic and isotype IgG-injected group, respectively) in each experiment. amCOL: anti-murine collagen, KO: knockout, WT: wild type.

3.3.3. Histological analysis of mice with MRP-14 protein deficiency in experimental EBA and BP

Although the investigation of the *Mrp-14*-deficient mouse strain at the level of clinical symptoms did not revealed differences between knokout and wild types in experimental EBA or BP, differences may occure within the inflamed tissue. Therefore, IgG binding, complement deposition and tissue inflammation was analyzed by histology.

From the experiments described in 3.1.1 and 3.1.3, skin samples of the mice were taken on day 16 for frozen sections. By using immunofluorescence staining, deposition of the injected amCOLVII IgG as well as deposition of complement C3 in the experiment was detected. Appropriate controls of the fluorescent staining, i.e. negative control (uncolored), isotype control (replacement of the primary antibody by IgG of the same isotype), and secondary antibody control (no primary antibody staining) were used and showed no unspecific fluorescence signal (data not shown). Binding of the amCOLVII IgG and complement C3 could be detected in skin samples of both knockout and wild type controls treated with amCOLVII IgG (Fig. 17A). Both proteins were located in close proximity to each other in the DEJ. As expected, no deposit of rabbit IgG or complement C3 could be observed in the samples from mice treated with the isotype control (Fig. 17A). In consistent with the observation in experimental EBA, IgG and C3 deposition were observed in both knockout and wildtypes controls treated with amCOL17 IgG but not in the mice treated with control antibodies (Fig. 17B).

In addition, changes in the tissue sections were examined by using H&E Staining. All animals treated with pathogenic amCOLVII IgG showed inflammation of the skin by infiltration of inflammatory cells in the dermis, thickening of the epidermis, and blister formation (Figure 19). Moreover, blister formation seen as splitting of the epidermis from the dermis could be observed. Animals treated with irrelevant rabbit IgG had no cell infiltration as well as having a thin epidermis without blistering. In both model of EBA and BP, no difference between *Mrp-14*$^{-/-}$ and wild type mice could be observed with regard to their clinical or histological phenotype.

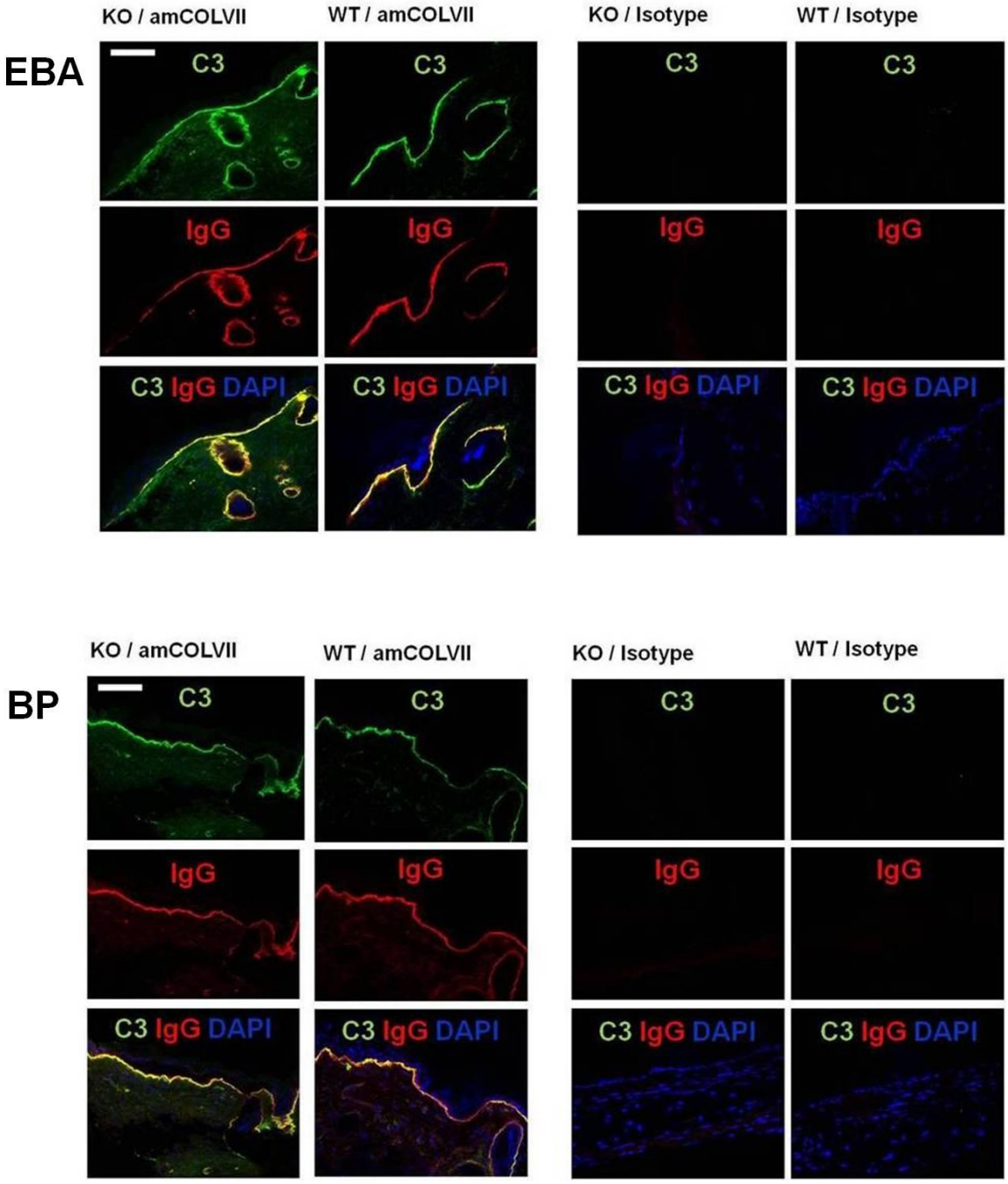

Figure 17 Deposition of rabbit IgG and complement C3 in *Mrp-14*-deficient mice and corresponding wild types. Cryosections of skin samples from knockout mice and the corresponding wild type controls were derived from the experiment described in section 3.1.1. Deposition of rabbit IgG (top panel) and the complement factor C3 (middle panel) was assessed by immunofluorescece staining and colocalization of both proteins was shown the overlay (lower panel) in EBA and BP. Skin samples of mice treated with pathogenic antibody are shown on the left side and animals treated with irrelevant rabbit IgG of the same isotype in the right side. Data of one representative experiment out of three is shown. Scale bar: 50 µm.

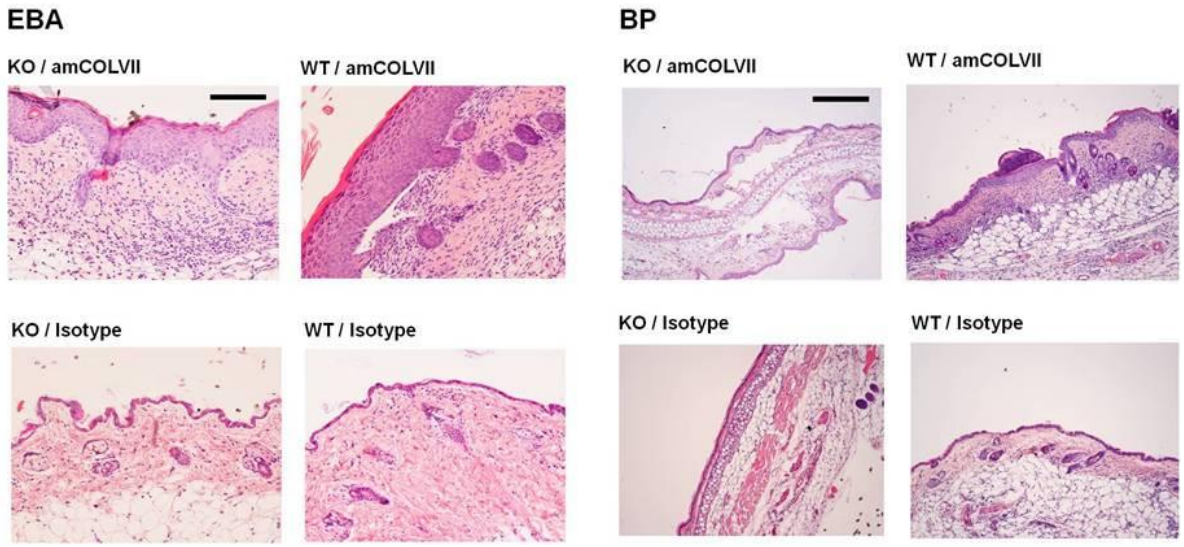

Figure 18 Histology of the skin of *Mrp-14*$^{-/-}$ and control mice in EBA and BP mouse models. Paraffin sections of skin samples from *Mrp-14*$^{-/-}$ mice and the corresponding wild type controls from the experiment described in sections 3.1.1 and 3.1.3. Skin inflammation in experimental EBA and BP in *Mrp-14*$^{-/-}$ and wild type mice. Infiltration of inflammatory cells and dermal-epidermal separation was determined at day 16 (EBA) or day 2 (BP) in sections of skin with H&E staining. *Mrp-14*$^{-/-}$ and wild type controls do not differ in the histopathology of both disease model. Data of one representative experiment out of three is shown. Scale bar: 100 µm.

In summary, the results of this study clearly show that expression of MRP-8/-14 is elevated in both human and experimental AIBD. However, although a significant increase in MRP-8/-14 expression in lesional skin of mice with experimental EBA and BP could be observed, the lacking difference in clinical symptoms as well as in histopathology between wild type controls and MRP-14$^{-/-}$ mice indicate that MRP-8/-14 proteins do not contributed in the development of these diseases. Therefore, it has to be concluded that MRP-8/-14 are upregulated but not functionally involved in the pathogenesis of experimental AIBD.

3.4. Imaging of neutrophil elastase enzyme activity in the effector phase of AIBD

As evident from the results of the previous part of this study, MRP-8/-14 proteins appear to be not functionally involved in the pathogenesis of experimental AIBD during the effector phase of the disease. As a consequence, a direct or indirect regulation of neutrophil effector mechanisms like the release of elastase by these proteins in EBA and BP models can not be expected and will not further be investigated here. Regardless to the role of MRPs, the determination of where and how neutrophils are activated as well as where and when neutrophil proteases mediate tissue damage in autoimmune inflammation represents a hallmark in the understanding of the pathogenesis of AIBD. Although the significant pathogenic role of neutrophil elastase in experimental AIBD has been clearly investigated, so far the role of this enzyme in disease has been shown only indirectly, either by determination of protease activity in cell extracts and supernatants, by inhibitor studies, or by histological localization of the protein in the diseased tissue. For better understanding of the pathophysiological mechanism of neutrophil elastase in disease, a direct approach allowing their quantification and localization of the enzyme activity at its site of action *in vitro* and *in vivo* is required. Therefore in this part, a method was established by using NE FRET reporter NEmo-2 to visualize NE activity on Jurkat T cells, human and murine neutrophils *in vitro* as well as in experimental EBA *in vivo*.

3.4.1. Human blood and murine BM-derived neutrophils

To analyze the activity of neutrophil elastase, highly purified neutrophils isolated from humans and mice were required. While human neutrophils could be isolated in sufficient amounts from peripheral blood, adequate numbers of murine cells could be isolated only from the bone marrow. Since a relevant portion of these BM-cells represent immature neutrophils, BM-cells were isolated and neutrophil precursors were terminally differentiated by culture in presence of G-CSF for 24h. The purity of neutrophils was assessed by analysis in flow cytometry. Samples were labeled with monoclonal antibodies CD16 and Ly-6G to identify the human and murine neutrophilic lineage, respectively. For human neutrophils, there was a clear

population with purity of 91.23% determined using CD16 antibody (Figure 19A). Isolated murine bone marrow derived neutrophils were tested with Ly-6G antibody and a purity of 93.46% was achieved (Figure 19B).

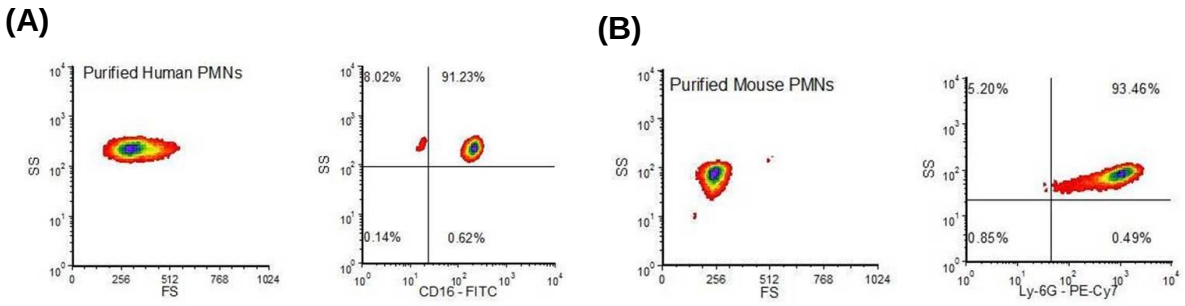

Figure 19 Purity of human and murine neutrophils. Neutrophils were purified from human blood **(A)** or differentiated from murine bone marrow cells **(B)**. Purified neutrophils were analyzed by flow cytometry and their distributions according to their forward scatter (FS) and side scatter (SS) are given (left panels). Neutrophils were identified by their surface expression of CD16 (> 91% purity) or Ly-6G (> 93% purity), respectively (right panels). Results of one representative experiment out of two are shown.

3.4.2. IC-induced neutrophil activation

In AIBD, neutrophils become activated after recruitment into the skin by the immobilized IC leading to the generation of ROS and the release of granule constituents including elastase, all of which have been proven to be essential factors for autoantibody-mediated tissue damage[117,137,139]. It has been shown that neutrophils are not only required but also sufficient to cause the tissue damage[141]. However, to protect the tissue from unwanted damage, in blood serum as well as peripheral tissues high amounts of protease inhibitors as well as oxygen radical scavengers are expressed. For this reasons, it is still unclear how neutrophils can mediate and execute tissue damage in AIBD and other inflammatory diseases. Neutrophil activation proceeds in a sequence of extravasation, directed migration towards the site of inflammation, adhesion, and, finally, execution of potential damaging functions such as the release of ROS and proteases. To investigate how

neutrophil proteases mechanistically mediate tissue damage under physiological conditions, the interdependency between the different steps was investigated by a delineation of the process. In a first approach an *in vitro* model was established, were neutrophils were activated by immobilized immune complexes (IC) and the physiological relevance of cell adherence for the subsequent release of ROS and elastase was analyzed.

Activation of neutrophils was performed by using immobilized IC *in vitro*. Immobilized IC was prepared using recombinant murine COLVII and rabbit amCOLVII IgG. Neutrophils immediately adhered to surfaces coated with immobilized IC as seen by a dramatic change of their morphology while after contact to uncoated surfaces cells remained round shaped (Figure 20A). To get a first hint on the molecules involved in IC-induced adhesion, cells were preincubated with blocking antibodies against CD18, the common β-chain of β2-integrins. These type of integrins have been shown to mediate many inflammatory adhesion processes in neutrophils[254–257]. As expected, inhibition of CD18 by blocking antibodies dramatically reduced the IC-induced morphological changes of neutrophils (Figure 20A) while no such effect was observed in samples which received antibodies of an unrelated isotype control.

These results provide first evidence of a CD18-mediated neutrophil adhesion to immobilized IC. However, to monitor and quantify the cell adhesion in a real time process, neutrophil adhesion on immobilized IC was analyzed by using impedance measurement[226]. In this detection system, increased cell adhesion directly correlates with an increase of the electrical impedance (expressed as cell index) of the cell layer. Confirming the previous microscopical analysis, neutrophil adhesion increased immediately after addition of the cells to the IC-coated wells and reached a peak after 25 min. Thereafter, a continuous decrease was observed and background levels were reached after 150 min (Figure 20B). The cell index of the control neutrophils exposed to uncoated surfaces increased only slightly over the 3 h (Figure 20B) and these results were confirmed after quantification of cell adhesion by integration of the cell indices which are represented as the area under the curve (Figure 20C). As seen in the microscope before, treatment of cells with CD18 resulted in a significant partial inhibition by approximately 50% (Figure 20B, C). A comparable effect was observed when murine neutrophils were used instead of human cells and β2-integrin were

blocked with an anti-murine CD18 antibody, indicating no principal difference between both species with regard to this function (Figure 20D, E).

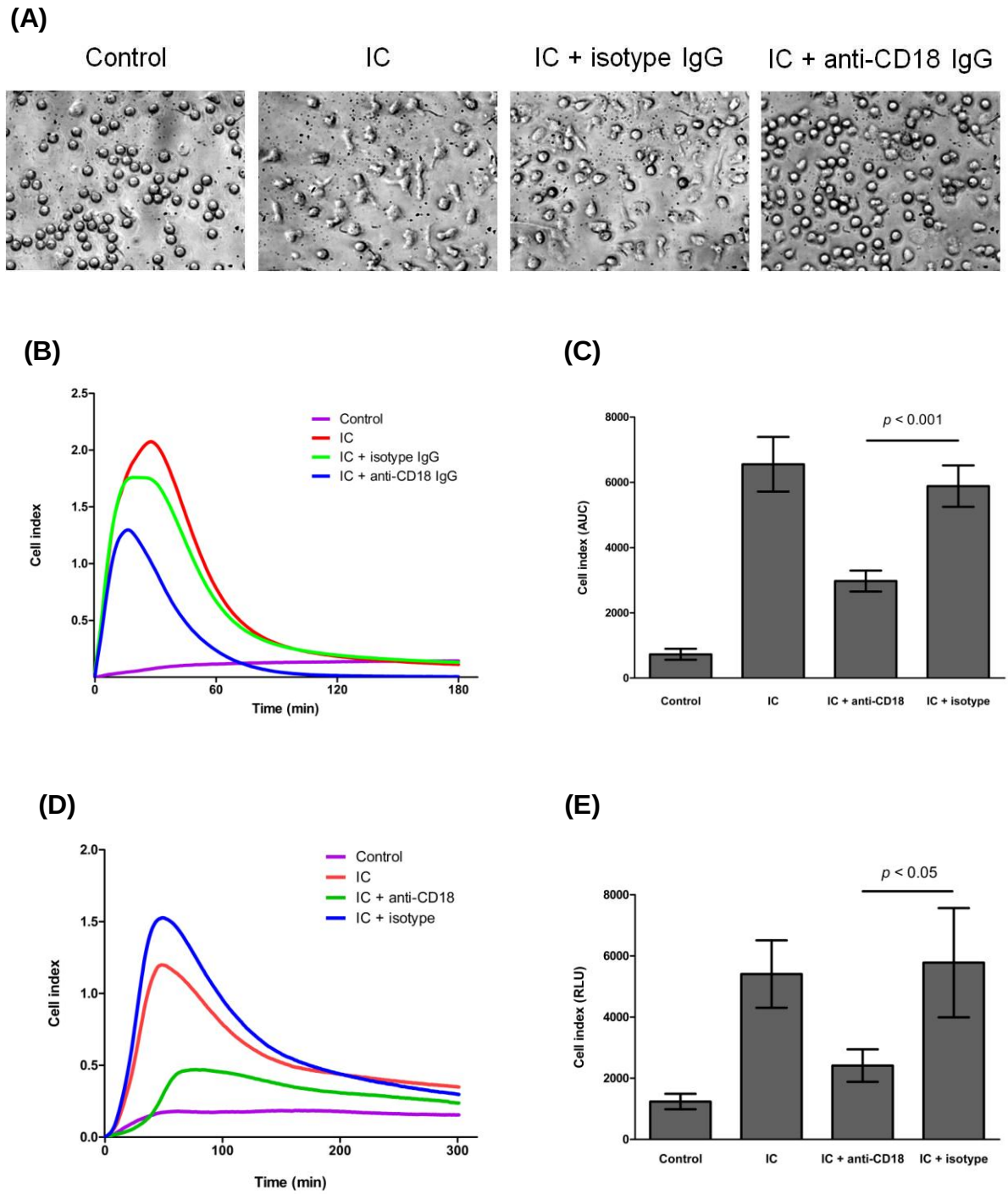

Figure 20 IC-induced neutrophil adhesion. Neutrophils were exposed for 1 to 3 h to immobilized IC or uncoated surfaces (control) alone or in presence of anti-CD18 IgG (IC + anti-CD18 IgG) or isotype control (IC + isotype IgG), respectively. **(A)** Morphology of human neutrophils was

analyzed by phase-contrast microscopy 1 h after the stimulation. **(B)** Adhesion kinetics was determined by real-time impedance measurement for 3 h and **(C)** data were integrated and represented as the area under the curve (AUC). **(D)** For IC-induced adhesion in murine neutrophils, cells were exposed for up to 5 h to the uncoated surfaces (control) or surfaces coated with IC (IC) in the presence of anti-mCD18 IgG (IC + anti-CD18 IgG) or an corresponding isotype control (IC + isotype IgG) and cell adhesion was determined by real-time impedance measurement. **(E)** Adhesion was further quantified by integration of cell indices and represented as AUC. Data of one representative out of 3 experiments is shown. Statistically significant differences between groups treated with IC/anti-CD18 IgG and IC/isotype-treated controls are indicated.

In the next step, the functional impact of IC-induced neutrophil adhesion on further cell functions like degranulation and ROS generation was analyzed. After exposure to IC, neutrophils immediately started to generate ROS which peaked after 10 min and reached background levels after 40-60 min. Noteworthy, this process was not affected by the blockage of CD18 (Figure 21A, B). Furthermore, determination of the elastase enzyme activity in the same supernatants revealed that blocking CD18 did not result in a reduced but slightly enhanced IC-induced liberation of the protease (Figure 21C).

Taken together, these results show that immobilized IC induces a tight neutrophil adhesion which is at least partially dependent on β2-integrins. Furthermore, these data indicate that tissue-damaging neutrophil functions like ROS production and elastase release are clearly independent from CD18-mediated neutrophil adhesion. From these findings, one would conclude that neutrophil-mediated tissue damage should not be affected by modulation of cell adhesion. By contrast, in a most recent study, Xinhua Yu in our group could show in an *ex vivo* model of EBA that blocking adhesion with CD18-antibodies results in a complete abrogation of neutrophil-induced tissue destruction. Vice versa, increasing adhesion of neutrophils by co-stimulation of cells with the chemokine CXCL4 resulted in augmented tissue damage (unpublished results). It becomes clear that the role of neutrophil adhesion in the conflicting findings between elastase release as IC-induced cell function and

observed proteolytic tissue damage cannot be resolved by the classical methods of determination of protease activities in cell free supernatants.

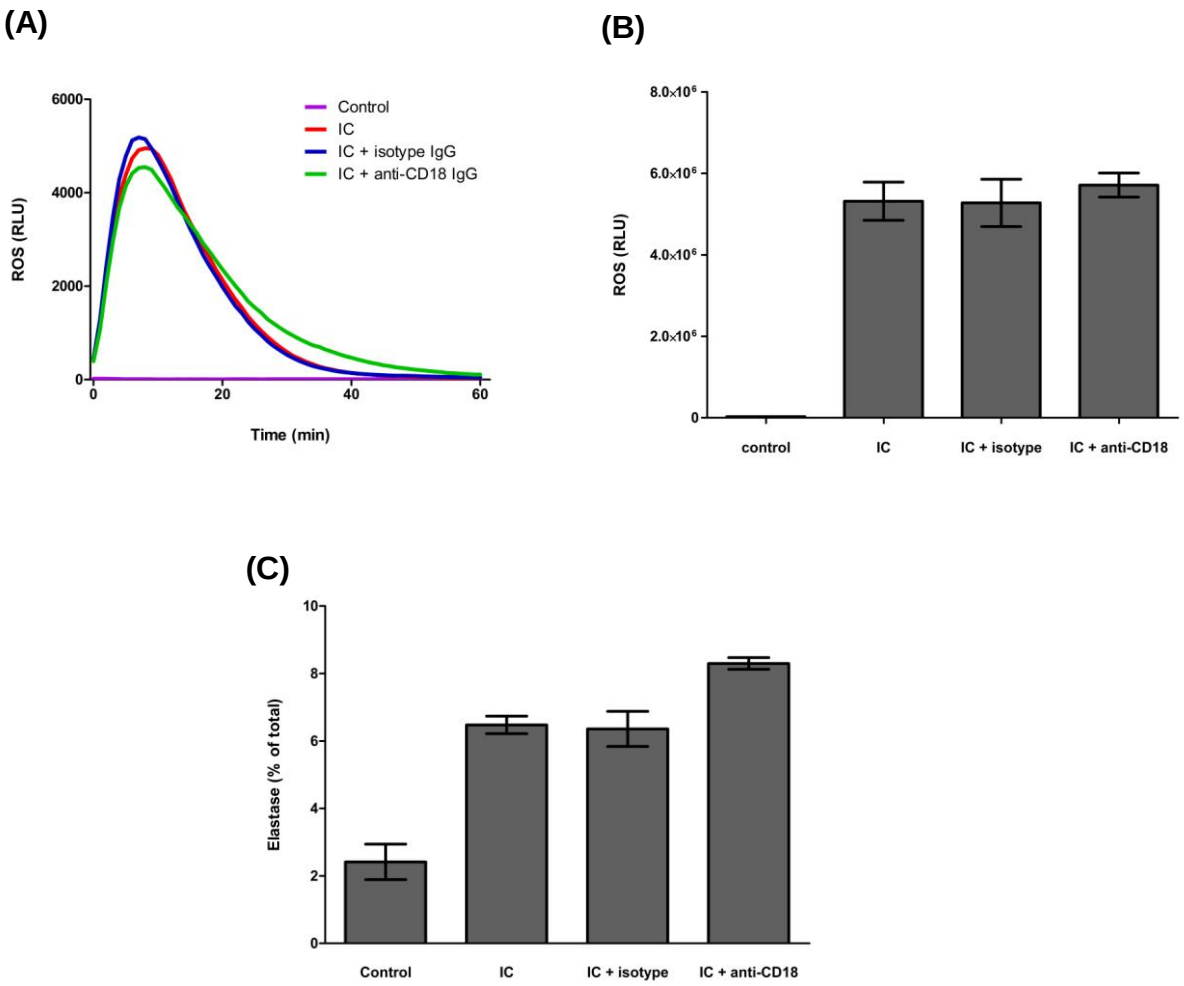

Figure 21 Effect of anti-CD18 antibodies on IC-induced activation. Neutrophils were exposed for 1 h to immobilized IC or uncoated surfaces (control) alone or in presence of anti-CD18 IgG (IC+anti-CD18 IgG) or isotype control (IC+isotype IgG), respectively. ROS production was determined by measurement of chemiluminescence in the presence of luminol in parallel samples for 60 min **(A)** and data were represented as integrals of light intensity determined for 1 h **(B)**. Degranulation was determined by the amount of elastase released into the supernatant and given as percentage of their respective total amount **(C)**. Data are presented as mean ± SEM derived of 3 experiments.

3.4.3. Visualiziation of lipidated FRET-protease reporter NEmo-2 on Jurkat T cells

The analysis of free elastase activity in supernatants provides no information of the local activity of the enzyme in small microenvironments which may be of high physiological relevance. For this reasons, a method for measuring elastase activity in close proximity to cell membranes using the lipidated FRET-based elastase substrate NEmo-2 was established. To analyze the characteristics and the performance of the reporter on cells, NEmo-2 was applied to Jurkat T cells. Since these cells do not express endogenous elastase, they are unable to cleave or modulate the reporter by themselves. Cells were incubated with the reporter for 5 min and subsequently analyzed by confocal microscopy. Coumarin 343 (donor; D) was excited with a 405 nm diode laser and emission was sampled between 470-510 nm. Sensitized emission of TAMRA (acceptor; A) was sampled between 570-610 nm. Donor fluorescence and sensitized acceptor emission was imaged and D/A ratio images were calculated. Donor emission and sensitized emission of the acceptor were sampled by confocal fluorescence microscopy and D/A-ratio images were calculated using ImageJ software.

The NEmo-2 was found to accumulate exclusively on the cell membrane and no intracellular signal was observed (Figure 22A, video 1A-C). For the intact reporter the D/A-ratio was low. In the next step, cleavage of the cell-bound reporter was induced by addition of exogenous neutrophil elastase. While the D/A ratio remained unchanged in control samples without NE, addition of NE resulted in a time-dependent increase of the D/A-ratio (Figure 22B, video 1D-F), indicating an effective proteolytical cleavage of the reporter. Normalization of the D/A-ratio to the starting value resulted in 3-fold increase (Figure 22C). The condition was reproduced using at least three cells and normalization of the mean of D/A-ratio to the starting value resulted in more than 2-fold increase (Figure 22D).

Of note, the TAMRA signal disappeared after cleavage, indicating that the TAMRA bearing fragment was lost from the cell-surface. TAMRA did not get internalized, since no intracellular signal was observed. Interestingly, the Coumarin 343 bearing lipidated part was not internalized, but stayed at the cell membrane. Nevertheless, all changes were applied as the D/A ratio.

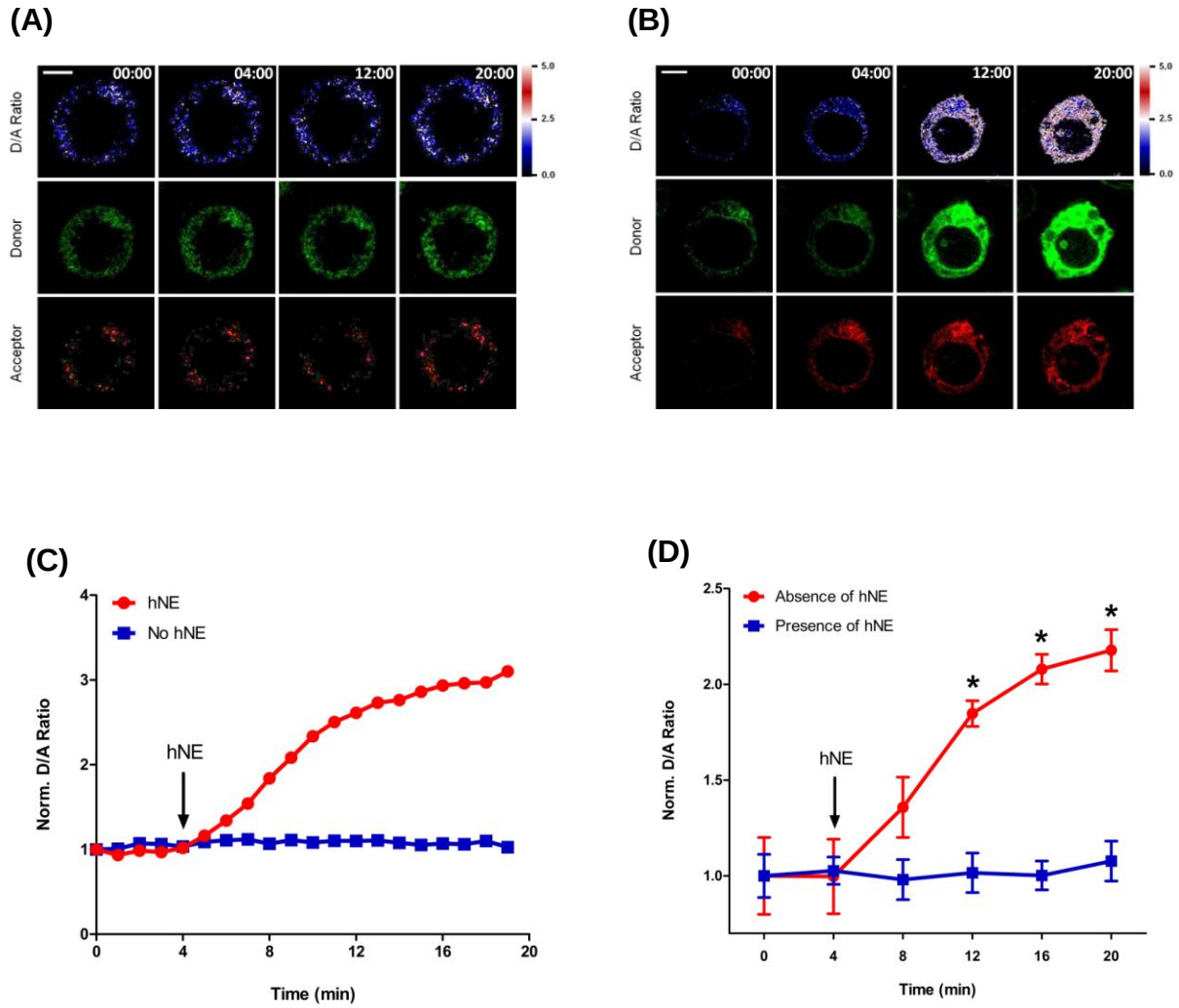

Figure 22 Elastase-mediated cleavage of NEmo-2 FRET reporter on Jurkat T cells. Jurkat T cells were incubated with the reporter for 5 min and bound reporter was determined by confocal microscopy. NEmo-2 localized exclusively on the cell membrane. Donor fluorescence and sensitized acceptor emission was imaged and D/A ratio images were calculated. NE was added after 4 min of incubation. **(A, B)** Representative confocal images of donor (D) and acceptor (A) fluorescence intensities and the corresponding D/A ratios are shown. Look up table (LUT): blue = low D/A ratio, intact NEmo-2; red = high D/A ratio, indicative for cleaved NEmo-2. Scale bar: 5 µm. **(C)** D/A ratios were normalized to the starting value and plotted over time. After addition of exogenous NE (min 4), a strong increase in the D/A emission ratio (3-fold) was observed. **(D)** D/A-ratio normalized to the starting value for at least three cells resulted in more than 2-fold increase. Asterisks indicate statistically significant differences ($p < 0.05$).

3.4.4. Determination of the FRET efficiency by acceptor photobleaching

The FRET effect is based on a transmission of a part of the emission energy of the donor to the acceptor fluorophore resulting in reduction of the donor signal. The best straight forward approach to prove that an observed FRET signal reflects a true interaction between two molecules is to use direct acceptor photobleaching to remove (photo-inactivate) the acceptor, thus frustrating the occurrence of FRET and monitor the reappearance of the donor fluorescence[258–260]. To confirm an operational FRET process for the NEmo-2 reporter, the acceptor fluorophore was bleached on Jurkat T cells which do not express NE. Acceptor photobleaching was performed by elimination the acceptor fluorophore with a high energy laser pulse at the excitation maximum of the acceptor. As a consequence, intensity of donor fluorophore will increase and can be measured quantitatively. This procedure was carried out before and after addition of hNE. In the absence of hNE, acceptor photobleaching results in enhancement of fluorescent signal of the donor in Jurkat cells and as a consequence, the emission ratio of post-bleach donor/pre-bleach donor was highly increased (Figure 23A). Therefore, bleaching of the acceptor in the intact reporter resulted in an increasing donor and decreasing acceptor fluorescence intensity and consequently, the D/A ratio increased (Figure 23A). However, such an increase was not observed when the reporter was enzymatically degraded by the addition of hNE prior to the bleaching process (Figure 23B). While the method is quantitative, the efficiency was calculated for the Jurkat cells and fluorescence intensity of donor, acceptor, and respective efficiency was shown (Figure 23C). In absence of hNE, the efficiency of acceptor photobleaching was ~37% which in presence of hNE, it was reduced to ~9% (Figure 23C). This result shows directly the presence of an operational FRET energy transfer between the molecules of the fluorophores on the cell membrane of Jurkat T cells.

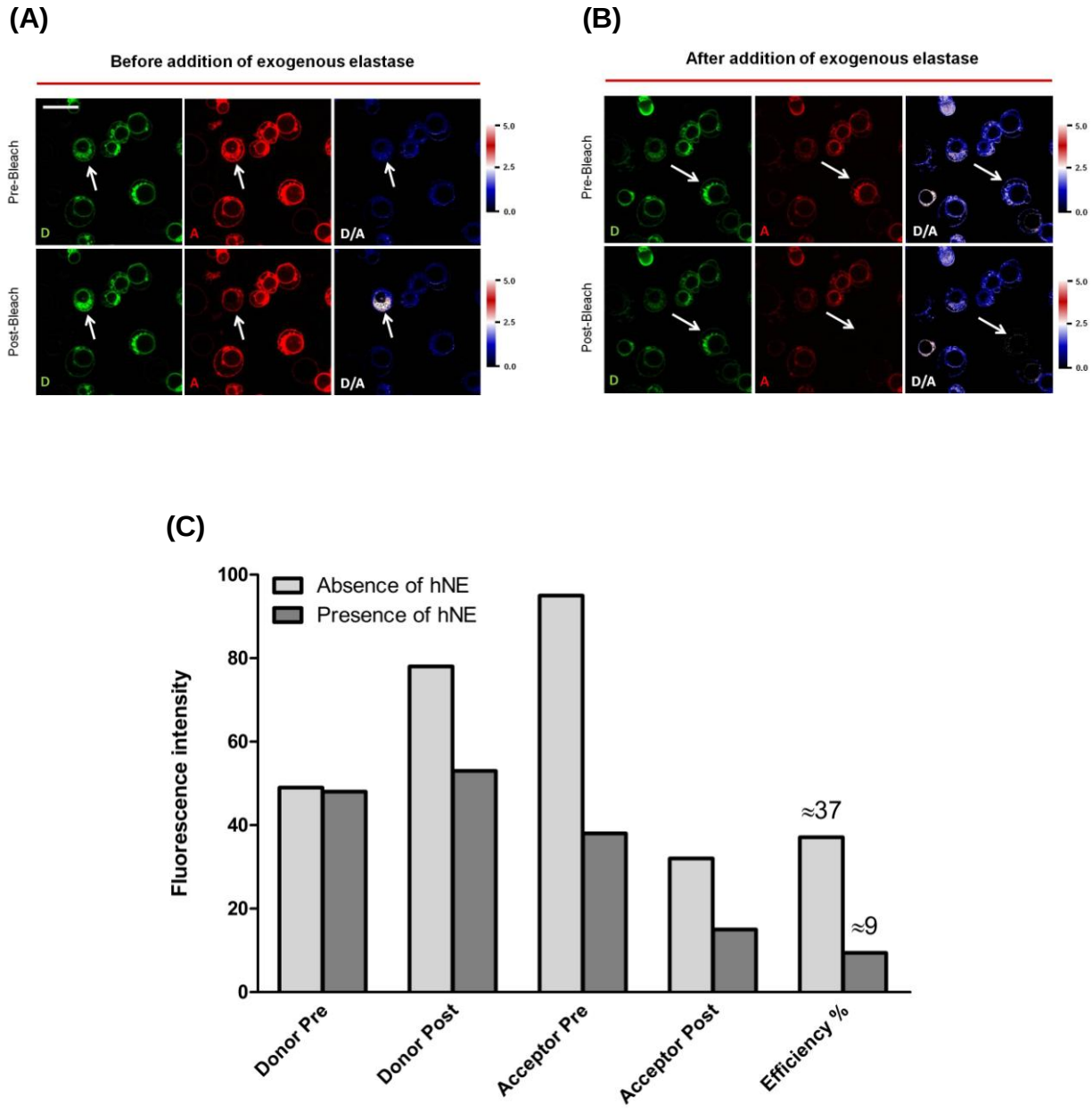

Figure 23 Analysis of operational FRET phenomenon by acceptor bleaching on Jurkat T cells. Coumarin 343 (donor; D) was excited with a 405 nm diode laser and emission was sampled between 470-510 nm. Sensitized emission of TAMRA (acceptor; A) was sampled between 570-610 nm. Donor fluorescence and sensitized acceptor emission was imaged and D/A ratio images were shown **(A)** in absence of hNE or **(B)** in presence of hNE. Photobleaching was carried out on a half of a single cell, indicated by an arrow. LUT: blue = low D/A ratio, intact NEmo-2; red = high D/A ratio, indicative of cleaved NEmo-2. Scale bar: 20 µm. **(C)** Acceptor photobleaching was quantified for Jurkat T cells. Donor and acceptor fluorescence intensities as well as FRET efficiency were calculated in the absence or presence of hNE.

3.4.5. Binding and stability of NEmo-2 on neutrophils

After having shown the stable membrane-binding of NEmo-2 to Jurkat cells, in the next step the interaction of the reporter with neutrophils was analyzed. In a first approach murine and human neutrophils were incubated with NEmo-2 and cells were analyzed by fluorescence microscopy. Surprisingly, the reporter was cleaved on the neutrophil membrane even in absence of any exogenous elastase (Figure 24A, B left panel). Therefore, no difference was observed after addition of exogenous hNE (Figure 24A, B middle panel). Since during cell culture always a low amount of dead or dying cells occur, this effect could be caused by elastase derived from leaking cells leading to unwanted reporter cleavage. To overcome this problem, neutrophils were incubated with the protease inhibitor A1AT. This macromolecular inhibitor is membrane-impermeable and, thus, selectively blocks the extracellular pool of NE. In presence of A1AT, no spontaneous FRET loss was observed indicating that cleavage of NEmo-2 was efficiently prevented (Figure 24A, B right panel). Under these conditions, donor as well as acceptor fluorescence remained stable as evident from spectral analysis (Figure 24C).

Taken together, this set of experiments showed that NEmo-2 binds to Jurkat T cells as well as murine neutrophils and reporter cleavage by elastase can be detected by a loss of FRET. Furthermore, neutrophil-derived elastase is able to cleave NEmo-2 enabeling the detection of this enzyme activity on single cell level.

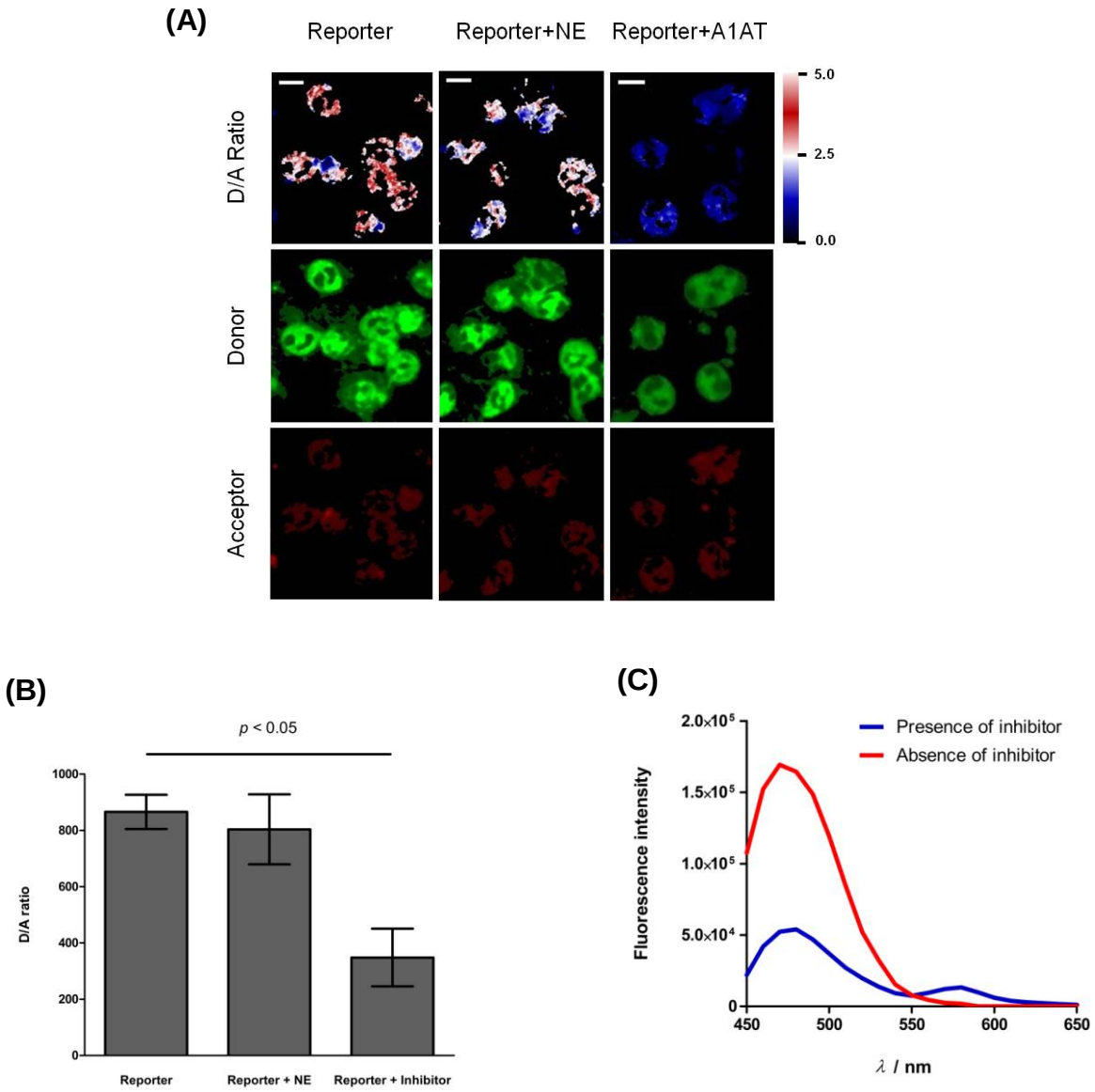

Figure 24 Determination of NE activity on murine BM neutrophils. Neutrophils from wild type mice were incubated with NEmo-2 in the presence or absence of inhibitor (A1AT). HNE was added to neutrophils to achieve maximal reporter cleavage. **(A)** Donor fluorescence and sensitized acceptor emission were imaged and D/A ratio images were calculated. NEmo-2 was rapidly cleaved on neutrophils in the absence of A1AT but no cleavage was found in the presence of A1AT. LUT: blue = low D/A ratio, intact NEmo-2; red = high D/A ratio, indicative of cleaved NEmo-2. Scale bar, 10 µm. **(B)** D/A ratios showed a ~4-fold increase in the absence of inhibitor over the presence of A1AT. Data of one representative experiment with >5 cells per group is shown. **(C)** Change in fluorescence emission spectrum of NEmo-2. Neutrophils were analyzed in presence or absence of inhibitor and the emission spectra between 450 and 650 nm were recorded. Enzymatic cleavage of the probe leads to strong increase in donor fluorescence and a decrease in acceptor fluorescence in absence of inhibitor.

3.4.6. Elastase activity in adherent neutrophils

The establishment of a method which enables the detection of elastase enzyme activity in close proximity to the cell membrane provides a new tool for tackling the question how cell adhesion can modulate tissue damage without affecting elastase release or ROS production (section 3.4.2). To prevent damage from the host, the potentially harmful proteinases such as neutrophil elastase are under tight control of various proteinase inhibitors such as A1AT which are ubiquitous presented in vasculature and surrounding tissues. Although neutrophil elastase has been shown to be the key proteinase excuting tissue damage in the experimental EBA, it is unclear how this enzyme executes its proteolytical function in the presence of inhibitor molecules. To clarify this, elastase activity was determined on neutrophils on single cell level by using NEmo-2. To mimic the situation *in vivo* where proteinase inhibitor are present in the local inflamed tissue, the protease activity was evaluated in neutrophils in an *in vitro* experimental setting where neutrophils were activated by immobilized IC in presence of A1AT. Neutrophils firmly attached to the surface with immobilized IC but not to the control surface coated with irrelevant IgG. Surprisingly, although A1AT was present, cleavage of Nemo-2 was observed on the surface of neutrophils stimulated with IC, which became visible after 5 min and significant after 10 min of incubation as compared to the controls (Figure 25A, video 2A-F). As expected, no change of the D/A ratio and, therefore, no elastase activity was detectable under the latter conditions (Figure 25B). Based on these observations, it can be hypothesized that the IC-induced neutrophil adhesion creates a closed space between cell and surface where macromolecular inhibitors have no or limited access to and in which the released elastase can accumulate in an active state.

Since the CD18 blockage could specifically inhibit the IC-induced neutrophil adhesion, it provides a tool to investigate the role of adhesion in elastase activity using this FRET-based *in vitro* experiment. In accordance to the data presented in Figure 26, cleavage of Nemo-2 was observed on neutrophils attached to IC-coated surfaces but not to surfaces with unrelated antibodies (Figure 26A). However, elastase enzyme activity was significantly reduced on neutrophils which attached to IC in the presence of adhesion-blocking antibodies directed against CD18. These findings were confirmed by quantitative analysis of the D/A ratios of several cells under the same conditions after normalization to the starting value and plotting over time. Normalization of the D/A-ratio to the starting value for IC-situmulated

neutrophils in the presence of CD18 antibody resulted in an increase of 1.2-fold which is lower than D/A ratio for those in absence of CD18 antibody (Figure 26B).

In summary, these results show for the first time that IC-activated adherent neutrophils secrete enzymatically active elastase in close proximity of their cell membrane which is resistant to blockade by macromolecular proteinase inhibitors. Since blocking of adhesion led to a complete abrogation of this effect, it is likely that cell adhesion protects proteases from an access of inhibitors.

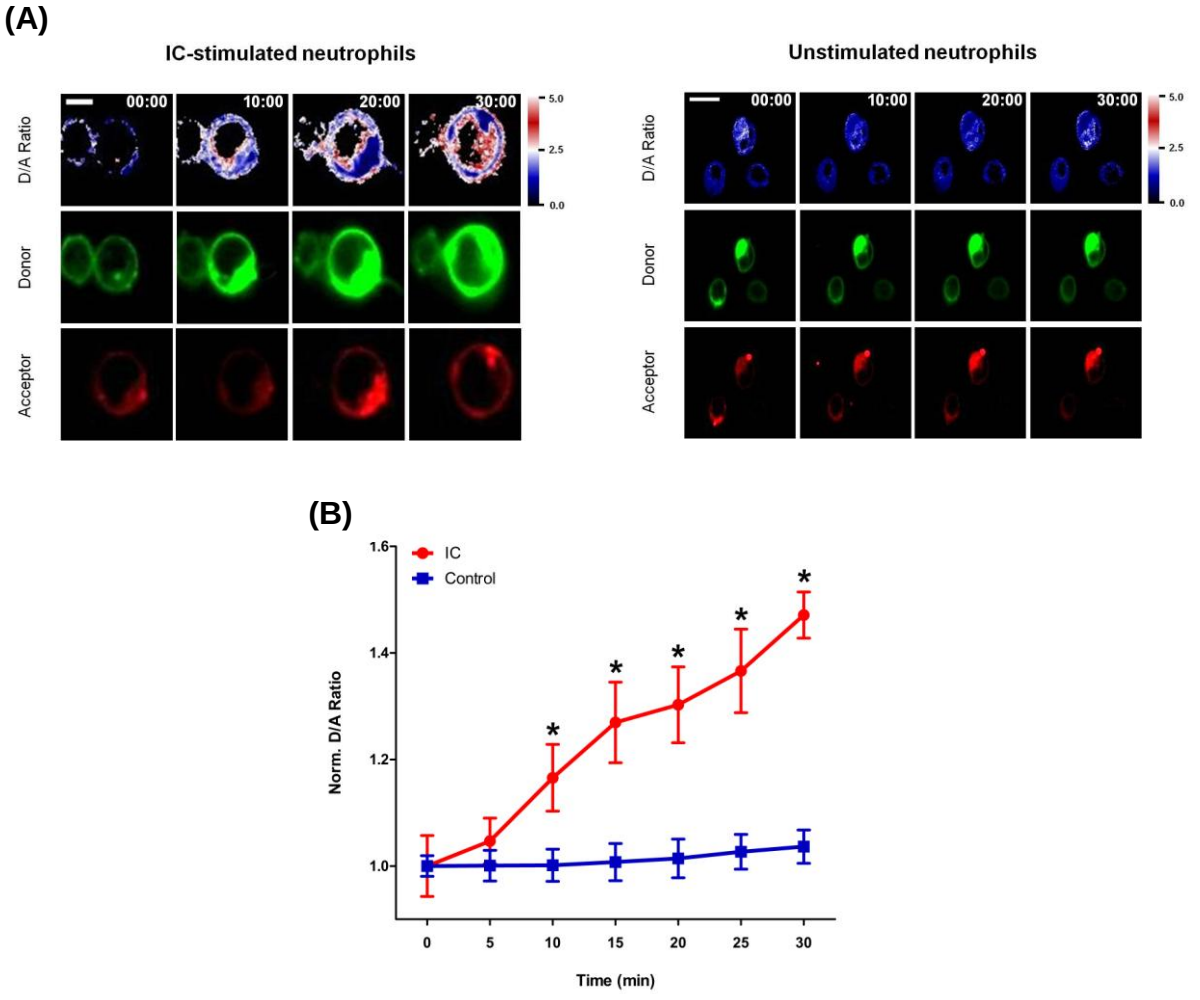

Figure 25 Elastase enzyme activities on IC-activated neutrophils in presence of protease inhibitors. Neutrophils were preincubated with NEmo-2 in presence of A1AT and allowed to adhere to immobilized IC or irrelevant antibodies of the same isotype. Cells were analyzed by confocal microscopy and fluorescence intensities of the donor and acceptor as well as the ratio of the intensities of D/A are shown. **(A)** Cells were able to spread on immobilized IC (but not unrelated antibodies) and as a consequence, cleavage of reporter was observed even in the presence of inhibitors which became visible after 5 min and significant after 10 min of incubation as compared to

the controls. LUT: blue = low D/A ratio, intact NEmo-2; red = high D/A ratio, indicative of cleaved NEmo-2. Scale bars: 5 µm for IC-stimulated and 20 µm for unstimulated neutrophils. **(B)** D/A ratios were normalized to the starting value and plotted over time. Data of three independent experiments were quantified and compared among these groups. Data are presented as mean ± SEM. Statically significant differences were indicated by asterics (*p<0.05).

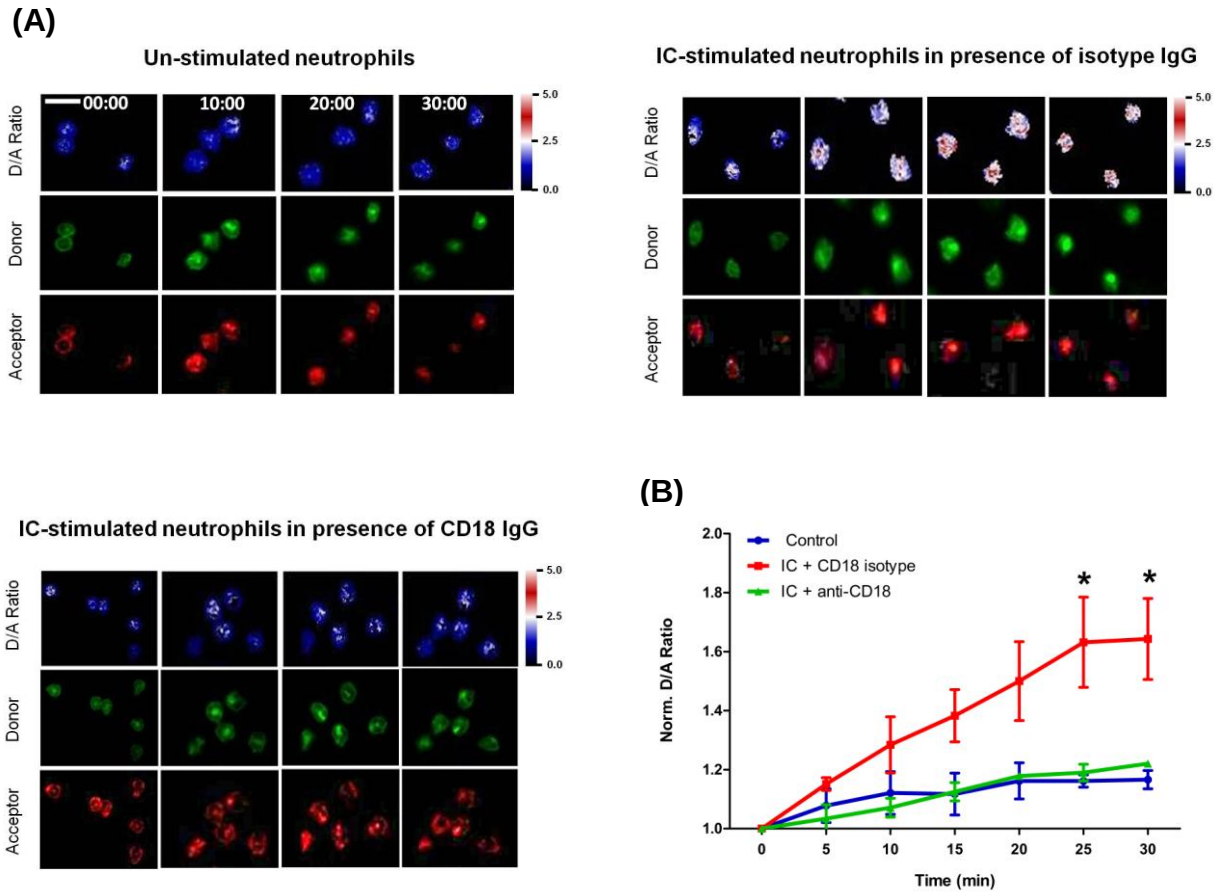

Figure 26 Effect of CD18-antibodies on elastase activities of IC-activated neutrophils. (A) Neutrophils were loaded with the elastase FRET probe NEmo-2 in presence of A1AT and subsequently exposed to uncoated surfaces (upper left panel), to immobilized IC in presence of unrelated IgG (upper right panel), or IC in presence of anti-CD18 antibodies (lower left panel) and cells were analyzed by confocal microscopy. Fluorescence intensities of the donor and acceptor as well as the ratio of the intensities of D/A are shown.Representative data drived from three independent experiments are shown. LUT: blue = low D/A ratio, intact NEmo-2; red = high D/A ratio, indicative of cleaved NEmo-2. Scale bar: 20 µm. **(B)** Donor and sensitized acceptor emission was collected for different time points and normalized D/A ratio images were calculated. Data of three independent experiments were quantified and compared among these groups. Data are presented as mean ± SEM. Statically significant differences were indicated by asterics (*p<0.05).

3.5. Monitoring neutrophil elastase activity *in vivo*

NE has been implicated in the pathogenesis of several key pathologies of AIBDs[149,261,262]. Results from the section above provide a reasonable model how neutrophils could exert a proteolytical damage even in the presence of high concentrations of proteinase inhibitors. However, the situation *in vivo* differs substantially from the rather linear and defined conditions of the *in vitro* experiment. In the living organism, neutrophils are exposed not only to a single stimulus like immobilized IC but to a variety of different activators and inhibitors which may vary during different phases of the inflammatory process. Furthermore, inflammation appears as a highly dynamic process where neutrophil migration, adhesion, detachment, and degranulation may occur in several repeated sequences. Therefore, the determination of elastase activity under conditions *in vivo* appears to be mandatory to prove the relevance of this model. Elastase protein has been detected in intact tissues so far only by immunohistology which provides no information of the activity status of the enzyme. Alternatively, the determination of protease activity in tissue extracts leads to the loss of the spatial information. Consequently, in the next series of experiments the application of FRET reporters for the analysis of elastase activity by MPM *in vivo* was performed.

3.5.1. FRET reporter performance on Jurkat and neutrophil cells *in vitro* by MPM

In a first approach, settings on the multi-photon microscope were established, which allow the detection of intact and processed reporter as shown previously for confocal microscopy (section 3.4.3 and 3.4.5). Therefore, both Jurkat cells and neutrophils were incubated with the reporter and donor (D) fluorescent emission and the sensitized emission of the acceptor (A) was imaged by MPM. For neutrophils, the inhibitor A1AT was used to prevent unwanted cleavage of the reporter. NEmo-2 was exited with 920 nm. Emitted light was detected by 4 wavelength separated PMTs (<435 nm, 453-495 nm, 495-560-560 nm and >560 nm). NEmo-2 was rapidly cleaved in the presence of exogenous elastase on Jurkat cells (Figure 27A) and by activation of neutrophils by immobilized IC (Figure 27B). Therefore, results obtained previously by confocal microscopy could be directly reproduced by using the MPM.

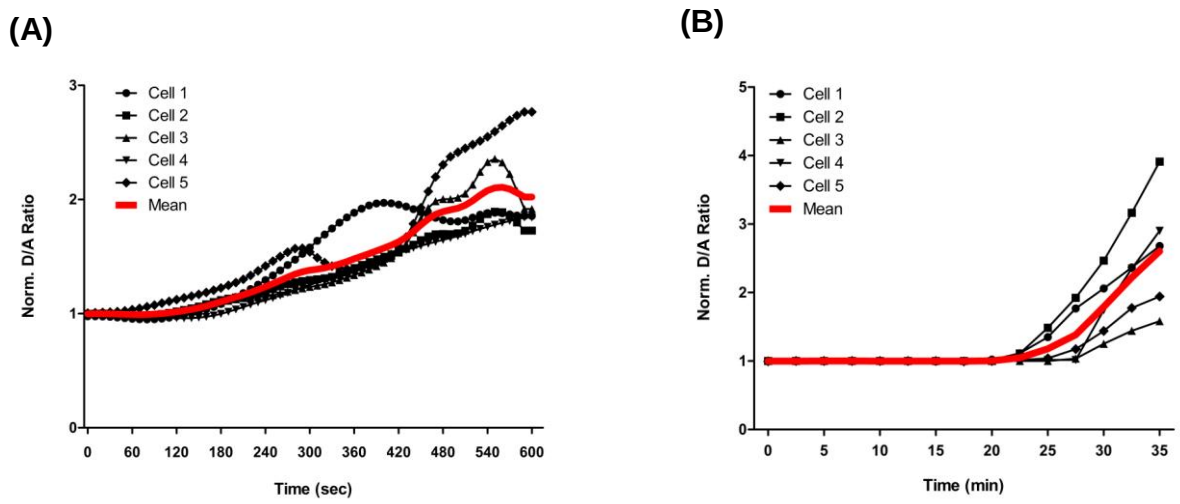

Figure 27 Performance of NEmo-2 reporter on Jurkat cells and neutrophils by using 2-photon microscopy. To study NEmo-2 performance in the context of a living cell-based model by 2-photon microscopy, Jurkat T cells and neutrophils were incubated with the reporter. Donor fluorescence and sensitized acceptor emission was imaged and D/A ratio images were calculated. D/A ratios were normalized to the starting value and plotted over time. After addition of exogenous NE (min 4) in the case of Jurkat cells **(A)** and activation of neutrophils by IC **(B)**, a strong increase in the D/A emission ratio was observed.

3.5.2. Monitoring of neutrophil responses to tissue damage

To analyze elastase activity *in vivo,* a local model of EBA was established in mice by application of a single dose of amCOLVII IgG into the ventral side of the ear. In this model, neutrophils were raised and labeled *in vitro* and subsequently adoptively transferred in to the inflamed ear.

However, as a prerequisite to this technique, infiltration of neutrophils and their migration towards the pathogenic antibody have to be documented in inflamed tissue. To examine the migration and influx of neutrophils following binding of pathogenic antibodies to their antigens *in vivo*, experimental EBA was induced locally by application of anti-mCOLVII IgG labeled with DyLight 649 intradermally into the ear of *lys-eGFP* mice. In these mice, *eGFP* gene is inserted into lysozyme M (*lys*)

locus which is expressed specifically in myelomonoytic cells[263,264]. Consequently, eGFP is present specifically in the myelomonocytic lineage with the strongest expression in mature neutrophils, while cells from other lineages remain non-labeled[211]. Recruitment of GFP-labeled neutrophils to the site of damage was investigated 24h after antibody injection in inflamed ear. Green neutrophils could be observed in high numbers in regions where the red-labeled pathogenic antibodies were present (Figure 28A, video 3A). A virtual side view based on the combining of several stacked images confirmed these data and indicated the presence of neutrophils in close proximity to the antibodies (Figure 28B, video 3B). These results show that the intrinsic neutrophils migrate to the area of tissue damage which antibody is present.

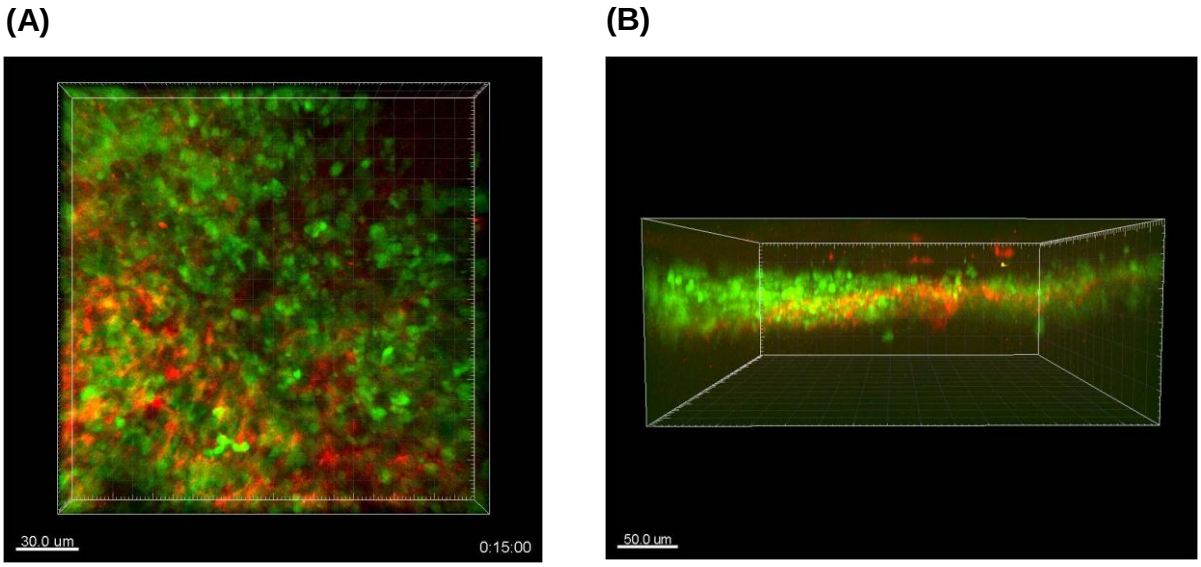

Figure 28 Migration of intrinsic neutrophils to the site of pathogenic antibodies. Local antibody transfer model of EBA was induced by a single dose injection of anti-mCOLVII labeled with DyLight 649 intradermally into the ventral ear skin of *lys-eGFP* mice. Neutrophil migration towards pathogenic antibody was monitored by two-photon microscopy. Results indicate the recruitment of neutrophils in close proximity of the antibody. Top image **(A)** as well as a side view generated by stack analysis demonstrates the close proximity of neutrophils to the pathogenic IgG **(B)**. EGFP appears as green color while deposition of anti-mCOLVII is shown in red. Results of one experiment are shown.

In the next step, the functional integrity of adoptively transferred neutrophils was monitored by their capacity to move within the tissue. To identify exogeneous neutrophils and to examine their cellular dynamics, neutrophils were first labeled by cell tracker component and injected into the ventral side of the mouse ear. To induce migration of these cells, an inducible model of sterile skin injury was used in which a brief intense two-photon laser pulse causes focal, dermis-restricted tissue damage. Focal tissue damage was set 2 h after injection of neutrophils and cell migration was imaged by MPM. Focal injury induced a first neutrophil migration into the area of tissue damage after 5 min and cells accumulated as an increasing cluster at the damage site that lasted more than 30 min (Figure 29A, video 4A). Track analysis was performed to provide a clear state of neutrophils as well as their direction toward the tissue damage (Figure 29B, video 4B, C). Red dots represent neutrophils and lines show the direction of these cells from the early step to the final area by shifting their colors from blue to red, respectively. These data indicate that the injected neutrophils respond adequately to a damage signal and that quality and numbers of cells are suitable for the further experiments.

(A)

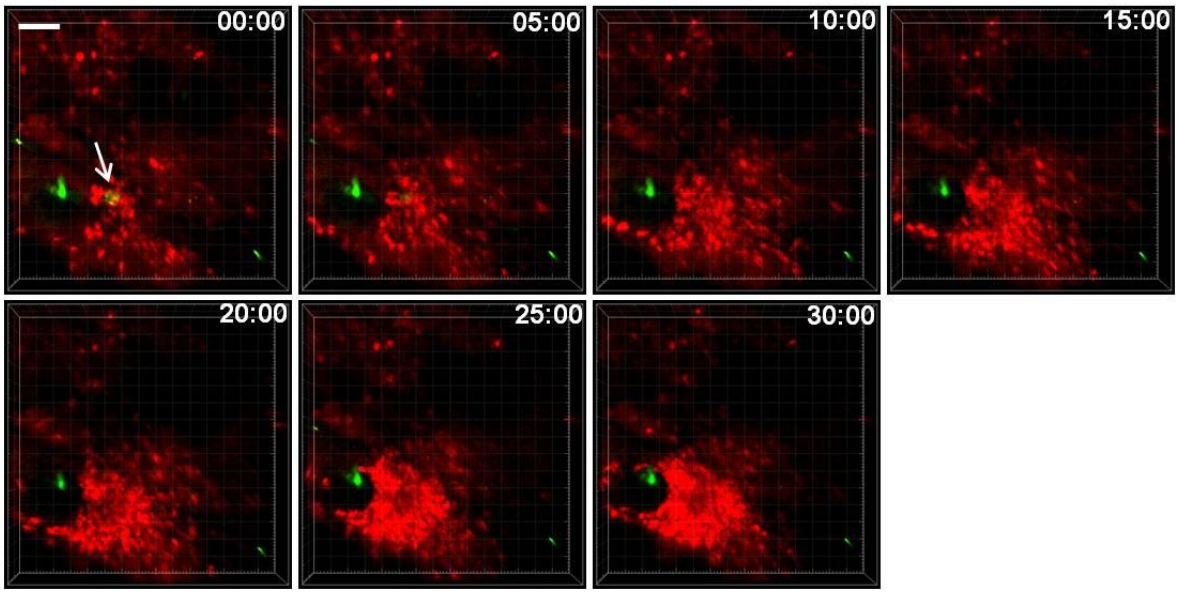

(Figure legend on the following page)

(B)

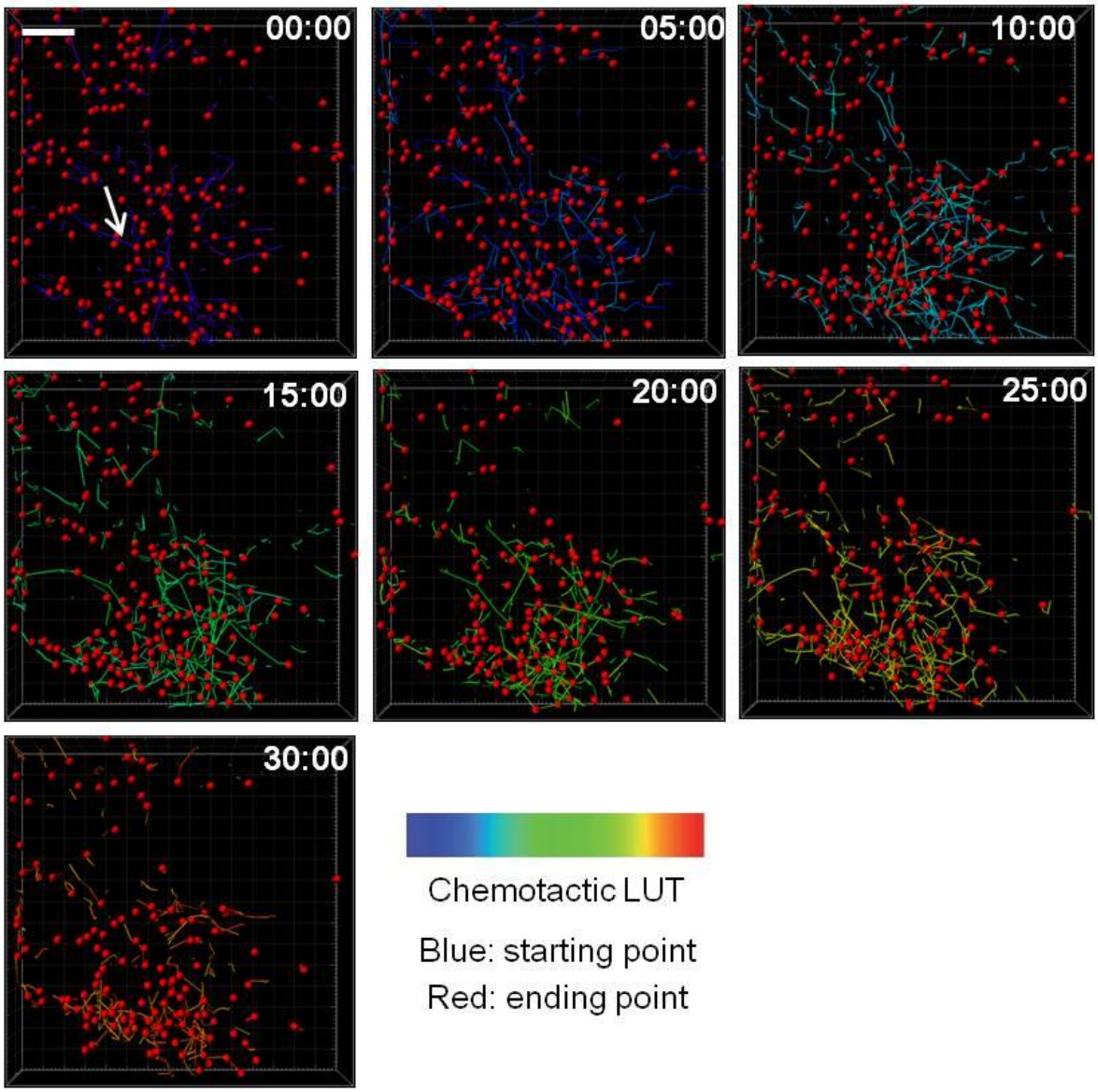

Figure 29 Response of adoptively transferred neutrophils to focal tissue damage. BM-derived neutrophils from Balb/c mice were labeled with cell tracker and injected intradermally into the ventral ear skin 2 h before laser-induced focal tissue damage was set. Neutrophil recruitment towards focal damage (white arrow; green spot) was recorded by multi-photon microscopy over a 30 min time-lapse **(A)**. Neutrophils (red dots) were identified and cell migration was followed by track analyses **(B)**. Tracks are indicated by colored lines. Migration areas of neutrophils are shown by direction lines which their color shifts from blue to red reflecting from the early step to the final area, respectively. Results of one representative experiment out of three experiments are shown. Scale bar: 50 µm.

3.5.3. Neutrophil activation in experimental EBA *in vivo*

To analyze NE activity *in vivo*, experimental EBA was induced locally in the ear by application of anti-mCOLVII IgG intradermally simultaneously with administration of inhibited and FRET probe-labeled BM-derived neutrophils into the ear of wildtype Balb/c mice. Irrelevant isotype antibody was injected together with neutrophils as a control. Intravital multi-photon imaging of NE activity on the surface of injected neutrophils by NEmo-2 probe indicate elastase enzyme activity on neutrophils in pathogenic antibody treated mice ear (Figure 30A) as compared to the controls (Figure 30B). Neutrophils accumulated in regions of anti-mCOLVII IgG deposition (Figure 30A). Monitoring of neutrophils confirmed the FRET loss on NEmo-2 sensor as cleaved by NE released from activated neutrophils by IC even in the presence of A1AT. While only low elastase activity could be detected in ears treated with the irrelevant isotype antibody, the percentage of activated cells significantly increased in neutrophils in ears treated with the pathogenic antibody (Figure 30C). The percentage of activated cells was defiened as the D/A ratio value comparing with the cell number observed in donor chanel. Since the donor signal of the cells is different, some value exceeds the maximum percent. These results provide clear evidence that, despite the presence of tissue protease inhibitors, NE activity is detectable in diseased tissue.

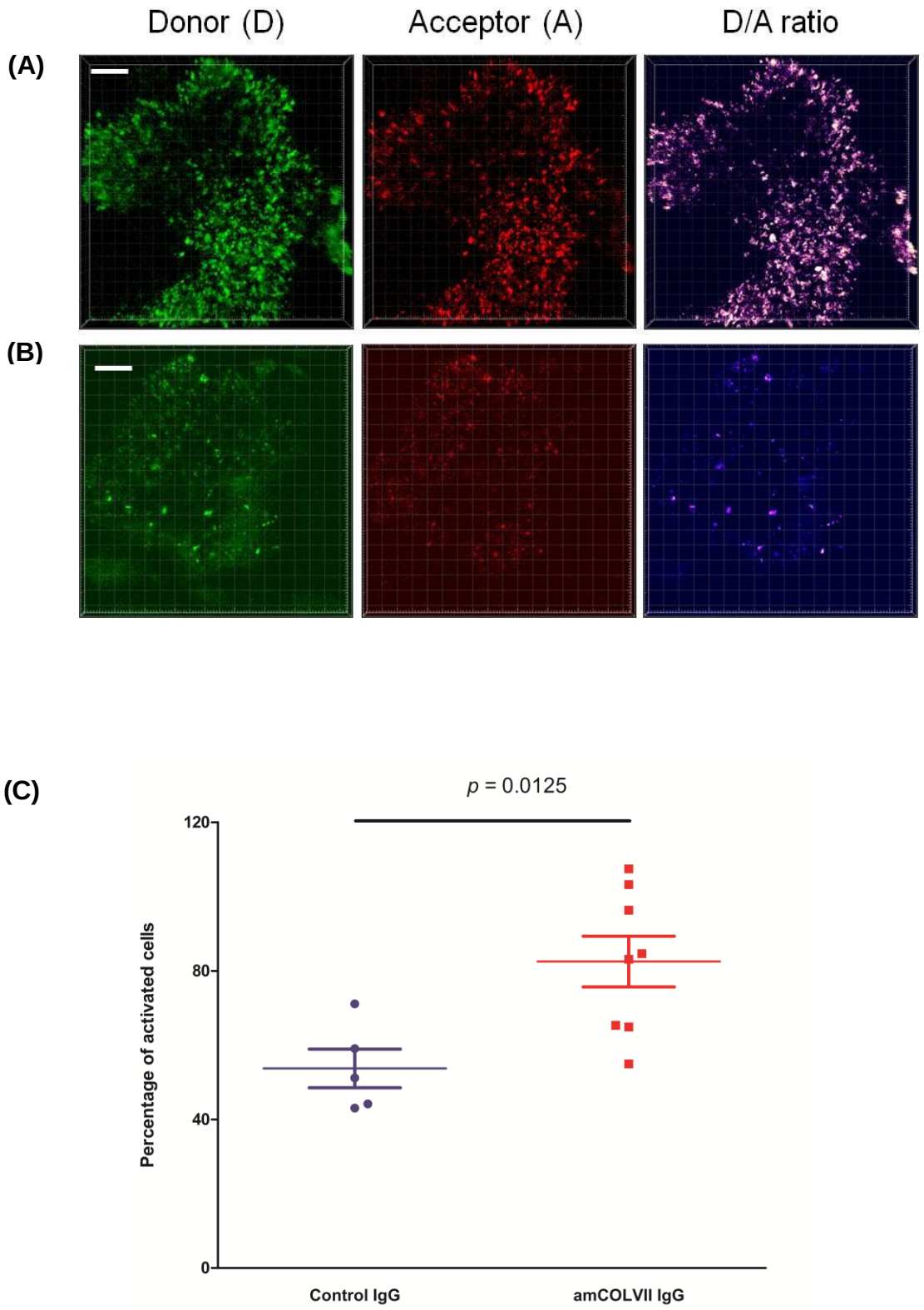

Figure 30 NE activities on activated neutrophils by IC in an *in vivo* mouse model of EBA. NEmo-2-labeled neutrophils as well as anti-mCOLVII antibody were injected in presence of A1AT into the ear of wildtype Balb/c mice **(A)**. Irrelevant isotype antibody served as control **(B)**. NE activity on the

surface of administrated neutrophils in mice ears was quantified by multi-photon microscopy. Images of donor and acceptor fluorescence were processed to calculate ratio values **(A, B)**. Scale bars: 30 and 50 µm for **(A)** and **(B)**, respectively. Results of one representative experiment out of 13 are shown. NE activity was quantified as the percentage of activated cells which was defined as the D/A ratio value comparing with the cell number observed in donor chanel **(C)**. Data are given as mean value out of 8 (amCOLVII IgG) and 5 (control isotype IgG) independent experiments. Observations indicated significantly increased the number of activated neutrophils comparing with unstimulated cells.

According to the current models of neutrophil activation, neutrophils should migrate from the periphery to the site of inflammation where they undergo a tight adhesion and exert further effector functions. Following our model, this tight adhesion is a prerequisite for protecting neutrophil proteases from an access to proteinase inhibitors. To examine whether the observed elastase activity in anti-mCOLVII-treated tissue is indeed associated with an increased adhesion of the cells, the capacity of neutrophils to migrate to a second inflammatory signal after first contact to pathogenic antibody was determined. To this end, focal tissue damage was applied in the area which anti-mCOLVII antibodies were bound to their antigens (Figure 31, video 5; blue area). The tissue damage signal still induced the attraction of injected neutrophils from distant sites, which became visible after 10 min. However, different to the result obtained in tissue treated with the pulse alone (Figure 29A, video 4A), in presence of pathogenic antibody, neutrophils became adherent during their migration and did not accumulate around the damage site (Figure 31, video 5). In summary, these findings suggest that increased elastase activity indeed correlates with enhanced adhesion of the cells.

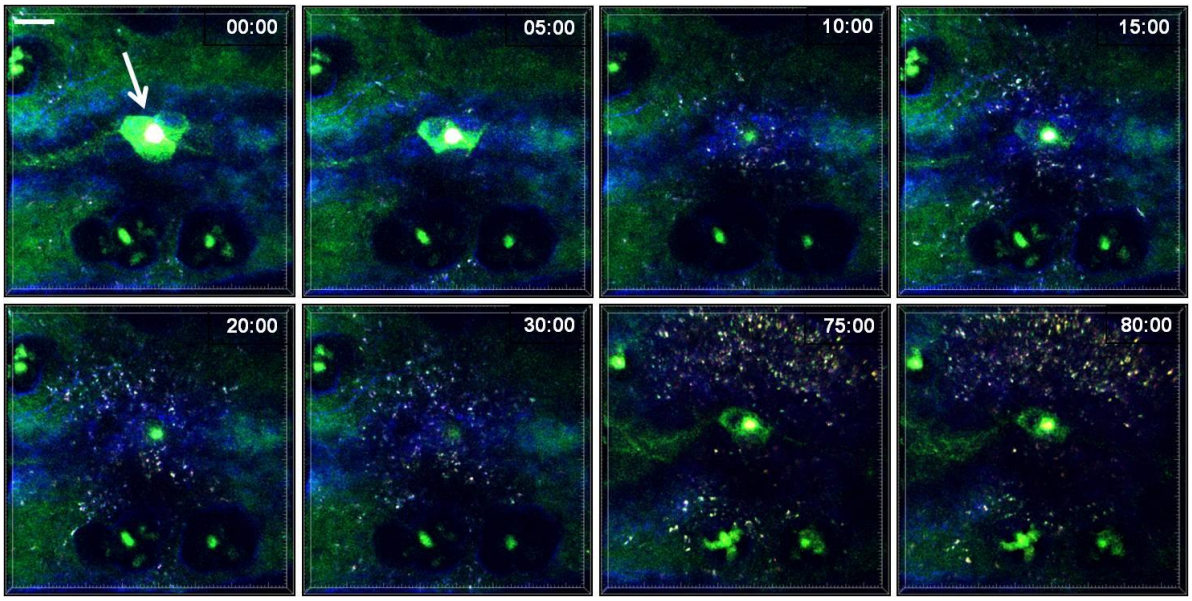

Figure 31 Damage-induced neutrophil migrations in presence of IC. NEmo-2-labeled neutrophils (fluorescence depicted as D/A ratio together with donor signal, bright small dots) as well as anti-mCOLVII antibody conjugated to DyLight 649 (blue color) were simultaneously injected in presence of A1AT into the ear of wildtype Balb/c mice. After 2h, focal tissue injury was applied (arrow) and the dynamics of administrated neutrophils was subsequently monitored over 90 min. Results of one representative experiment out of three are shown. Scale bar: 50 µm.

In the next step, spatial dynamics of elastase activity on the cells *in vivo* was analyzed. According to the findings derived from the static model *in vitro*, FRET reporter cleavage appeared to be rather homogenously distributed on the surface, most likely on the side of attachment to the surface with no significant changes over time (Figure 25A, video 2A-C). However, analysis of single cells *in vivo* revealed a completely different pattern. When neutrophils were bound to the pathogenic antibody, NE activity was only seen in very small defined areas on the cell surface (Figure 32, Video 6). Furthermore, regions of enzyme activity displayed high temporal dynamics and persisted mainly less than 30 sec (Figure 32, Video 6). As a result, increased D/A ratio were emitted only in some of the time sequences which the adhesion site might be visible.

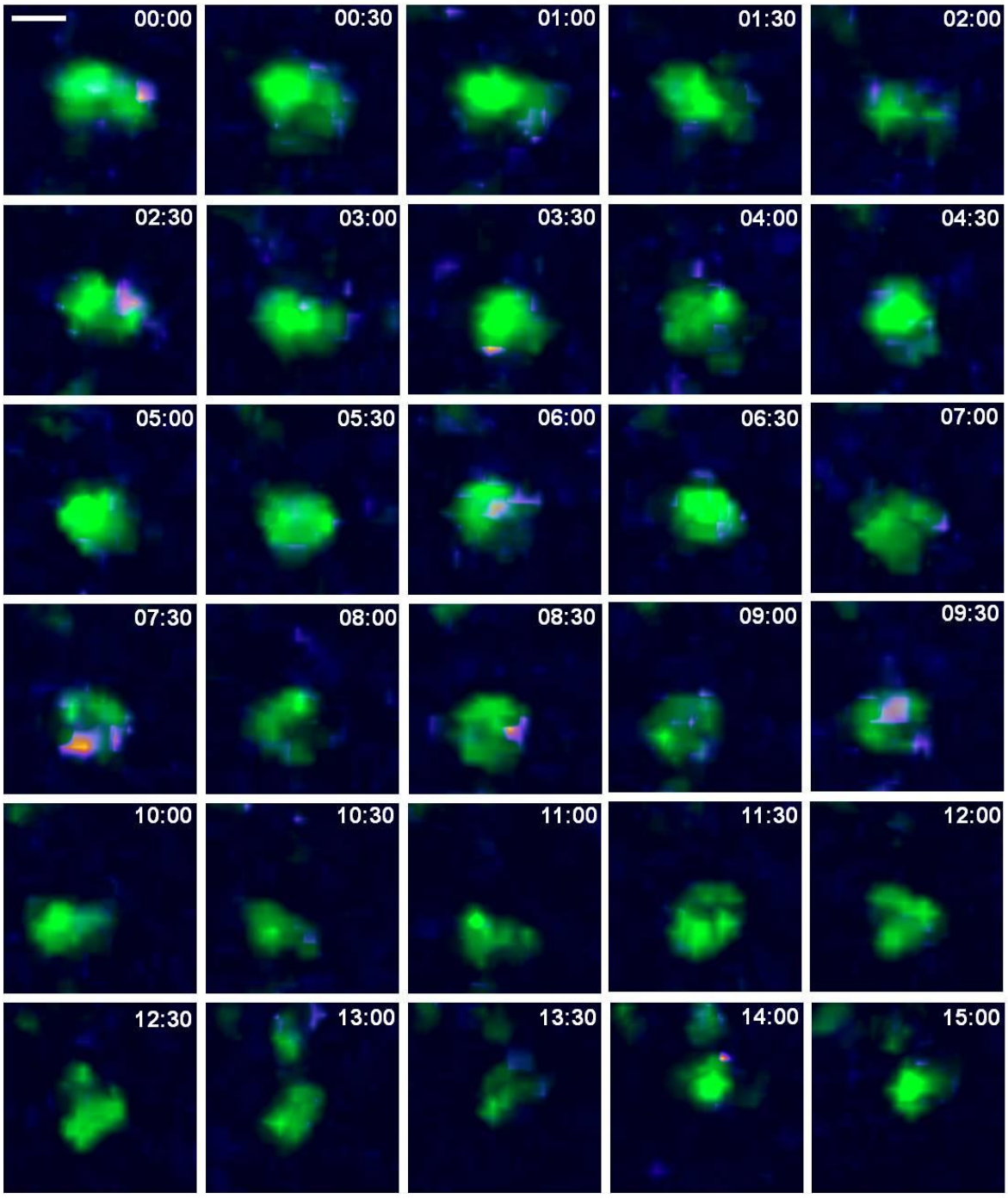

Figure 32 NE activities at the adhesion site of activated neutrophils *in vivo*. Local EBA was induced by single injection of anti-mCOLVII to the ventral side of ear. Thereafter, neutrophils were labeled with NEmo-2 reporter in presence of A1AT. NE activities were determined on single neutrophil at different time-points over a 15 min time-lapse by multi-photon microscopy. D/A ratio (violet color) together with donor signal (green color) are shown. Result of one representative experiment is shown. Scale bar: 10 µm.

Based on findings shown in the previous part, neutrophils respond to the signals derived from tissue damage and migrate to this point. Irrespective to adoptively transferred cells, endogenous neutrophils are also recruited to the site of damage. As a consequence, activation of endogenous neutrophils and the subsequent release of NE may also affect the sensitive reporter on the transferred neutrophils. To analyze the potential cleavage of NEmo-2 on the transferred neutrophils by elastase derived from endogenous sources, a NE-deficient ($NE^{-/-}$) mouse strain was used. For this purpose, experimental EBA was induced locally by administration of anti-mCOLVII IgG intradermally simultaneously with administration of inhibited and FRET probe-labeled neutrophils into the ear of NE-deficient mice. NE activity was observed on the surface of injected NEmo-2-labeled neutrophils as imaged by intravital multi-photon which indicate elastase enzyme activity on neutrophils in inflamed area of pathogenic antibody treated mice ear (Figure 33). Imaging of neutrophils confirmed the FRET loss on NEmo-2 sensor as cleaved by NE derived from exogenous activated neutrophils by IC in the presence of A1AT. These results provide obvious state that NE activity is detectable in diseased tissue by NE released by exogenous neutrophils which NE-derived from intrinsic neutrophils are excluded.

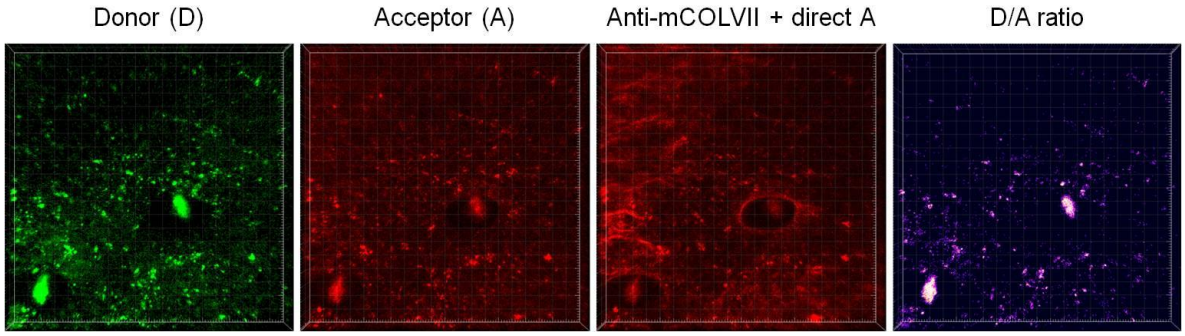

Figure 33 NE activities on exogenous activated neutrophils in an *in vivo* $NE^{-/-}$ mouse model of EBA. NEmo-2-labeled neutrophils as well as anti-mCOLVII antibody were injected into the ear of NE-deficient ($NE^{-/-}$) mouse in presence of A1AT. NE activity on the surface of administrated neutrophils in mice ears was quantified in presence of IC. Images of donor and acceptor fluorescence were processed to calculate ratio values. Since the excitation wavelengths of anti-mCOLVII and acceptor are in the same range, antibody and direct acceptor emissions are shown as a single image (lower left panel).Scale bars: 30 µm. Results of one representative experiment are shown.

Taken together, a novel method allowing the detection of NE activity in close proximity to cell membranes of living cells has been established in this study. By using a lipidated FRET-based proteases sensor, NE enzyme activity could be detected in experimental models of EBA *in vitro* and *in vivo* even in the presence of protease inhibitors. Although elastase release from activated neutrophils was shown to be independent from cell adhesion, resistance of protease activity to macromolecular inhibitors was strictly reliant on neutrophil adherence. These findings provide evidence for a model, in which adherent neutrophils release proteases in a sealed gap between cell and the attached surface where an access of the inhibitors to the proteases is prevented.

4. DISCUSSION

Neutrophils are involved in the pathomechanism of AIBDs as an important component of effector and regulatory pathways[124]. They contributed as executors of tissue damage in the concept of effector function by releasing several aggressive components such as ROS and serine proteases like elastase[126,149]. In addition to this effector phase, neutrophils are considered as regulators of inflammation which communicate with other immune cells by cell-cell contacts or secretion of mediators[124]. Although the fundamental pathogenic function of neutrophils has been under broad investigation in the tissue damage of human and experimental AIBDs, the neutrophil regulatory mechanisms as well as their mode of action in execution of the disease remain unclear. In the current study, the potential of neutrophils to regulate disease by MRP-8/-14 proteins as well as to execute tissue damage by NE was investigated. Currently, *in vitro* and *in vivo* quantification of NE activity on a single cell at the site of action as well as expression and potential function of MRP-8/-14 in AIBDs is not described so far. Therefore, the understanding of MRP-8/-14 proteins as well as NE contribution in the pathogenesis of EBA or BP diseases could help to identify novel therapeutical targets for developing new strategies in the treatment of AIBDs.

4.1. Involvement of neutrophils as executors of tissue damage

In experimental models of AIBDs, neutrophils are present at high numbers at the autoimmune lesional sites[136,265] which are recruited in a successive multistep fashion of adhesion, chemotaxis, and migration from the blood to inflammatory sites[266]. They are well equipped with an arsenal of microbicidal effector molecules, including ROS and proteinases. That weaponry may not only be harmful for pathogens but it could also damage components of the host tissues. Moreover, aberrant activation of neutrophils is believed to be an important factor of several disease processes, associated with immune-mediated damage to host tissues[267]. Of the various enzymes secreted by neutrophils at the sites of inflammation, NE represents an inflammatory serine protease mediating important protective functions under physiological and pathophysiological conditions including remodeling of the ECM and host defense against infections[128,268]. While it plays a beneficial role in innate host defense, unbalanced NE can lead to organ damage and dysfunction[269,270]. Beside

the reports of NE implication in numerous inflammatory and chronic diseases like AIBD, COPD, or cystic fibrosis[149,271–274], there is also some evidence of the presence of lesional elastase activity in dermatitis[275] and a destructive role of NE in bullous diseases such as EBA and BP[139,276]. NE-deficient mice do definitely not develop experimental BP despite a normal IgG and C3 deposition found at the basal membrane zone[149]. Reconstitution of NE-deficient mice with intradermal injection of wild type neutrophils results in a recovered susceptibility to experimental BP[149], indicating a significant role of neutrophils in disease pathogenesis. Therefore, neutrophil counts and NE activity can be considered as clinical parameters to determine the inflammatory status in many diseases such as AIBDs. Moreover, it has been shown that inhibition of neutrophil proteases could reduce neutrophil infiltration and neutrophil-mediated injury in different models of inflammation, such as collagen-induced arthritis, endotoxin-induced acute lung injury, and ischaemia and reperfusion injury[131–133]. Consequently, a specific imaging agent would prove invaluable for understanding the biological functions of NE and the development of NE inhibitors.

Under inflammatory condition, neutrophils transmigrate from the blood vessels into the tissue and become activated at sites where large amounts of inhibitory molecules are present[277,278]. Nevertheless, proteolytic properties of neutrophil proteases remain active despite the presence of inhibitors[277,278]. It has long been unclear how neutrophil activation and elastase activity can occure *in vivo* and how neutrophil elastase subsequently mediate tissue damage in presence of protecting proteases inhibitors. This highlights the relevance of novel tools for the detection of NE activity and the understanding of the contribution of NE in the pathogenesis of neutrophil-dominant inflammatory diseases. Until now, analysis of neutrophil activation in terms of protease release is limited to the determination of the enzymes or the corresponding enzyme activity in solution, e.g. in body fluids or culture supernatants. A site-specific analysis of neutrophil degranulation on single-cell level in diseased tissue, organs, or living animals was not possible so far. In this study, a method was established by using a FRET reporter to visualize neutrophil protease activity (NE) in experimental models of autoimmunity to COLVII (EBA) *in vitro* and *in vivo*. Therefore, the providing better visualization of neutrophil activation and subsequently enzyme release in disease could help to develop new strategies to prevent the host from harmful attacks by these cells.

NE activity was visualized on mouse BM differentiated as well as human peripheral neutrophils by using lipidated FRET reporter NEmo-2. The lipidated reporter NEmo-2 has been synthetized for monitoring of NE activity on neutrophil cell membranes which were previously successfully applied for *in vitro* analysis[165]. However, before analyzing the NE activity on the neutrophils, Jurkat T cells were used as controls which do not express endogenous elastase. As shown, NE activity could be detected on the cell surface in the presence of exogenous NE. In the absence of the exogenous elastase, the reporter was stable on the cell membrane for several hours. This provides first evidence of a proper interation between donor and acceptor fluorophores which are in close apposition on the cell membrane whereby the excitation energy of the donor fluorophore is transferred to the nearby acceptor. To confirm this interaction between the two fluorophores and to prove the presence of appropriate FRET efficiency, acceptor photobleaching was performed by comparing donor fluorescence intensity on the cell surface of Jurkat T cells before and after quenching the acceptor. Photo-inactivation of the acceptor fluorophore results in an increase of the donor signal, confirming the occurrence of FRET process between the molecules of the fluorophores.

NE activity was also found to be localized on neutrophils. However, the reporter was not stable here and rapidly degraded also on the surface of unstimulated cells. This unwanted cleavage resulted most likely from NE derived from leaking neutrophils which is seen also as background activity in the supernatants of unstimulated cell (Figure 21C). To avoid this cleavage and to stabilize the reporter on the cell membrane, the inhibitor A1AT was used. Antiprotease A1AT, a 55-kDa serum glycoprotein, is primarily synthesized in the liver and inactivates NE which is a monomeric, approximately 30-kDa glycoprotein[270]. Its major function is to protect tissue elastin from NE-mediated destruction by irreversible covalent binding to the enzyme[279–281]. Since NE is capable of degrading most of the constituents of connective tissue matrices, its inhibitor A1AT is thought to play a critical role in connective tissue turnover in homeostasis and tissue injury/inflammation[279,282]. In presence of A1AT, no elastase activity was detected on neutrophils and the reporter remains stable on the surface comparable to Jurkat cells.

Apart from the advantage of using inhibitor which helps for stabilizing the reporter on neutrophils, the complete blocking of NE by inhibitory molecules disable

determination of NE as a consequence of neutrophil activation. However, although elastase activity is inhibited on neutrophils in presence of A1AT *in vitro*, it does not neccessarily reflect the physiological conditions. *In vivo*, neutrophil protease activity is preserved in the extracellular environment even when inhibitors are present. The accurate and detailed process is not completely clear and remains a topic of some debate. Nevertheless, it has been shown that a massive quantity of the proteases released from neutrophil granules bind to the plasma membrane where their catalytic activity is preserved[283–285]. Therefore, it is suggested that this tight binding to the cell membrane makes the extracellular neutrophil proteases inaccessible to circulating, large molecule endogenous inhibitors, and therefore remain resistant[130,283–285]. Other studies have proven that protease inhibitors can be suppressed and inactivated by the large proportions of proteases and oxidants released by neutrophils that accumulate to the site of inflammation[285]. Soluble mediators such as proteases, cationic peptides, and ROS released by transmigrating leukocytes may influence epithelial permeability and function[286,287]. This influence together with the importance of soluble substances in neutrophil-epithelial interactions is emphasized where toxic mediators are not released by neutrophils into circulation, but they are released only once they are adherent to the endothelium, interstitium, or epithelium[286,287]. It is hypothesized that released proteases are compartmentalized between the adherent neutrophil and the ECM. This microenvironment excludes the large, circulating protease inhibitors and results in achievement of high concentrations of proteases[130,285,288,289]. This hypothesis so called ‘‘protected space’’ or ‘‘closed space’’ hypothesis which has been proposed three decades ago and used to explain the role of neutrophil adhesion in antibody dependent cellular cytotoxicity and anti-tumor immunity[254–257]. However, to my knowledge, this hypothesis has not been proven experimentally.

By using a membrane-bound protease sensor in this study, this hypothesis is supported by the direct evidence that IC-induced neutrophil adhesion is required for elastase to escape from the access of proteinase inhibitors. Our results suggest that a fine cooperation exists between IC-induced adhesion and NE in the tissue damage. To test this hypothesis, the neutrophil protease activity was determined in an *in vitro* experimental setting where neutrophils were activated by immobilized IC in presence of A1AT. Therefore, neutrophils were preincubated with Nemo-2 reporter and A1AT as NE inhibitor was applied to the neutrophils. NE has no membrane domain, but its

overall positive electrostatic potential is thought to induce interaction with the negative electrostatic potential of the membrane[290]. Under physiological conditions, this pool of NE might allow a controlled proteolysis directed by migration of the neutrophil to the target tissue. As shown here, neutrophils tightly attached to the surface with immobilized IC release their elastase enzymes which remain active in presence of A1AT. Cleavage of Nemo-2 reporter became visible on the surface of neutrophils stimulated with IC shortly after incubation. Noteworthy, IC-induced neutrophil adhesion establishes a secluded region between cell and surface whereby macromolecular inhibitors are excluded and released elastase can accumulate in an active state. Partial blocking of adhesion by anti-human CD18 antibody, which did not affect the IC-induced release of elastase, resulted in the complete loss of elastase activity in the presence of A1AT. This may indicate that already a limited disturbance of the closed space could be sufficient to allow the entry of inhibitory molecules.

4.2. NE activity *in vivo*

Due to the importance of NE in the pathogenesis of various diseases, the development of techniques to spatiotemporally visualize and quantify disease-associated NE *in vivo* is an active field of research in many laboratories. Advances in optical imaging techniques could provide new tools for understanding the roles of NE in disease onset and progression, as well as in the development and assessment of specific NE inhibiting therapies. Clinical applications of NE imaging may also help in diagnosis, staging of disease, and monitoring of treatment efficacy. In recent years, intense research efforts have been done in recognition of immune responses in the skin which lead to better understanding of the immune cell functions in the skin. This could help to develop new strategies or improved treatments for inflammatory skin diseases and preventing the host more effectively from harmful attacks by immune cells. Local microenvironment within a specific tissue such as skin can influence the immune cell function. Therefore, as compartment-specific imaging can be readily performed[291–296], using intravital imaging approaches could be an opportunity to address biological questions. Relatively low depth of light penetration and/or spatial resolution[296] in conventional microscopy techniques such as confocal or fluorescence microscopy could influence the quality of *in vivo* imaging of immune responses in the skin. Multi-photon intravital imaging represents a powerful technique with the

capacity to address complex immunological questions quantitatively. MPM enables the direct *in vivo* visualization, with high spatial and temporal resolution, of fluorescently tagged immune cells, ECM and vasculature in tissues. Therefore, this technique has this capacity to perform dynamic and multidimensional imaging and track the cell populations at the single-cell level *in vivo*[291,293]. Thus, common methods of determining immune cell function in the skin are mainly based on histology and flow cytometry can be obviously replaced by this powerful alternative approach.

In the present study, an experimental procedure[241] of intravital multi-photon imaging was used in mouse ear skin, to address a couple of questions regarding NE activity *in vivo*. Animal models offer an oppourtunity to analyze and understand disease mechanisms on a molecular level[297]. An experimental mouse model of EBA was used to address the role of NE on disease pathogenesis *in vivo*. The response of neutrophils during skin inflammation and analysis of neutrophil behavior in the context of the skin microanatomy are important points which by using novel FRET probes as well as a powerful imaging technique could be addressed. The ultimate goal of this part of study was to visualize NE activity *in vivo* and to proof its potential dependency on cell adherence. Although some attempts have been done to detect and quantify NE activity *in vivo* by using a NE-specific near-infrared fluorescence imaging agent[298,299], but still reliable monitoring of protease activity in a complex matrix at the level of intact cells is missing. Moreover, it should be considered that the protease activity, rather than its protein quantity, is indicative of disease status. Consequently, the immunological methods are limited and rarely applied in screening protease inhibitors. Classical biochemical methods for measuring activity of proteases[300] including liquid chromatography and gel electrophoresis are time consuming, and thus, can not be easily adapted for high throughput analysis of samples. The commercially available NE detection substrate is optimized towards the enzyme of human origin and moreover they can only be used for an *in vitro* analysis. As a consequence, although a substrate sequence with increased specificity towards murine NE has been recently identified and optimized[146], both sensitivity and specificity towards the murine counterpart are insufficient to monitor enzyme activity *in vivo*. Therefore in present study, the use of a newly developed specific NE reporter agent, NEmo-2, was described to detect and quantify NE activity *in vivo*, in real time in a mouse model of EBA. To this end, a local EBA mouse model was first validated which induced by injecting antibody against COLVII into the ear and results in

inflammation and tissue damage in the skin characterized by massive neutrophil infiltration and degranulation. As expected and observed in the histopathology of the ear skin, antibody administration resulted in a significant increase in the number of inflammatory cells, particularly neutrophils. Since neutrophil activation and corresponding NE release could be a very fast procedure and because of applying a single injection into the ear skin, NEmo-2 reporter-labeled neutrophils were administrated intradermally together with pathogenic antibody or irrelevant isotype antibody into the ventral side of mouse ear. The fluorescence signal emitting from the reporter inside the skin of mouse ear was detected by a multi-photon imaging microscopy. Significantly higher D/A ratios indicating increased levels of NE activity were visualized in the ear skin of EBA mice as compared to controls which had very low detectable D/A ratio emmision fluorescence. The activation of administrated neutrophils immediately started after binding to the pathogenic antibody. By using a fluorescent-labeled pathogenic antibody, activated neutrophils which bound to the antibody were detectable. Focal skin tissue damage was applied and restricted to the dermal layers near to the injection part to attract neutrophils. In control experiment, neutrophils migrate rapidly to the site of laser shooting. Interestingly when pathogenic antibody is present, neutrophils recruit to the area of tissue damage and they are trapped by the antibody. These findings are in agreement with the results indicating secretion of active elastase from IC-activated adherent neutrophils in close proximity of their cell membrane to the pathogenic antibody which is resistant to blockade by proteinase inhibitors in protected space. NE released by non-adherent neutrophils lacked activity and, most likely, was blocked by inhibitory molecules penetrating to the exposed space. As shown in Figure 32, NE activitiy was observed only in temporal regions of the cell surface by cleavage of NEmo-2 reporter at the adhesion site of activated neutrophils *in vivo*. This could be due to a gradient of NE located on the membrane which might be controlled by an opposing gradient of antiproteases and thus restricting highest NE activity in close proximity to the membrane. However as mentioned before, NE activity is observed inside the protected space which most likely is free of inhibitors. Therefore, observing a partial cleavage by NE on the surface of neutrophils is expected. This shows the advantage of the lipidated reporter on which the signal is accumulated on single cells. Specificity of the signal was shown by using control NE-deficient mice or irrelevant isotype antibody in wild type.

Based on these findings, a model can be proposed how IC-activated neutrophils contribute to tissue damage in experimental EBA (Figure 34). After recruitment to the skin, neutrophils are activated by the immobilized anti-COLVII/COLVII IC via FcγR. During activation, neutrophils tightly adhere to the DEJ and form a protected space preventing a molecular exchange with the environment. The subsequent degranulation process leads on the one hand to a production of ROS which are capable to destroy residual amounts macromolecular inhibitors and on the other hand to a strong accumulation of proteinases which together results in an overrun the inhibitory control mechanisms. As a consequence, uncontrolled elastase activity inaccessible to exogenous inhibitors will attack and destroy the structure proteins of the DEJ.

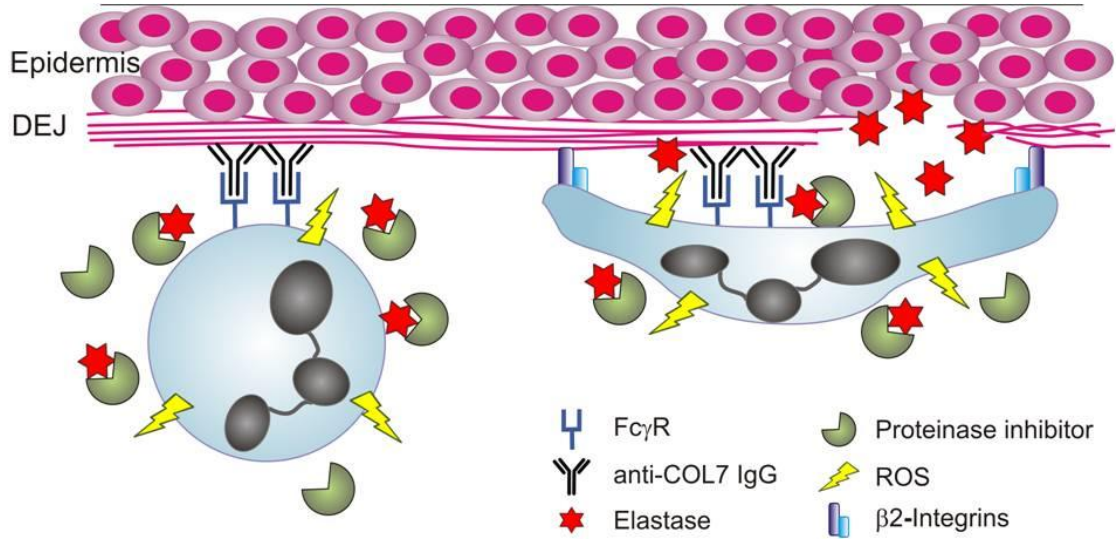

Figure 34 Model of autoantiboy-induced tissue damage. Neutrophils are activated by the anti-COLVII-COLVII immune complex via FcγR. Consequently, the activated neutrophils generate ROS and release elastase and other proteinases. When neutrophil adhesion is prevented (left panel), proteinases will be bound to inhibitors and ROS will be deactivated by scavengers resulting in tissue protection. If neutrophils can properly adhere to the target structure during activation (right panel), a β2-integrin-stabilized closed space will prevent the access of inhibitors and scavangers to proteinases and ROS enabling uncontrolled activity of these mediators leading to tissue damage.

Inhibition of proteinases as a therapeutic concept has been under broad investigation since more than 30 years. Despite this scientific effort only the elastase inhibitor Sivelestat has been approved for clinical use in Japan[301]. Patients suffering

from EBA and other AIBDs are currently treated with systemic immunosuppressive drugs or IVIG and no agents targeting the effector phase of these disorders have been developed until now[68,302]. The ideal treatment of the terminal phase of the disease should reduce efficiently neutrophil-mediated tissue damage without provoking side-effects like a broad restriction of the host defense against microbial invaders. Imaging of NE release in the protected space which is protected from the inhibitory effects of inhibitors might open a therapeutic avenue for EBA and other related diseases. Breaking the closed space of adherent neutrophils could facilitate the access of intrinsic as well as therapeutic inhibitors at the site of tissue damage.

4.3. Neutrophil MRP-8/-14 proteins in the regulation of EBA and BP

The results of the present study revealed a mechanistic explanation how proteases released by IC-activated neutrophils could promote tissue damage and destruction *in vivo*. This pathway obviously refers to the mechanisms by which neutrophils execute their effector functions in pathophysiology of AIBDs and directly cause tissue destruction. However, understanding of the direct pathogenic effects mediated by neutrophils covers only a part of the pathogenic potential of these cells. Today, it becomes more and more clear that neutrophils have also the capacity to regulate the immune response and as a consequence, indirectly influence the pathogenesis of the diseases. Therefore, it is hypothesized that neutrophils most likely contribute to the effector phase indirectly by the secretion soluble mediators like MRP-8/-14 proteins leading to amplification and maintenance of the inflammatory loop. Nevertheless, while some evidence have indicated the contribution of MRP-8/-14 in the regulatory phase of autoimmune-mediated diseases in human and experimental models[190,205,208], other studies provide a number of question marks on these results[209], so that the importance of these proteins in autoimmune diseases remains as a matter of debate. At the beginning of my studies, the potential role of MRP-8/-14 in AIBDs was not investigated.

Beside their critical functions in normal physiological pathways within cells, increased expression of MRP-8 and MRP-14 proteins is associated with many chronic diseases in humans such as autoimmune disorders, cancer, atherosclerosis,

cardiomyopathies and neurodegenerative diseases[194,205,303–306]. In most cases, these proteins are associated to proinflammatory mechanisms and a significant overexpression of them at the sites of inflammation as well as a strong correlation of their serum concentrations to inflammation have been indicated[190,207,307–309]. In this study, increased serum concentrations of MRP-8/-14 were observed in EBA and BP patients as well as in experimental disease. These results are in agreement of previous studies concerning to other AIDs. For example, MRP-8/-14 has been detected in serum and synovial fluid of patients suffering from juvenile idiopathic arthritis (JIA)[175] and a relationship has also been identified between their serum concentrations and individual disease activity in long-term studies in children[185,218,310]. Elevated serum concentrations of MRP-8/-14 have also been found in systemic AIDs such as systemic lupus erythematosus (SLE) and are related significantly with the SLE disease activity index[311].

Increased expression of MRP-8/-14 proteins in diseased tissue is frequently associated with an infiltration of neutrophils into regions of acute and chronic inflammatory lesions[186]. Initially, these proteins have been identified in RA, in which activated phagocytes expressing MRP proteins are among the first cells infiltrating inflammatory lesions in the synovium[190,307]. Furthermore, phagocytes expressing MRP-8/-14 have been observed as proinflammatory cells at sites of intestinal inflammation in chronic inflammatory bowel disease[312,313]. Based on several investigations, this heterodimeric protein complex was designated as a potential biomarker of disease activity in inflammatory arthritis and other AID states where myeloid cells play a crucial role[202,207]. In AIBDs such as inflammatory EBA and BP as well as in their corresponding mouse models, subepidermal blistering is associated with varying extents of cellular infiltrates[68,90,116,314] in which neutrophils represent the most abundant inflammatory cell type. This massive infiltration of inflammatory cells into regions of skin lesions could be confirmed in my models of EBA and BP where the diseases were induced by transfer of amCOL VII or XVII antibodies, respectively. Furthermore, significant numbers of neutrophils identified by their expression of NIMP were detected in these infiltrates. Noteworthy, the numbers of neutrophils correlated with the numbers of MRP-8/-14-positively stained cells in the lesional skin. These data confirm on the cellular level the previously observed increase in expression of MRP-8/-14 genes and proteins in diseased tissue. Furthermore, since these proteins are mainly expressed by neutrophils, the data suggest that this upregulation is most

likely caused by an infiltration of neutrophils. These finding clearly indicate that MRP-8/-14 proteins as a biomarker of chronic inflammation are not limited to rheumatoid arthritis (RA) or inflammatory bowel disease but may be also relevant to detect an ongoing inflammation in AIBD.

While the correlation between disease manifestation and MRP-8/-14 expression appears to be rather clear, their functional role in chronic disorders is a matter of a controversial debate. To delineate MRP-functions *in vivo*, we and others have used *Mrp-14*-deficient mice in different disease models. MRP-8 (10 kDa) and MRP-14 (14 kDa) proteins are constitutively expressed in circulating neutrophils and monocytes[186,315]. Although it has been shown that these two proteins can exist as homo- and heterocomplexes, they preferentially form heterodimers or heterotetramers in a Ca^{2+} and Zn^{2+} dependent way[192,316–320]. Although MRP-8/-14 homo- and hetero-oligomers may have distinct roles in cell physiology, it is well accepted that the predominant form in which MRP-8/-14 associates in physiological and pathological conditions is the heterodimer, even if it has been observed that MRP-8 and MRP-9 could also form homodimers[318,321]. *Mrp-8* deficient mice show a lethal phenotype[322], while *Mrp-14* knockout mice are perfectly viable and no major differences in inflammatory response have been observed compared to wild type animals[197]. Importantly, I could confirm previous findings that due to the instability of MRP-8 in *Mrp-14* knockout mice, in these strains both MRPs are not detectable. In contrast to my initial hypothesis that a lack of MRP-8/-14 may be protective in AIBD, *Mrp-14*$^{-/-}$ and wild type controls in systemic EBA developed a comparable clinical phenotype of the disease. The percentage of regional affected skin did not significantly differ between knockout mice and wild type controls. Moreover, histological examination of the skin revealed no differences in antibody or complement deposition as well as in cell infiltration in both mouse strains. Comparable to these results obtained in the EBA model, no significant difference could be observed between knockout and wild type mice in local mouse model of BP.

Mrp-14 deficient animals were capable of developing disease and outcome measures of cellular inflammation in the *Mrp-14* knock out did not differ significantly with the controls. Therefore, MRP-8/-14 proteins do not contribute to the disease expression in the antibody transfer models of EBA and BP used here. While these findings are in line with results published by Rampersad et al.[209] who analyzed the

role of MRP-14 in two models of RA, they are in sharp contrast to observations of van Lent et al.[205] who could show that *Mrp-14*-deficient animals are significantly protected from inflammatory arthritis in a further model of this disease. How can such diametrically opposed results be explained? One possibility is that the role of MRP-8/-14 is different in the respective animal models. In the model of van Lent, an antigen-induced arthritis is induced by immunization against methylated bovine serum albumin (mBSA). Disease was established by a booster injection of mBSA locally in the joint resulting in a chronic destructive localized arthritis. By contrast, Rampersad used two models, an acute model by systemic antibody transfer of K/BxN serum and the chronic collagen-induced arthritis (CIA) model, which is a *de novo*-induced immune response dependent on the H-2^q haplotype. Therefore, the mBSA model may represent more a general inflammatory response induced in the joints by soluble immune complexes with cartilage damage as side effect, while the K/BxN and CIA models are systemic models where specifically the cartilage is attacked as an immobilized immune complex. Within this view, the models of EBA and BP used here may be closer related to the K/BxN model than to the mBSA system.

Moreover, although the role of MRP-8/-14 in numerous intracellular functions in phagocytes has been documented[175,191,202,323,324], several conflicting reports exists regarding their specific activities, making assessment of some functions difficult. Although my results argue against a prominent role of MRP-8/-14 in the pathogenesis of AIBDs, a regulatory function of these proteins in the autoimmune diseases can not be excluded. First of all, the experimental models used here mainly represent the effector phase of the disease. Therefore, a potential role of MRP-8/-14 during the initial phase of AIBDs is still possible. Indeed, Loser et al. reported on a crucial role of MRP-8/-14 on the development of autoreactive $CD8^+$ T cells in a model of cutaneous lupus erythematosus[206]. Furthermore, Petersen and coworkers described an effect of these proteins on the maturation of dendritic cells in experimental contact dermatitis[325]. Both reports provide evidence that MRP-8/-14 may be rather involved in the regulation of the initial phases of chronic inflammation than in the effector phase of these diseases. Furthermore, since the MRP-8/-14 genes are regulated by pro- and anti-inflammatory mediators, together with their emerging anti-inflammatory properties, the functions of these proteins might be affected by several factors including the cell type and mediator involved in their induction in a particular inflammatory milieu, the receptors involved in their

recognition and their post-translational modification. For example, although there are correlation between MRP-8/-14 and chondrocyte-mediated cartilage destruction in RA[205], anti-inflammatory properties of the injected proteins are reported in rodent models of arthritis[326], autoimmune myocadritis[327] and endotoxin-mediated inflammation[328]. Therefore, it might be a point that they are mislabeled as 'proinflammatory' and in some circumstances; their high expression levels may actually mediate host protection. For example, MRP-8 and MRP-14 expression patterns in incision wounds in skin lead to the suggestion that elevated levels may have a therapeutic effect against inflammation in wound healing[329], and their positive expression in skin may be crucial for the protection against bacterial infections[330] and UVA-mediated oxidative damage[331]. In addition, MRP-14 has antinociceptive properties that are effective in various acute inflammatory pain models, and the use of a C-terminal peptide may represent a potential therapeutic[332]. Taken together with the pro-inflammatory properties described for these proteins, their ability to modulate inflammation should also be considered. Functions may be governed by the receptors that are activated by the calgranulins. Additionally, post-translational modifications may occur in oxidative environments and other factors such as proteolytic cleavage by proteases released as a consequence of phagocyte activation[333], and zinc binding may also have important functional ramifications.

Finally, a further possible explanation for the lacking disease phenotype of *Mrp-14* knockouts in our experimental systemic EBA and local BP model could be compensatory or overlapping mechanisms in *Mrp-14*$^{-/-}$ mouse. Specifically, MRP-6 (or S100A12) has been also shown to exhibit its pro-inflammatory activities via interaction with RAGE[178]. This protein has been described as a biomarker of neutrophil activation in inflammatory diseases, including RA[207,334]. Alternatively, either other proinflammatory mediators could be involved in compensatory mechanisms for MRP-8/-14 protein deficiency or these heterodimer proteins may play a less significant role in mouse models of inflammation than in human disease.

Taken together, my results strongly suggest that MRP-8/-14 proteins are not involved in the regulation of the effector phase of EBA and BP. Nevertheless, they may represent interesting new biomarkers for autoantibody-mediated immune dermatoses. Further studies are required to define a potential role of these proteins during the initial phase of AIBD.

4.4. Outlook and future perspectives

NE activity was visualized with FRET reporter as a direct effector in blister formation in bullous disease. However, monitoring the activity of different proteases which are also involved in the pathogenesis of the disease may help to examine complex biological processes in the concept of diseases[335]. For instance, presence of MMP-9 which is an important neutrophil enzyme has been confirmed in the blister fluid of lesional skin[336]. NE can be activated by MMP-9 through cleaving A1AT inhibitor[262] which confirms a link between MMP-9 and NE in skin pathogenesis. Therefore, visualization and monitoring of proteases which contribute to the disease pathogenesis could help to provide an outlook for strategies concerning treatment of skin diseases. Furthermore, since proteases are active when neutrophils detach to the surface, monitoring of simultaneous targeting of adhesion and proteases as a therapeutical concept could also be helpful.

As it was mentioned before, MRP-8/-14 proteins might be involved in the regulation of the induction phase of chronic inflammation than in the effector phase of these diseases. Therefore, providing an active model of bullous diseases EBA and BP by immunization of mice against autologous COLVII or COLXVII, respectively could be helpful. However, the self-tolerance has to be overcome for developing animal models of autoimmune diseases. Since susceptibility to the inflammatory-type EBA is strongly associated with the H2s haplotype[19], animals with a C57BL/6 background develop no clinical symptoms in active models of AIBD[120]. To circumvent this problem, *Mrp-14*-deficient mice could be backcrossed to a mouse strain like SJL, in which the suitable haplotype is expressed.

5. SUMMARY

The prevalence of chronic inflammatory diseases, especially autoimmune disorders (AID), has increased dramatically during the last decades in the world. Most diseases require a life-long non-curative treatment which is largely limited to the application of immunosuppressive drugs. The permanent and severe reduction in the quality of life of the patients as well as the enormous economical burden associated with these diseases emphasizes the high medical need for the development of novel therapeutic options. Since many years, the contribution of the different components of immune system to the pathogenesis of AID has been under intensive investigation. In the context of autoimmune bullous diseases (AIBDs), neutrophils have been identified as essential players in the effector phase of AIBDs. Neutrophil-derived mediators are involved in tissue damage and skin blister formation which is the hallmark of AIBDs including epidermolysis bullosa acquisita (EBA) and bullous pemphigoid (BP). However, although the principal participation of neutrophil proteases and ROS has clearly been shown in this course, the precise regulatory and executive mechanisms of neutrophils in the disease still remain unclear. In this study, it is hypothesized that neutrophils contribute to the effector phase by two ways, indirectly by the secretion of myeloid-related proteins (MRP)-8 and -14 leading to amplification and maintenance of the inflammatory loop as well as directly by the release of tissue-destructing elastase. Therefore, delineation of the mechanisms how neutrophils cause tissue damage will establish further information about the pathomechanisms of EBA and BP and provide a novel therapeutic avenue specifically targets the terminal phase of the disease.

MRP-8/-14 proteins belong to the group of alarmins or danger-associated molecular pattern (DAMPs) and their association with numerous human disorders, including acute and chronic inflammatory conditions and autoimmune diseases has been shown. In this study it is shown that elevated levels of MRP-8/-14 occur also in EBA and BP patients as well as in experimental disease. To clarify whether these functions are also relevant in the pathological process of the skin bullous diseases, *Mrp-14*-deficient mice, which are also functional deficient in MRP-8, were tested in antibody transfer models of EBA and BP. However, the knockout mice were not protected against disease development and their phenotype did not differ from that of the wild type controls. In contrast to the original hypothesis, these results indicate

that MRP-8/-14 proteins are not involved in the effector phase of EBA and BP. As a consequence, MRP-8/-14 do not appear as suitable therapeutic targets for the treatment of the effector phase of EBA or BP.

Neutrophil proteases such as elastase are essentially involved in many pathophysiologcal processes and uncontrolled proteolysis is a major reason for tissue damage and destruction in chronic inflammatory diseases like asthma, COPD, or AIDs. However, due to their low efficacy or severe side effects, antiproteinase therapies failed so far as treatment concept for these diseases. Therefore, the understanding of the mode of action of proteases under physiological conditions could help to develop new strategies to prevent the host from harmful attacks by these proteins. So far the role of these enzymes in disease has been shown only indirectly, either by appropriate knockout mice or inhibitor studies, determination of protease activity in cell extracts and supernatants, or by histological localization of the protein in the diseased tissue. For better understanding of the pathophysiological mechanism of neutrophil elastase in disease, a direct approach allowing their quantification and localization of the enzyme activity at its site of action *in vitro* and *in vivo* is required. Therefore, a method was established by using NE FRET reporter NEmo-2 to visualize NE activity on neutrophils *in vitro* as well as in experimental EBA *in vivo*. Using these novel tools, an interdependency between immune complex (IC)-induced neutrophil adhesion and elastase enzyme activity was discovered.

According to my results, exposure of neutrophils to immobilized IC induces their rapid activation in terms of cell adhesion, ROS production and the release of elastase. Surprisingly, although blocking of neutrophil adhesion with antibodies to CD18 did not affect the release of elastase or ROS, it has been shown in our group that IC-mediated tissue damage is significantly reduced under these conditions. Analysis of membrane-associated elastase activity *in vitro* by using the novel FRET-based protease sensor NEmo-2 revealed the presence of protease activity on adherent cells which is resistant to macromolecular protease inhibitors. Most likely, the escape of elastase from inhibitor access is enabled by the formation of a closed space between cell and surface. This fine cooperation among IC-induced neutrophil adhesion and elastase activity in tissue damage was further confirmed in a model ob EBA *in vivo*, where elastase enzyme activity could be imaged on the surface of adherent neutrophils in presence of protease inhibitors.

Taken together, this study demonstrates that during the effector phase of experimental AIBD, MRP-8/-14 proteins do not contribute to these diseases and, therefore, may not represent suitable therapeutical targets in this stage. However, highly sensitive detection of neutrophil elastase protease activity reveals an essential dependency of protease activity *in vitro* and *in vivo* on IC-induced neutrophil adhesion. Therefore, prevention of adhesion process in neutrophils by breaking the protected space could facilitate the access of intrinsic as well as therapeutic inhibitors at the site of tissue damage. These results help to better understand the pathophysiological functions of neutrophils in the effector phase of the disease particularly the direct effects of NE on tissue degradation and enable us to open a previous unseen window for novel therapeutical approaches of AIBD and other neutrophil-mediated disorders.

6. ZUSAMMENFASSUNG

Die Prävalenz chronischer Erkrankungen, insbesondere die der Autoimmunität, ist während der letzten Dekaden weltweit dramatisch angestiegen. Der überwiegende Teil dieser Krankheiten erfordert eine lebenslange Behandlung der Symptome durch immunsuppressive Medikation. Auf Grund dem damit verbundenen dauerhaften Verlust an Lebensqualität wie auch der enormen sozio-ökonomischen Belastung ist die Entwicklung neuer therapeutischer Optionen dringend erforderlich. Seit vielen Jahren wird daher die Beteiligung verschiedener Komponenten des Immunsystems an der Pathogenese von Autoimmunerkrankungen intensiv erforscht. In der Effektorphase von bullösen Autoimmunerkrankungen (autoimmune bullous diseases; AIBDs) konnten neutrophilen Granulozyten (Neutrophile) eine zentrale pro-pathogene Funktion zugewiesen werden. Mediatoren dieser Zellen sind an der Gewebeschädigung wie auch der Ausbildung von Blasen beteiligt, beides Charakteristika von AIBDs wie der Epidermolysis bullosa acquisita (EBA) oder dem bullösen Pemphigoid (BP). Obwohl die prinzipielle Beteiligung von Neutrophilen an der Pathogenese von AIBDs über die Freisetzung von Proteasen und reaktiven Sauerstoffderivaten bekannt ist, so sind die exakten regulatorischen und exekutiven Mechanismen dieser Zellen in dem Krankheitsprozess nicht geklärt. Nach der Hypothese der vorliegenden Studie beteiligen sich Neutrophile an der Effektorphase dieser Erkrankungen über zwei verschiedene Wege. Über den indirekten Weg einer Freisetzung der Myeloid-related Proteine (MRP)-8 und -14 könnte eine Amplifikation und Aufrechterhaltung der Entzündung vermittelt werden während über einen direkten Weg sezernierte Elastase eine Gewebsschädigung bewirken könnte. Die Aufklärung der Mechanismen über die Neutrophile zum Krankheitsbild der EBA und des BP beitragen könnte damit zu einem neuen therapeutischen Konzept zur Behandlung insbesondere bei bereits manifestierten Erkrankungen führen.

MRP-8 und -14 gehören zu der Gruppe der Alarmine oder DAMPs (danger-associated molecular pattern) und ihre Assoziation mit verschiedensten chronisch-entzündlichen Erkrankungen, insbesondere Autoimmunerkrankungen, konnte bereits erfolgreich nachgewiesen werden. In dieser Studie wurde gezeigt, dass sich erhöhte Spiegel von MRP-8/-14 auch in EBA- und BP-Patienten und Mäusen mit experimenteller AIBD nachweisen lassen. Um zu klären, ob diese Proteine auch eine funktioneller Relevanz in bullösen Erkrankungen besitzen, wurden die

Krankheitsbilder experimentell durch Übertragung pathogener Antikörper in *Mrp-14*-defizienten Mäusen, in welchen ebenfalls kein MRP-8 nachweisbar ist, induziert. Es zeigte sich jedoch, dass die Phänotypen der *Mrp-14*-defizienten Tiere keine signifikanten Unterschiede zu den Wildtypen aufwiesen. Entgegen der initialen Hypothese muss daher geschlossen werden, dass MRP-8/-14 nicht an der Regulation der Effektorphase der AIBS beteiligt sind und damit auch nicht als ein brauchbares therapeutisches Ziel zur Behandlung von AIBD erscheinen.

Neutrophile Proteasen wie Elastase sind an einer Vielzahl von pathophsiologischen Prozessen beteiligt und unkontrollierte Proteolyse ist ein Hauptgrund für die Gewebsschädigung in chronisch-entzündlichen Erkrankungen wie beispielsweise im Asthma, der COPD oder in Autoimmunerkrankungen. Auf Grund ihrer geringen Effizienz oder ihren schweren Nebeneffekten haben sich jedoch Antiprotease-Therapien als Behandlungskonzept nicht durchsetzen können. Ein besseres Verstehen der Wirkungsweise von Proteasen unter physiologischen Bedingungen könnte jedoch zur Entwicklung neuer Strategien zum Schutz des Wirtes vor einem Angriff durch diese Proteine führen. Auf die potentielle Rolle von Proteasen im Krankheitsgeschehen konnte bisher nur indirekt geschlossen werden, sei es durch geeignete Knockout Mäuse oder Inhibitorstudien, histologische Untersuchungen oder der Bestimmung von Enzymaktivitäten in Gewebsextrakten oder Kulturüberständen. Um die pathophysiologischen Prozesse jedoch erfassen zu können, ist ein direkter Ansatz notwendig, welcher gleichzeitig die Bestimmung von Enzymaktivität und deren lokale Zuordnung *in vitro* und *in vivo* erlaubt. Als Konsequenz wurde in dieser Arbeit unter Verwendung des FRET-basierten Elastase-Reporters NEmo-2 eine Methode entwickelt, welche einen Fluoreszenz-optischen Nachweis zellassoziierter Elastaseaktivität ermöglicht. Mithilfe dieser Methode konnte ein direkter Zusammenhang zwischen durch Immunkomplexe (IC) induzierter Adhärenz und Elastase-Enzymaktivität nachgewiesen werden.

Nach meinen Ergebnissen induziert die Stimulation mit immobilisierten IC in Neutrophilen eine schnelle Aktivierung in Form einer Zelladhärenz sowie der Freisetzung von Sauerstoffradikalen und Elastase. Obwohl die Blockade der Adhärenz mittel CD18-Antikörpern keinerlei Effekt auf die Freisetzung von Elastase oder Sauerstoffradikalen hatte, so konnte in unserer Gruppe gezeigt werden, dass die durch IC vermittelte Gewebsschädigung unter diesen Bedingungen drastisch reduziert ist. Mit Hilfe des FRET-Sensors NEmo-2 konnte auf adhärenten

Neutrophilen *in vitro* eine mit der Zellmembran assoziierten Elastaseaktivität nachgewiesen werden, welche sich als resistent gegenüber makromolekularen Proteaseinhibitoren erwies. Diese Resistenz basiert wahrscheinlich auf der Bildung eines abgeschlossenen Raumes ("closed space") auf der Anheftungsseite der Zellen, welcher den Zugang der Inhibitoren zu den Proteasen verhindert. Ein solches Zusammenspiel von Zelladhärenz und Proteaseaktivität konnte in einem Tiermodell der EBA *in vivo* bestätigt werden, bei dem sich Elastaseaktivität in Gegenwart hoher Konzentrationen von Proteaseinhibitoren in adhärenten Neutrophilen nachweisen ließ.

Nach den Befunden dieser Studie tragen die Proteine MRP-8 und -14 nicht zur Pathogenese in der Effektorphase von experimentellen AIBDs bei und repräsentieren damit auch keine potentiellen therapeutischen Ziele zur Behandlung dieser Erkrankungen in diesem Stadium. Jedoch konnte mittels einer hochempfindlichen zellbasierten Methode zur Bestimmung der Elastaseaktivität eine direkte Abhängigkeit zwischen Proteaseaktivität und Zelladhärenz nachgewiesen werden. Damit könnte die Interferenz mit dem Adhäsionsprozess, welche einen Zugang von intrinsischen oder therapeutischen Inhibitoren zu den pathogenen Proteasen ermöglicht, eine vielversprechende neue Strategie zur Behandlung von AIBD und anderen Erkrankungen darstellen.

7. REFERENCES

1. Kanitakis, J. Anatomy, histology and immunohistochemistry of normal human skin. *Eur. J. Dermatol. EJD* **12,** 390–399; quiz 400–401 (2002).

2. Kolarsick, P. A. J., Kolarsick, M. A. & Goodwin, C. Anatomy and Physiology of the Skin: *J. Dermatol. Nurses Assoc.* **3,** 203–213 (2011).

3. James, W. D., Berger, T. & Elston, D. *Andrew's Diseases of the Skin: Clinical Dermatology*. (Elsevier Health Sciences, 2011).

4. Lever, W. F., Elder, D. E. & Elenitsas, R. *Lever's Histopathology of the Skin*. (Lippincott Williams & Wilkins, 2005).

5. Prost-Squarcioni, C., Fraitag, S., Heller, M. & Boehm, N. [Functional histology of dermis]. *Ann. Dermatol. Vénéréologie* **135,** 1S5–20 (2008).

6. Gayraud, B., Höpfner, B., Jassim, A., Aumailley, M. & Bruckner-Tuderman, L. Characterization of a 50-kDa component of epithelial basement membranes using GDA-J/F3 monoclonal antibody. *J. Biol. Chem.* **272,** 9531–9538 (1997).

7. Briggaman, R. A. & Wheeler, C. E. The epidermal-dermal junction. *J. Invest. Dermatol.* **65,** 71–84 (1975).

8. Weber, L., Krieg, T. & Timpl, R. [Basement membranes--structure, function, pathology]. *Hautarzt Z. Für Dermatol. Venerol. Verwandte Geb.* **35,** 279–286 (1984).

9. Sakai, L. Y., Keene, D. R., Morris, N. P. & Burgeson, R. E. Type VII collagen is a major structural component of anchoring fibrils. *J. Cell Biol.* **103,** 1577–1586 (1986).

10. Paulsson, M. Basement membrane proteins: structure, assembly, and cellular interactions. *Crit. Rev. Biochem. Mol. Biol.* **27,** 93–127 (1992).

11. Villone, D. *et al.* Supramolecular interactions in the dermo-epidermal junction zone: anchoring fibril-collagen VII tightly binds to banded collagen fibrils. *J. Biol. Chem.* **283,** 24506–24513 (2008).

12. Encyclopedia Britannica, Inc.: http://www.britannica.com/EBchecked/topic/547591/human-skin.

13. Charles A Janeway, J., Travers, P., Walport, M. & Shlomchik, M. J. Principles of innate and adaptive immunity. (2001).

14. Zhernakova, A., van Diemen, C. C. & Wijmenga, C. Detecting shared pathogenesis from the shared genetics of immune-related diseases. *Nat. Rev. Genet.* **10,** 43–55 (2009).

15. Selgrade, M. K., Cooper, G. S., Germolec, D. R. & Heindel, J. J. Linking environmental agents and autoimmune disease: an agenda for future research. *Environ. Health Perspect.* **107 Suppl 5,** 811–813 (1999).

16. Kalies, K., Blessenohl, M., Nietsch, J. & Westermann, J. T cell zones of lymphoid organs constitutively express Th1 cytokine mRNA: specific changes during the early phase of an immune response. *J. Immunol. Baltim. Md 1950* **176,** 741–749 (2006).

17. Tashiro, H., Arai, H., Hashimoto, T., Takezaki, S. & Kawana, S. Pemphigoid nodularis: two case studies and analysis of autoantibodies before and after the development of generalized blistering. *J. Nippon Med. Sch. Nippon Ika Daigaku Zasshi* **72,** 60–65 (2005).

18. Gammon, W. R. *et al.* Increased frequency of HLA-DR2 in patients with autoantibodies to epidermolysis bullosa acquisita antigen: evidence that the expression of autoimmunity to type VII collagen is HLA class II allele associated. *J. Invest. Dermatol.* **91,** 228–232 (1988).

19. Ludwig, R. J. *et al.* Generation of antibodies of distinct subclasses and specificity is linked to H2s in an active mouse model of epidermolysis bullosa acquisita. *J. Invest. Dermatol.* **131,** 167–176 (2011).

20. Zumelzu, C. *et al.* Black patients of African descent and HLA-DRB1*15:03 frequency overrepresented in epidermolysis bullosa acquisita. *J. Invest. Dermatol.* **131,** 2386–2393 (2011).

21. Ludwig, R. J. *et al.* Identification of quantitative trait loci in experimental epidermolysis bullosa acquisita. *J. Invest. Dermatol.* **132,** 1409–1415 (2012).

22. Yancey, K. B. & Fairley, J. A. Introduction to the milestones in autoimmune bullous diseases. *J. Invest. Dermatol.* **128,** E15 (2008).

23. Yancey, K. B. & Egan, C. A. Pemphigoid: clinical, histologic, immunopathologic, and therapeutic considerations. *JAMA* **284,** 350–356 (2000).

24. Hertl, M., Eming, R. & Veldman, C. T cell control in autoimmune bullous skin disorders. *J. Clin. Invest.* **116,** 1159–1166 (2006).

25. Kouno, M. *et al.* Ahnak/Desmoyokin is dispensable for proliferation, differentiation, and maintenance of integrity in mouse epidermis. *J. Invest. Dermatol.* **123,** 700–707 (2004).

26. Simpson, C. L., Patel, D. M. & Green, K. J. Deconstructing the skin: cytoarchitectural determinants of epidermal morphogenesis. *Nat. Rev. Mol. Cell Biol.* **12,** 565–580 (2011).

27. Tsuruta, D., Hashimoto, T., Hamill, K. J. & Jones, J. C. R. Hemidesmosomes and focal contact proteins: functions and cross-talk in keratinocytes, bullous diseases and wound healing. *J. Dermatol. Sci.* **62,** 1–7 (2011).

28. Hashimoto, T., Ishii, N., Ohata, C. & Furumura, M. Pathogenesis of epidermolysis bullosa acquisita, an autoimmune subepidermal bullous disease. *J. Pathol.* **228,** 1–7 (2012).

29. Mihai, S. & Sitaru, C. Immunopathology and molecular diagnosis of autoimmune bullous diseases. *J. Cell. Mol. Med.* **11,** 462–481 (2007).

30. Kneisel, A. & Hertl, M. Autoimmune bullous skin diseases. Part 1: Clinical manifestations. *J. Dtsch. Dermatol. Ges. J. Ger. Soc. Dermatol. JDDG* **9,** 844–856; quiz 857 (2011).

31. Otten, J. V., Hashimoto, T., Hertl, M., Payne, A. S. & Sitaru, C. Molecular diagnosis in autoimmune skin blistering conditions. *Curr. Mol. Med.* **14,** 69–95 (2014).

32. Amagai, M. & Stanley, J. R. Desmoglein as a target in skin disease and beyond. *J. Invest. Dermatol.* **132,** 776–784 (2012).

33. Hashimoto, T. Immunopathology of IgA pemphigus. *Clin. Dermatol.* **19,** 683–689 (2001).

34. Hashimoto, T. Immunopathology of paraneoplastic pemphigus. *Clin. Dermatol.* **19,** 675–682 (2001).

35. Hashimoto, T. Treatment strategies for pemphigus vulgaris in Japan. *Expert Opin. Pharmacother.* **9,** 1519–1530 (2008).

36. Joly, P. *et al.* A comparison of oral and topical corticosteroids in patients with bullous pemphigoid. *N. Engl. J. Med.* **346,** 321–327 (2002).

37. Langan, S. M. *et al.* Bullous pemphigoid and pemphigus vulgaris--incidence and mortality in the UK: population based cohort study. *BMJ* **337,** a180 (2008).

38. LEVER, W. F. Pemphigus. *Medicine (Baltimore)* **32,** 1–123 (1953).

39. Labib, R. S., Anhalt, G. J., Patel, H. P., Mutasim, D. F. & Diaz, L. A. Molecular heterogeneity of the bullous pemphigoid antigens as detected by immunoblotting. *J. Immunol. Baltim. Md 1950* **136,** 1231–1235 (1986).

40. Stanley, J. R., Tanaka, T., Mueller, S., Klaus-Kovtun, V. & Roop, D. Isolation of complementary DNA for bullous pemphigoid antigen by use of patients' autoantibodies. *J. Clin. Invest.* **82,** 1864–1870 (1988).

41. Sawamura, D., Li, K., Chu, M. L. & Uitto, J. Human bullous pemphigoid antigen (BPAG1). Amino acid sequences deduced from cloned cDNAs predict biologically important peptide segments and protein domains. *J. Biol. Chem.* **266,** 17784–17790 (1991).

42. Stanley, J. R. Cell adhesion molecules as targets of autoantibodies in pemphigus and pemphigoid, bullous diseases due to defective epidermal cell adhesion. *Adv. Immunol.* **53,** 291–325 (1993).

43. Liu, Z. *et al.* A passive transfer model of the organ-specific autoimmune disease, bullous pemphigoid, using antibodies generated against the hemidesmosomal antigen, BP180. *J. Clin. Invest.* **92,** 2480–2488 (1993).

44. Nishie, W. *et al.* Humanization of autoantigen. *Nat. Med.* **13,** 378–383 (2007).

45. Schaumburg-Lever G, Orfanos CE & Lever WF. ELectron microscopic study of bullous pemphigoid. *Arch. Dermatol.* **106,** 662–667 (1972).

46. Dvorak, A. M. *et al.* Bullous pemphigoid, an ultrastructural study of the inflammatory response: eosinophil, basophil and mast cell granule changes in multiple biopsies from one patient. *J. Invest. Dermatol.* **78,** 91–101 (1982).

47. Della Torre, R. *et al.* Clinical presentation and diagnostic delay in bullous pemphigoid: a prospective nationwide cohort. *Br. J. Dermatol.* **167,** 1111–1117 (2012).

48. Kasperkiewicz, M. & Zillikens, D. The pathophysiology of bullous pemphigoid. *Clin. Rev. Allergy Immunol.* **33,** 67–77 (2007).

49. Tanaka, T., Parry, D. A., Klaus-Kovtun, V., Steinert, P. M. & Stanley, J. R. Comparison of molecularly cloned bullous pemphigoid antigen to desmoplakin I confirms that they define a new family of cell adhesion junction plaque proteins. *J. Biol. Chem.* **266,** 12555–12559 (1991).

50. Green, K. J., Virata, M. L., Elgart, G. W., Stanley, J. R. & Parry, D. A. Comparative structural analysis of desmoplakin, bullous pemphigoid antigen and plectin: members of a new gene family involved in organization of intermediate filaments. *Int. J. Biol. Macromol.* **14,** 145–153 (1992).

51. Hopkinson, S. B., Riddelle, K. S. & Jones, J. C. Cytoplasmic domain of the 180-kD bullous pemphigoid antigen, a hemidesmosomal component: molecular and cell biologic characterization. *J. Invest. Dermatol.* **99,** 264–270 (1992).

52. Hirako, Y., Usukura, J., Nishizawa, Y. & Owaribe, K. Demonstration of the molecular shape of BP180, a 180-kDa bullous pemphigoid antigen and its potential for trimer formation. *J. Biol. Chem.* **271,** 13739–13745 (1996).

53. Balding, S. D., Diaz, L. A. & Giudice, G. J. A recombinant form of the human BP180 ectodomain forms a collagen-like homotrimeric complex. *Biochemistry (Mosc.)* **36,** 8821–8830 (1997).

54. Bédane, C. *et al.* Bullous pemphigoid and cicatricial pemphigoid autoantibodies react with ultrastructurally separable epitopes on the BP180 ectodomain: evidence that BP180 spans the lamina lucida. *J. Invest. Dermatol.* **108,** 901–907 (1997).

55. Masunaga, T. *et al.* The extracellular domain of BPAG2 localizes to anchoring filaments and its carboxyl terminus extends to the lamina densa of normal human epidermal basement membrane. *J. Invest. Dermatol.* **109,** 200–206 (1997).

56. Giudice, G. J. *et al.* Bullous pemphigoid and herpes gestationis autoantibodies recognize a common non-collagenous site on the BP180 ectodomain. *J. Immunol. Baltim. Md 1950* **151,** 5742–5750 (1993).

57. Perriard, J. *et al.* IgG autoantibodies from bullous pemphigoid (BP) patients bind antigenic sites on both the extracellular and the intracellular domains of the BP antigen 180. *J. Invest. Dermatol.* **112,** 141–147 (1999).

58. Hofmann, S. *et al.* Severity and phenotype of bullous pemphigoid relate to autoantibody profile against the NH2- and COOH-terminal regions of the BP180 ectodomain. *J. Invest. Dermatol.* **119,** 1065–1073 (2002).

59. Di Zenzo, G. *et al.* Multicenter prospective study of the humoral autoimmune response in bullous pemphigoid. *Clin. Immunol. Orlando Fla* **128,** 415–426 (2008).

60. Di Zenzo, G. *et al.* Characterization of the anti-BP180 autoantibody reactivity profile and epitope mapping in bullous pemphigoid patients. *J. Invest. Dermatol.* **122,** 103–110 (2004).

61. Schmidt, E. & Zillikens, D. Diagnosis and clinical severity markers of bullous pemphigoid. *F1000 Med. Rep.* **1,** (2009).

62. Kromminga, A. *et al.* Patients with bullous pemphigoid and linear IgA disease show a dual IgA and IgG autoimmune response to BP180. *J. Autoimmun.* **15,** 293–300 (2000).

63. Döpp, R. *et al.* IgG4 and IgE are the major immunoglobulins targeting the NC16A domain of BP180 in Bullous pemphigoid: serum levels of these immunoglobulins reflect disease activity. *J. Am. Acad. Dermatol.* **42,** 577–583 (2000).

64. Iwata, Y. *et al.* Correlation of IgE autoantibody to BP180 with a severe form of bullous pemphigoid. *Arch. Dermatol.* **144,** 41–48 (2008).

65. Christophoridis, S. *et al.* IgG, IgA and IgE autoantibodies against the ectodomain of BP180 in patients with bullous and cicatricial pemphigoid and linear IgA bullous dermatosis. *Br. J. Dermatol.* **143,** 349–355 (2000).

66. Joly, P. *et al.* Incidence and mortality of bullous pemphigoid in France. *J. Invest. Dermatol.* **132,** 1998–2004 (2012).

67. Cortés, B. *et al.* Mortality of bullous pemphigoid in Switzerland: a prospective study. *Br. J. Dermatol.* **165,** 368–374 (2011).

68. Schmidt, E. & Zillikens, D. Pemphigoid diseases. *Lancet* **381,** 320–332 (2013).

69. Di Zenzo, G., Marazza, G. & Borradori, L. Bullous pemphigoid: physiopathology, clinical features and management. *Adv. Dermatol.* **23,** 257–288 (2007).

70. Schmidt, E., della Torre, R. & Borradori, L. Clinical features and practical diagnosis of bullous pemphigoid. *Immunol. Allergy Clin. North Am.* **32,** 217–232, v (2012).

71. Kobayashi, M. *et al.* BP180 ELISA using bacterial recombinant NC16a protein as a diagnostic and monitoring tool for bullous pemphigoid. *J. Dermatol. Sci.* **30,** 224–232 (2002).

72. Yoshida, M. *et al.* Enzyme-linked immunosorbent assay using bacterial recombinant proteins of human BP230 as a diagnostic tool for bullous pemphigoid. *J. Dermatol. Sci.* **41,** 21–30 (2006).

73. Sitaru, C. *et al.* Enzyme-linked immunosorbent assay using multimers of the 16th non-collagenous domain of the BP180 antigen for sensitive and specific detection of pemphigoid autoantibodies. *Exp. Dermatol.* **16,** 770–777 (2007).

74. Blöcker, I. M. *et al.* Epitope mapping of BP230 leading to a novel enzyme-linked immunosorbent assay for autoantibodies in bullous pemphigoid. *Br. J. Dermatol.* **166,** 964–970 (2012).

75. Elliott, G. T. Two cases of epidermolysis bullosa. *J. Cutan. Genitourin. Dis.* **13,** 10-18 (1895).

76. Bernard, P. *et al.* Incidence and distribution of subepidermal autoimmune bullous skin diseases in three French regions. Bullous Diseases French Study Group. *Arch. Dermatol.* **131,** 48–52 (1995).

77. Wong, S. N. & Chua, S. H. Spectrum of subepidermal immunobullous disorders seen at the National Skin Centre, Singapore: a 2-year review. *Br. J. Dermatol.* **147,** 476–480 (2002).

78. Bertram, F., Bröcker, E.-B., Zillikens, D. & Schmidt, E. Prospective analysis of the incidence of autoimmune bullous disorders in Lower Franconia, Germany. *J. Dtsch. Dermatol. Ges. J. Ger. Soc. Dermatol. JDDG* **7,** 434–440 (2009).

79. Ludwig, R. J. Clinical presentation, pathogenesis, diagnosis, and treatment of epidermolysis bullosa acquisita. *ISRN Dermatol.* **2013,** 812029 (2013).

80. Sitaru, C. & Zillikens, D. Mechanisms of blister induction by autoantibodies. *Exp. Dermatol.* **14,** 861–875 (2005).

81. Hallel-Halevy, D., Nadelman, C., Chen, M. & Woodley, D. T. Epidermolysis bullosa acquisita: update and review. *Clin. Dermatol.* **19,** 712–718 (2001).

82. Gammon, W. R., Briggaman, R. A., Woodley, D. T., Heald, P. W. & Wheeler, C. E., Jr. Epidermolysis bullosa acquisita--a pemphigoid-like disease. *J. Am. Acad. Dermatol.* **11,** 820–832 (1984).

83. Stewart, M. I., Woodley, D. T. & Briggaman, R. A. Epidermolysis bullosa acquisita and associated symptomatic esophageal webs. *Arch. Dermatol.* **127,** 373–377 (1991).

84. Lunstrum, G. P., Sakai, L. Y., Keene, D. R., Morris, N. P. & Burgeson, R. E. Large complex globular domains of type VII procollagen contribute to the structure of anchoring fibrils. *J. Biol. Chem.* **261,** 9042–9048 (1986).

85. Lunstrum, G. P. *et al.* Anchoring fibrils contain the carboxyl-terminal globular domain of type VII procollagen, but lack the amino-terminal globular domain. *J. Biol. Chem.* **262,** 13706–13712 (1987).

86. Christiano, A. M. *et al.* A missense mutation in type VII collagen in two affected siblings with recessive dystrophic epidermolysis bullosa. *Nat. Genet.* **4,** 62–66 (1993).

87. Heinonen, S. *et al.* Targeted inactivation of the type VII collagen gene (Col7a1) in mice results in severe blistering phenotype: a model for recessive dystrophic epidermolysis bullosa. *J. Cell Sci.* **112 (Pt 21),** 3641–3648 (1999).

88. Fritsch, A. *et al.* A hypomorphic mouse model of dystrophic epidermolysis bullosa reveals mechanisms of disease and response to fibroblast therapy. *J. Clin. Invest.* **118,** 1669–1679 (2008).

89. Hundorfean, G., Neurath, M. F. & Sitaru, C. Autoimmunity against type VII collagen in inflammatory bowel disease. *J. Cell. Mol. Med.* **14,** 2393–2403 (2010).

90. Sitaru, C. Experimental models of epidermolysis bullosa acquisita. *Exp. Dermatol.* **16,** 520–531 (2007).

91. Chen, M. *et al.* Development of an ELISA for rapid detection of anti-type VII collagen autoantibodies in epidermolysis bullosa acquisita. *J. Invest. Dermatol.* **108,** 68–72 (1997).

92. Saleh, M. A. *et al.* Development of NC1 and NC2 domains of type VII collagen ELISA for the diagnosis and analysis of the time course of epidermolysis bullosa acquisita patients. *J. Dermatol. Sci.* **62,** 169–175 (2011).

93. Komorowski, L. *et al.* Sensitive and specific assays for routine serological diagnosis of epidermolysis bullosa acquisita. *J. Am. Acad. Dermatol.* **68,** e89–95 (2013).

94. Gammon, W. R. *et al.* Autoantibodies to type VII collagen recognize epitopes in a fibronectin-like region of the noncollagenous (NC1) domain. *J. Invest. Dermatol.* **100,** 618–622 (1993).

95. Engineer, L. & Ahmed, A. R. Emerging treatment for epidermolysis bullosa acquisita. *J. Am. Acad. Dermatol.* **44,** 818–828 (2001).

96. Kim, J. H. & Kim, S.-C. Epidermolysis bullosa acquisita. *J. Eur. Acad. Dermatol. Venereol. JEADV* **27,** 1204–1213 (2013).

97. Ishii, N. *et al.* Epidermolysis bullosa acquisita: what's new? *J. Dermatol.* **37,** 220–230 (2010).

98. Hellberg, L. *et al.* Methylprednisolone blocks autoantibody-induced tissue damage in experimental models of bullous pemphigoid and epidermolysis bullosa acquisita through inhibition of neutrophil activation. *J. Invest. Dermatol.* **133,** 2390–2399 (2013).

99. Remington, J., Chen, M., Burnett, J. & Woodley, D. T. Autoimmunity to type VII collagen: epidermolysis bullosa acquisita. *Curr. Dir. Autoimmun.* **10,** 195–205 (2008).

100. Connolly, S. M. & Sander, H. M. Treatment of epidermolysis bullosa acquisita with cyclosporine. *J. Am. Acad. Dermatol.* **16,** 890 (1987).

101. Khatri, M. L., Benghazeil, M. & Shafi, M. Epidermolysis bullosa acquisita responsive to cyclosporin therapy. *J. Eur. Acad. Dermatol. Venereol. JEADV* **15,** 182–184 (2001).

102. Maize, J. C., Jr & Cohen, J. B. Cyclosporine controls epidermolysis bullosa acquisita co-occurring with acquired factor VIII deficiency. *Int. J. Dermatol.* **44,** 692–694 (2005).

103. Kim, J. H., Kim, Y. H. & Kim, S.-C. Epidermolysis bullosa acquisita: a retrospective clinical analysis of 30 cases. *Acta Derm. Venereol.* **91,** 307–312 (2011).

104. Bauer, J. W. *et al.* Ocular involvement in IgA-epidermolysis bullosa acquisita. *Br. J. Dermatol.* **141,** 887–892 (1999).

105. Megahed, M. & Scharffetter-Kochanek, K. Epidermolysis bullosa acquisita--successful treatment with colchicine. *Arch. Dermatol. Res.* **286,** 35–46 (1994).

106. Cunningham, B. B., Kirchmann, T. T. & Woodley, D. Colchicine for epidermolysis bullosa acquisita. *J. Am. Acad. Dermatol.* **34,** 781–784 (1996).

107. Arora, K. P., Sachdeva, B., Singh, N. & Bhattacharya, S. N. Remission of recalcitrant epidermolysis bullosa acquisita (EBA) with colchicine monotherapy. *J. Dermatol.* **32,** 114–119 (2005).

108. Tanaka, N. *et al.* A case of epidermolysis bullosa acquisita with clinical features of Brunsting-Perry pemphigoid showing an excellent response to colchicine. *J. Am. Acad. Dermatol.* **61,** 715–719 (2009).

109. Kiniwa, Y. *et al.* A case of epidermolysis bullosa acquisita associated with laryngeal stenosis. *Acta Derm. Venereol.* **92,** 93–94 (2012).

110. Ishii, N., Hashimoto, T., Zillikens, D. & Ludwig, R. J. High-dose intravenous immunoglobulin (IVIG) therapy in autoimmune skin blistering diseases. *Clin. Rev. Allergy Immunol.* **38,** 186–195 (2010).

111. Ahmed, A. R. & Gürcan, H. M. Treatment of epidermolysis bullosa acquisita with intravenous immunoglobulin in patients non-responsive to conventional therapy: clinical outcome and post-treatment long-term follow-up. *J. Eur. Acad. Dermatol. Venereol. JEADV* **26,** 1074–1083 (2012).

112. Sadler, E. *et al.* Treatment-resistant classical epidermolysis bullosa acquisita responding to rituximab. *Br. J. Dermatol.* **157,** 417–419 (2007).

113. Schmidt, E., Benoit, S., Bröcker, E.-B., Zillikens, D. & Goebeler, M. Successful adjuvant treatment of recalcitrant epidermolysis bullosa acquisita with anti-CD20 antibody rituximab. *Arch. Dermatol.* **142,** 147–150 (2006).

114. Kim, J. H., Lee, S. E. & Kim, S.-C. Successful treatment of epidermolysis bullosa acquisita with rituximab therapy. *J. Dermatol.* **39,** 477–479 (2012).

115. Kirtschig, G., Murrell, D., Wojnarowska, F. & Khumalo, N. Interventions for mucous membrane pemphigoid and epidermolysis bullosa acquisita. *Cochrane Database Syst. Rev.* CD004056 (2003). doi:10.1002/14651858.CD004056

116. Bieber, K. *et al.* Animal models for autoimmune bullous dermatoses. *Exp. Dermatol.* **19,** 2–11 (2010).

117. Sitaru, C. *et al.* Induction of dermal-epidermal separation in mice by passive transfer of antibodies specific to type VII collagen. *J. Clin. Invest.* **115,** 870–878 (2005).

118. Woodley, D. T. *et al.* Evidence that anti-type VII collagen antibodies are pathogenic and responsible for the clinical, histological, and immunological features of epidermolysis bullosa acquisita. *J. Invest. Dermatol.* **124,** 958–964 (2005).

119. Woodley, D. T. *et al.* Induction of epidermolysis bullosa acquisita in mice by passive transfer of autoantibodies from patients. *J. Invest. Dermatol.* **126,** 1323–1330 (2006).

120. Sitaru, C. *et al.* Induction of complement-fixing autoantibodies against type VII collagen results in subepidermal blistering in mice. *J. Immunol. Baltim. Md 1950* **177,** 3461–3468 (2006).

121. Liu, Z. *et al.* Beta2-microglobulin-deficient mice are resistant to bullous pemphigoid. *J. Exp. Med.* **186,** 777–783 (1997).

122. Kobayashi, S. D., Voyich, J. M., Burlak, C. & DeLeo, F. R. Neutrophils in the innate immune response. *Arch. Immunol. Ther. Exp. (Warsz.)* **53,** 505–517 (2005).

123. Grassi, F. Purinergic control of neutrophil activation. *J. Mol. Cell Biol.* **2,** 176–177 (2010).

124. Mantovani, A., Cassatella, M. A., Costantini, C. & Jaillon, S. Neutrophils in the activation and regulation of innate and adaptive immunity. *Nat. Rev. Immunol.* **11,** 519–531 (2011).

125. Pham, C. T. N. Neutrophil serine proteases fine-tune the inflammatory response. *Int. J. Biochem. Cell Biol.* **40,** 1317–1333 (2008).

126. Raptis, S. Z., Shapiro, S. D., Simmons, P. M., Cheng, A. M. & Pham, C. T. N. Serine protease cathepsin G regulates adhesion-dependent neutrophil effector functions by modulating integrin clustering. *Immunity* **22,** 679–691 (2005).

127. Borregaard, N. Neutrophils, from marrow to microbes. *Immunity* **33,** 657–670 (2010).

128. Korkmaz, B., Horwitz, M. S., Jenne, D. E. & Gauthier, F. Neutrophil elastase, proteinase 3, and cathepsin G as therapeutic targets in human diseases. *Pharmacol. Rev.* **62,** 726–759 (2010).

129. Mittal, M., Siddiqui, M. R., Tran, K., Reddy, S. P. & Malik, A. B. Reactive oxygen species in inflammation and tissue injury. *Antioxid. Redox Signal.* **20,** 1126–1167 (2014).

130. Pham, C. T. N. Neutrophil serine proteases: specific regulators of inflammation. *Nat. Rev. Immunol.* **6,** 541–550 (2006).

131. Carden, D. L. & Korthuis, R. J. Protease inhibition attenuates microvascular dysfunction in postischemic skeletal muscle. *Am. J. Physiol.* **271,** H1947–1952 (1996).

132. Kawabata, K. *et al.* Delayed neutrophil elastase inhibition prevents subsequent progression of acute lung injury induced by endotoxin inhalation in hamsters. *Am. J. Respir. Crit. Care Med.* **161,** 2013–2018 (2000).

133. Kakimoto, K., Matsukawa, A., Yoshinaga, M. & Nakamura, H. Suppressive effect of a neutrophil elastase inhibitor on the development of collagen-induced arthritis. *Cell. Immunol.* **165,** 26–32 (1995).

134. Chen, M. *et al.* The cartilage matrix protein subdomain of type VII collagen is pathogenic for epidermolysis bullosa acquisita. *Am. J. Pathol.* **170,** 2009–2018 (2007).

135. Chen, M. & Woodley, D. T. Duplicating autoimmune bullous diseases by passively transferring autoantibodies into animals. *J. Invest. Dermatol.* **128,** E25–27 (2008).

136. Liu, Z. *et al.* A major role for neutrophils in experimental bullous pemphigoid. *J. Clin. Invest.* **100,** 1256–1263 (1997).

137. Chiriac, M. T. *et al.* NADPH oxidase is required for neutrophil-dependent autoantibody-induced tissue damage. *J. Pathol.* **212,** 56–65 (2007).

138. Liu, Z., Zhao, M., Li, N., Diaz, L. A. & Mayadas, T. N. Differential roles for beta2 integrins in experimental autoimmune bullous pemphigoid. *Blood* **107,** 1063–1069 (2006).

139. Shimanovich, I. *et al.* Granulocyte-derived elastase and gelatinase B are required for dermal-epidermal separation induced by autoantibodies from patients with epidermolysis bullosa acquisita and bullous pemphigoid. *J. Pathol.* **204,** 519–527 (2004).

140. Sitaru, C. *et al.* Autoantibodies to bullous pemphigoid antigen 180 induce dermal-epidermal separation in cryosections of human skin. *J. Invest. Dermatol.* **118,** 664–671 (2002).

141. Yu, X. *et al.* EndoS reduces the pathogenicity of anti-mCOL7 IgG through reduced binding of immune complexes to neutrophils. *PloS One* **9,** e85317 (2014).

142. Kuhn, C., 3rd, Slodkowska, J., Smith, T. & Starcher, B. The tissue response to exogenous elastase. *Bull. Eur. Physiopathol. Respir.* **16 Suppl,** 127–139 (1980).

143. Garwicz, D., Lennartsson, A., Jacobsen, S. E. W., Gullberg, U. & Lindmark, A. Biosynthetic profiles of neutrophil serine proteases in a human bone marrow-derived cellular myeloid differentiation model. *Haematologica* **90,** 38–44 (2005).

144. Borregaard, N. & Cowland, J. B. Granules of the human neutrophilic polymorphonuclear leukocyte. *Blood* **89,** 3503–3521 (1997).

145. Lominadze, G. *et al.* Proteomic analysis of human neutrophil granules. *Mol. Cell. Proteomics MCP* **4,** 1503–1521 (2005).

146. Kalupov, T. *et al.* Structural characterization of mouse neutrophil serine proteases and identification of their substrate specificities: relevance to mouse models of human inflammatory diseases. *J. Biol. Chem.* **284,** 34084–34091 (2009).

147. Walsh, D. E. *et al.* Interleukin-8 up-regulation by neutrophil elastase is mediated by MyD88/IRAK/TRAF-6 in human bronchial epithelium. *J. Biol. Chem.* **276,** 35494–35499 (2001).

148. Devaney, J. M. *et al.* Neutrophil elastase up-regulates interleukin-8 via toll-like receptor 4. *FEBS Lett.* **544,** 129–132 (2003).

149. Liu, Z. *et al.* A critical role for neutrophil elastase in experimental bullous pemphigoid. *J. Clin. Invest.* **105,** 113–123 (2000).

150. Oikarinen, A. I., Zone, J. J., Ahmed, A. R., Kiistala, U. & Uitto, J. Demonstration of collagenase and elastase activities in the blister fluids from bullous skin diseases. Comparison between dermatitis herpetiformis and bullous pemphigoid. *J. Invest. Dermatol.* **81,** 261–266 (1983).

151. Benabid, R. *et al.* Neutrophil elastase modulates cytokine expression: contribution to host defense against Pseudomonas aeruginosa-induced pneumonia. *J. Biol. Chem.* **287,** 34883–34894 (2012).

152. Heussen, C. & Dowdle, E. B. Electrophoretic analysis of plasminogen activators in polyacrylamide gels containing sodium dodecyl sulfate and copolymerized substrates. *Anal. Biochem.* **102,** 196–202 (1980).

153. Nakajima, K., Powers, J. C., Ashe, B. M. & Zimmerman, M. Mapping the extended substrate binding site of cathepsin G and human leukocyte elastase. Studies with peptide substrates related to the alpha 1-protease inhibitor reactive site. *J. Biol. Chem.* **254,** 4027–4032 (1979).

154. Castillo, M. J., Nakajima, K., Zimmerman, M. & Powers, J. C. Sensitive substrates for human leukocyte and porcine pancreatic elastase: a study of the merits of various chromophoric and fluorogenic leaving groups in assays for serine proteases. *Anal. Biochem.* **99,** 53–64 (1979).

155. Korkmaz, B. *et al.* Design and use of highly specific substrates of neutrophil elastase and proteinase 3. *Am. J. Respir. Cell Mol. Biol.* **30,** 801–807 (2004).

156. Wiesner, O. *et al.* Differences between human proteinase 3 and neutrophil elastase and their murine homologues are relevant for murine model experiments. *FEBS Lett.* **579,** 5305–5312 (2005).

157. Lane, A. A. & Ley, T. J. Neutrophil elastase cleaves PML-RARalpha and is important for the development of acute promyelocytic leukemia in mice. *Cell* **115,** 305–318 (2003).

158. Ntziachristos, V., Ripoll, J., Wang, L. V. & Weissleder, R. Looking and listening to light: the evolution of whole-body photonic imaging. *Nat. Biotechnol.* **23,** 313–320 (2005).

159. McDonald, D. M. & Choyke, P. L. Imaging of angiogenesis: from microscope to clinic. *Nat. Med.* **9,** 713–725 (2003).

160. Contag, C. H. & Bachmann, M. H. Advances in in vivo bioluminescence imaging of gene expression. *Annu. Rev. Biomed. Eng.* **4,** 235–260 (2002).

161. Wagnières, G. A., Star, W. M. & Wilson, B. C. In vivo fluorescence spectroscopy and imaging for oncological applications. *Photochem. Photobiol.* **68,** 603–632 (1998).

162. Jares-Erijman, E. A. & Jovin, T. M. FRET imaging. *Nat. Biotechnol.* **21,** 1387–1395 (2003).

163. Förster, T. Zwischenmolekulare Energiewanderung und Fluoreszenz. *Ann. Phys.* **437,** 55–75 (1948).

164. Cobos-Correa, A., Trojanek, J. B., Diemer, S., Mall, M. A. & Schultz, C. Membrane-bound FRET probe visualizes MMP12 activity in pulmonary inflammation. *Nat. Chem. Biol.* **5,** 628–630 (2009).

165. Gehrig, S., Mall, M. A. & Schultz, C. Spatially resolved monitoring of neutrophil elastase activity with ratiometric fluorescent reporters. *Angew. Chem. Int. Ed Engl.* **51,** 6258–6261 (2012).

166. Gambin, Y. & Deniz, A. A. Multicolor single-molecule FRET to explore protein folding and binding. *Mol. Biosyst.* **6,** 1540–1547 (2010).

167. Lu, S. & Wang, Y. Fluorescence resonance energy transfer biosensors for cancer detection and evaluation of drug efficacy. *Clin. Cancer Res. Off. J. Am. Assoc. Cancer Res.* **16,** 3822–3824 (2010).

168. Prasuhn, D. E. *et al.* Quantum dot peptide biosensors for monitoring caspase 3 proteolysis and calcium ions. *ACS Nano* **4,** 5487–5497 (2010).

169. Reits, E. *et al.* Peptide diffusion, protection, and degradation in nuclear and cytoplasmic compartments before antigen presentation by MHC class I. *Immunity* **18,** 97–108 (2003).

170. Adams, S. R., Harootunian, A. T., Buechler, Y. J., Taylor, S. S. & Tsien, R. Y. Fluorescence ratio imaging of cyclic AMP in single cells. *Nature* **349,** 694–697 (1991).

171. Miyawaki, A. *et al.* Fluorescent indicators for Ca2+ based on green fluorescent proteins and calmodulin. *Nature* **388,** 882–887 (1997).

172. Fonović, M. & Bogyo, M. Activity-based probes as a tool for functional proteomic analysis of proteases. *Expert Rev. Proteomics* **5,** 721–730 (2008).

173. Bachmann, M. F. & Kopf, M. On the role of the innate immunity in autoimmune disease. *J. Exp. Med.* **193,** F47–50 (2001).

174. Feldmann, M. & Maini, R. N. Anti-TNF alpha therapy of rheumatoid arthritis: what have we learned? *Annu. Rev. Immunol.* **19,** 163–196 (2001).

175. Foell, D., Wittkowski, H., Vogl, T. & Roth, J. S100 proteins expressed in phagocytes: a novel group of damage-associated molecular pattern molecules. *J. Leukoc. Biol.* **81,** 28–37 (2007).

176. Johnson, K. J. & Ward, P. A. Acute immunologic pulmonary alveolitis. *J. Clin. Invest.* **54,** 349–357 (1974).

177. Guo, R.-F. & Ward, P. A. Mediators and regulation of neutrophil accumulation in inflammatory responses in lung: insights from the IgG immune complex model. *Free Radic. Biol. Med.* **33,** 303–310 (2002).

178. Oppenheim, J. J. & Yang, D. Alarmins: chemotactic activators of immune responses. *Curr. Opin. Immunol.* **17,** 359–365 (2005).

179. Murao, S., Collart, F. R. & Huberman, E. A protein containing the cystic fibrosis antigen is an inhibitor of protein kinases. *J. Biol. Chem.* **264,** 8356–8360 (1989).

180. McNamara, M. P., Wiessner, J. H., Collins-Lech, C., Hahn, B. L. & Sohnle, P. G. Neutrophil death as a defence mechanism against Candida albicans infections. *Lancet* **2,** 1163–1165 (1988).

181. Steinbakk, M. *et al.* Antimicrobial actions of calcium binding leucocyte L1 protein, calprotectin. *Lancet* **336,** 763–765 (1990).

182. Sohnle, P. G., Collins-Lech, C. & Wiessner, J. H. Antimicrobial activity of an abundant calcium-binding protein in the cytoplasm of human neutrophils. *J. Infect. Dis.* **163,** 187–192 (1991).

183. Murthy, A. R., Lehrer, R. I., Harwig, S. S. & Miyasaki, K. T. In vitro candidastatic properties of the human neutrophil calprotectin complex. *J. Immunol. Baltim. Md 1950* **151,** 6291–6301 (1993).

184. Hogg, N., Allen, C. & Edgeworth, J. Monoclonal antibody 5.5 reacts with p8,14, a myeloid molecule associated with some vascular endothelium. *Eur. J. Immunol.* **19,** 1053–1061 (1989).

185. Berntzen, H. B., Olmez, U., Fagerhol, M. K. & Munthe, E. The leukocyte protein L1 in plasma and synovial fluid from patients with rheumatoid arthritis and osteoarthritis. *Scand. J. Rheumatol.* **20,** 74–82 (1991).

186. Hessian, P. A., Edgeworth, J. & Hogg, N. MRP-8 and MRP-14, two abundant Ca(2+)-binding proteins of neutrophils and monocytes. *J. Leukoc. Biol.* **53,** 197–204 (1993).

187. Kerkhoff, C., Eue, I. & Sorg, C. The regulatory role of MRP8 (S100A8) and MRP14 (S100A9) in the transendothelial migration of human leukocytes. *Pathobiol. J. Immunopathol. Mol. Cell. Biol.* **67,** 230–232 (1999).

188. Edgeworth, J., Gorman, M., Bennett, R., Freemont, P. & Hogg, N. Identification of p8,14 as a highly abundant heterodimeric calcium binding protein complex of myeloid cells. *J. Biol. Chem.* **266,** 7706–7713 (1991).

189. Lagasse, E. & Weissman, I. L. Mouse MRP8 and MRP14, two intracellular calcium-binding proteins associated with the development of the myeloid lineage. *Blood* **79,** 1907–1915 (1992).

190. Odink, K. *et al.* Two calcium-binding proteins in infiltrate macrophages of rheumatoid arthritis. *Nature* **330,** 80–82 (1987).

191. Roth, J., Vogl, T., Sorg, C. & Sunderkötter, C. Phagocyte-specific S100 proteins: a novel group of proinflammatory molecules. *Trends Immunol.* **24,** 155–158 (2003).

192. Heizmann, C. W., Fritz, G. & Schäfer, B. W. S100 proteins: structure, functions and pathology. *Front. Biosci. J. Virtual Libr.* **7,** d1356–1368 (2002).

193. Hunter, M. J. & Chazin, W. J. High level expression and dimer characterization of the S100 EF-hand proteins, migration inhibitory factor-related proteins 8 and 14. *J. Biol. Chem.* **273,** 12427–12435 (1998).

194. Vogl, T., Gharibyan, A. L. & Morozova-Roche, L. A. Pro-Inflammatory S100A8 and S100A9 Proteins: Self-Assembly into Multifunctional Native and Amyloid Complexes. *Int. J. Mol. Sci.* **13,** 2893–2917 (2012).

195. Lackmann, M., Cornish, C. J., Simpson, R. J., Moritz, R. L. & Geczy, C. L. Purification and structural analysis of a murine chemotactic cytokine (CP-10) with sequence homology to S100 proteins. *J. Biol. Chem.* **267,** 7499–7504 (1992).

196. Raftery, M. J., Harrison, C. A., Alewood, P., Jones, A. & Geczy, C. L. Isolation of the murine S100 protein MRP14 (14 kDa migration-inhibitory-factor-related protein) from activated spleen cells: characterization of post-translational modifications and zinc binding. *Biochem. J.* **316 (Pt 1),** 285–293 (1996).

197. Hobbs, J. A. R. *et al.* Myeloid cell function in MRP-14 (S100A9) null mice. *Mol. Cell. Biol.* **23,** 2564–2576 (2003).

198. Nacken, W., Sopalla, C., Pröpper, C., Sorg, C. & Kerkhoff, C. Biochemical characterization of the murine S100A9 (MRP14) protein suggests that it is functionally equivalent to its human counterpart despite its low degree of sequence homology. *Eur. J. Biochem. FEBS* **267,** 560–565 (2000).

199. Vogl, T. *et al.* Mrp8 and Mrp14 are endogenous activators of Toll-like receptor 4, promoting lethal, endotoxin-induced shock. *Nat. Med.* **13,** 1042–1049 (2007).

200. Sunahori, K. *et al.* The S100A8/A9 heterodimer amplifies proinflammatory cytokine production by macrophages via activation of nuclear factor kappa B and p38 mitogen-activated protein kinase in rheumatoid arthritis. *Arthritis Res. Ther.* **8,** R69 (2006).

201. Sinha, P. *et al.* Proinflammatory S100 proteins regulate the accumulation of myeloid-derived suppressor cells. *J. Immunol. Baltim. Md 1950* **181,** 4666–4675 (2008).

202. Nacken, W., Roth, J., Sorg, C. & Kerkhoff, C. S100A9/S100A8: Myeloid representatives of the S100 protein family as prominent players in innate immunity. *Microsc. Res. Tech.* **60,** 569–580 (2003).

203. Björk, P. *et al.* Identification of human S100A9 as a novel target for treatment of autoimmune disease via binding to quinoline-3-carboxamides. *PLoS Biol.* **7,** e97 (2009).

204. Van Zoelen, M. A. D. *et al.* Expression and role of myeloid-related protein-14 in clinical and experimental sepsis. *Am. J. Respir. Crit. Care Med.* **180,** 1098–1106 (2009).

205. Van Lent, P. L. E. M. *et al.* Myeloid-related proteins S100A8/S100A9 regulate joint inflammation and cartilage destruction during antigen-induced arthritis. *Ann. Rheum. Dis.* **67,** 1750–1758 (2008).

206. Loser, K. *et al.* The Toll-like receptor 4 ligands Mrp8 and Mrp14 are crucial in the development of autoreactive CD8+ T cells. *Nat. Med.* **16,** 713–717 (2010).

207. Foell, D., Frosch, M., Sorg, C. & Roth, J. Phagocyte-specific calcium-binding S100 proteins as clinical laboratory markers of inflammation. *Clin. Chim. Acta Int. J. Clin. Chem.* **344,** 37–51 (2004).

208. Zenz, R. *et al.* Psoriasis-like skin disease and arthritis caused by inducible epidermal deletion of Jun proteins. *Nature* **437,** 369–375 (2005).

209. Rampersad, R. R. *et al.* S100A9 is not essential for disease expression in an acute (K/BxN) or chronic (CIA) model of inflammatory arthritis. *Scand. J. Rheumatol.* **38,** 445–449 (2009).

210. Manitz, M.-P. *et al.* Loss of S100A9 (MRP14) results in reduced interleukin-8-induced CD11b surface expression, a polarized microfilament system, and diminished responsiveness to chemoattractants in vitro. *Mol. Cell. Biol.* **23,** 1034–1043 (2003).

211. Faust, N., Varas, F., Kelly, L. M., Heck, S. & Graf, T. Insertion of enhanced green fluorescent protein into the lysozyme gene creates mice with green fluorescent granulocytes and macrophages. *Blood* **96,** 719–726 (2000).

212. Tkalcevic, J. *et al.* Impaired immunity and enhanced resistance to endotoxin in the absence of neutrophil elastase and cathepsin G. *Immunity* **12,** 201–210 (2000).

213. Chua, F. *et al.* Mice lacking neutrophil elastase are resistant to bleomycin-induced pulmonary fibrosis. *Am. J. Pathol.* **170,** 65–74 (2007).

214. Yu, X. *et al.* FcγRIIA and FcγRIIIB are required for autoantibody-induced tissue damage in experimental human models of bullous pemphigoid. *J. Invest. Dermatol.* **130,** 2841–2844 (2010).

215. Kasprick, A. Die Beteiligung von Mastzellen in der Autoimmunerkrankung Epidermolysis bullosa acquisita. (Forschungszentrum Borstel-Universität zu lübeck, Deutschland, 2013).

216. Kiernan, J. A. *Histological and histochemical methods - Theory and practice.* (2008).

217. Zreiqat, H. *et al.* S100A8 and S100A9 in experimental osteoarthritis. *Arthritis Res. Ther.* **12,** R16 (2010).

218. Frosch, M. *et al.* Myeloid-related proteins 8 and 14 are specifically secreted during interaction of phagocytes and activated endothelium and are useful markers for monitoring disease activity in pauciarticular-onset juvenile rheumatoid arthritis. *Arthritis Rheum.* **43,** 628–637 (2000).

219. Laemmli, U. K. Cleavage of structural proteins during the assembly of the head of bacteriophage T4. *Nature* **227,** 680–685 (1970).

220. Mittendorf, E. A. *et al.* Breast cancer cell uptake of the inflammatory mediator neutrophil elastase triggers an anticancer adaptive immune response. *Cancer Res.* **72,** 3153–3162 (2012).

221. Brown, M. & Wittwer, C. Flow cytometry: principles and clinical applications in hematology. *Clin. Chem.* **46,** 1221–1229 (2000).

222. Döring, G. The role of neutrophil elastase in chronic inflammation. *Am. J. Respir. Crit. Care Med.* **150,** S114–117 (1994).

223. Agarwal, A., Allamaneni, S. S. R. & Said, T. M. Chemiluminescence technique for measuring reactive oxygen species. *Reprod. Biomed. Online* **9,** 466–468 (2004).

224. Pervushina, O. *et al.* Platelet factor 4/CXCL4 induces phagocytosis and the generation of reactive oxygen metabolites in mononuclear phagocytes independently of Gi protein activation or intracellular calcium transients. *J. Immunol. Baltim. Md 1950* **173,** 2060–2067 (2004).

225. Petersen, F., Van Damme, J., Flad, H. D. & Brandt, E. Neutrophil-activating polypeptides IL-8 and NAP-2 induce identical signal transduction pathways in the regulation of lysosomal enzyme release. *Lymphokine Cytokine Res.* **10,** 35–41 (1991).

226. Scrace, S., O'Neill, E., Hammond, E. M. & Pires, I. M. Use of the xCELLigence system for real-time analysis of changes in cellular motility and adhesion in physiological conditions. *Methods Mol. Biol. Clifton NJ* **1046,** 295–306 (2013).

227. Martinez-Serra, J. *et al.* xCELLigence system for real-time label-free monitoring of growth and viability of cell lines from hematological malignancies. *OncoTargets Ther.* **7,** 985–994 (2014).

228. Kustermann, S. *et al.* A label-free, impedance-based real time assay to identify drug-induced toxicities and differentiate cytostatic from cytotoxic effects. *Toxicol. Vitro Int. J. Publ. Assoc. BIBRA* **27,** 1589–1595 (2013).

229. Limame, R. *et al.* Comparative analysis of dynamic cell viability, migration and invasion assessments by novel real-time technology and classic endpoint assays. *PloS One* **7,** e46536 (2012).

230. Paddock, S. W. Principles and practices of laser scanning confocal microscopy. *Mol. Biotechnol.* **16,** 127–149 (2000).

231. Flaberg, E., Stuber, G. & Szekely, L. Multi-dimensional laser confocal microscopy on live cells in submicroliter volumes using glass capillaries. *Acta Histochem. Cytochem.* **39,** 103–106 (2006).

232. Mochizuki, N. *et al.* Spatio-temporal images of growth-factor-induced activation of Ras and Rap1. *Nature* **411,** 1065–1068 (2001).

233. Sato, M., Ozawa, T., Inukai, K., Asano, T. & Umezawa, Y. Fluorescent indicators for imaging protein phosphorylation in single living cells. *Nat. Biotechnol.* **20,** 287–294 (2002).

234. Gu, Y., Di, W. L., Kelsell, D. P. & Zicha, D. Quantitative fluorescence resonance energy transfer (FRET) measurement with acceptor photobleaching and spectral unmixing. *J. Microsc.* **215,** 162–173 (2004).

235. Van Munster, E. B., Kremers, G. J., Adjobo-Hermans, M. J. W. & Gadella, T. W. J., Jr. Fluorescence resonance energy transfer (FRET) measurement by gradual acceptor photobleaching. *J. Microsc.* **218,** 253–262 (2005).

236. FRET acceptor photobleaching. Leica confocal application letter. (2007).

237. Dunn, K. W. & Young, P. A. Principles of multiphoton microscopy. *Nephron Exp. Nephrol.* **103,** e33–40 (2006).

238. So, P. T., Dong, C. Y., Masters, B. R. & Berland, K. M. Two-photon excitation fluorescence microscopy. *Annu. Rev. Biomed. Eng.* **2,** 399–429 (2000).

239. Benninger, R. K. P. & Piston, D. W. Two-photon excitation microscopy for the study of living cells and tissues. *Curr. Protoc. Cell Biol. Editor. Board Juan Bonifacino Al* **Chapter 4,** Unit 4.11.1–24 (2013).

240. König, K. Multiphoton microscopy in life sciences. *J. Microsc.* **200,** 83–104 (2000).

241. Li, J. L. *et al.* Intravital multiphoton imaging of immune responses in the mouse ear skin. *Nat. Protoc.* **7,** 221–234 (2012).

242. Lämmermann, T. *et al.* Neutrophil swarms require LTB4 and integrins at sites of cell death in vivo. *Nature* **498,** 371–375 (2013).

243. Ng, L. G. *et al.* Migratory dermal dendritic cells act as rapid sensors of protozoan parasites. *PLoS Pathog.* **4,** e1000222 (2008).

244. Ng, L. G. *et al.* Visualizing the neutrophil response to sterile tissue injury in mouse dermis reveals a three-phase cascade of events. *J. Invest. Dermatol.* **131,** 2058–2068 (2011).

245. Celli, S., Albert, M. L. & Bousso, P. Visualizing the innate and adaptive immune responses underlying allograft rejection by two-photon microscopy. *Nat. Med.* **17,** 744–749 (2011).

246. Dudeck, A. *et al.* Mast cells are key promoters of contact allergy that mediate the adjuvant effects of haptens. *Immunity* **34,** 973–984 (2011).

247. Matheu, M. P. *et al.* Imaging of effector memory T cells during a delayed-type hypersensitivity reaction and suppression by Kv1.3 channel block. *Immunity* **29,** 602–614 (2008).

248. Peters, N. C. *et al.* In vivo imaging reveals an essential role for neutrophils in leishmaniasis transmitted by sand flies. *Science* **321,** 970–974 (2008).

249. Gaiser, M. R. *et al.* Cancer-associated epithelial cell adhesion molecule (EpCAM; CD326) enables epidermal Langerhans cell motility and migration in vivo. *Proc. Natl. Acad. Sci. U. S. A.* **109,** E889–897 (2012).

250. Davalos, D. *et al.* ATP mediates rapid microglial response to local brain injury in vivo. *Nat. Neurosci.* **8,** 752–758 (2005).

251. Kasperkiewicz, M. *et al.* Genetic identification and functional validation of FcγRIV as key molecule in autoantibody-induced tissue injury. *J. Pathol.* **228,** 8–19 (2012).

252. Chen, R. *et al.* Mast cells play a key role in neutrophil recruitment in experimental bullous pemphigoid. *J. Clin. Invest.* **108,** 1151–1158 (2001).

253. Lopez, A. F., Strath, M. & Sanderson, C. J. Differentiation antigens on mouse eosinophils and neutrophils identified by monoclonal antibodies. *Br. J. Haematol.* **57,** 489–494 (1984).

254. Tang, T. *et al.* A role for Mac-1 (CDIIb/CD18) in immune complex-stimulated neutrophil function in vivo: Mac-1 deficiency abrogates sustained Fcgamma receptor-dependent neutrophil adhesion and complement-dependent proteinuria in acute glomerulonephritis. *J. Exp. Med.* **186,** 1853–1863 (1997).

255. Ottonello, L. *et al.* Monoclonal Lym-1 antibody-dependent cytolysis by neutrophils exposed to granulocyte-macrophage colony-stimulating factor: intervention of FcgammaRII (CD32), CD11b-CD18 integrins, and CD66b glycoproteins. *Blood* **93,** 3505–3511 (1999).

256. Soriano, S. G. *et al.* Mice deficient in Mac-1 (CD11b/CD18) are less susceptible to cerebral ischemia/reperfusion injury. *Stroke J. Cereb. Circ.* **30,** 134–139 (1999).

257. Van Spriel, A. B. *et al.* Mac-1 (CD11b/CD18) is essential for Fc receptor-mediated neutrophil cytotoxicity and immunologic synapse formation. *Blood* **97,** 2478–2486 (2001).

258. Bastiaens, P. I., Majoul, I. V., Verveer, P. J., Söling, H. D. & Jovin, T. M. Imaging the intracellular trafficking and state of the AB5 quaternary structure of cholera toxin. *EMBO J.* **15,** 4246–4253 (1996).

259. Bastiaens, P. I. & Jovin, T. M. Microspectroscopic imaging tracks the intracellular processing of a signal transduction protein: fluorescent-labeled protein kinase C beta I. *Proc. Natl. Acad. Sci. U. S. A.* **93,** 8407–8412 (1996).

260. Wouters, F. S., Bastiaens, P. I., Wirtz, K. W. & Jovin, T. M. FRET microscopy demonstrates molecular association of non-specific lipid transfer protein (nsL-TP) with fatty acid oxidation enzymes in peroxisomes. *EMBO J.* **17,** 7179–7189 (1998).

261. Liu, Z. *et al.* The role of complement in experimental bullous pemphigoid. *J. Clin. Invest.* **95,** 1539–1544 (1995).

262. Liu, Z. *et al.* The serpin alpha1-proteinase inhibitor is a critical substrate for gelatinase B/MMP-9 in vivo. *Cell* **102,** 647–655 (2000).

263. Cross, M., Mangelsdorf, I., Wedel, A. & Renkawitz, R. Mouse lysozyme M gene: isolation, characterization, and expression studies. *Proc. Natl. Acad. Sci. U. S. A.* **85,** 6232–6236 (1988).

264. Brady, G. *et al.* Analysis of gene expression in a complex differentiation hierarchy by global amplification of cDNA from single cells. *Curr. Biol. CB* **5,** 909–922 (1995).

265. Chen, R. *et al.* Macrophages, but not T and B lymphocytes, are critical for subepidermal blister formation in experimental bullous pemphigoid: macrophage-mediated neutrophil infiltration depends on mast cell activation. *J. Immunol. Baltim. Md 1950* **169,** 3987–3992 (2002).

266. Springer, T. A. Traffic signals for lymphocyte recirculation and leukocyte emigration: the multistep paradigm. *Cell* **76,** 301–314 (1994).

267. Németh, T. & Mócsai, A. The role of neutrophils in autoimmune diseases. *Immunol. Lett.* **143,** 9–19 (2012).

268. Belaaouaj, A. *et al.* Mice lacking neutrophil elastase reveal impaired host defense against gram negative bacterial sepsis. *Nat. Med.* **4,** 615–618 (1998).

269. Lee, W. L. & Downey, G. P. Leukocyte elastase: physiological functions and role in acute lung injury. *Am. J. Respir. Crit. Care Med.* **164,** 896–904 (2001).

270. Shapiro, S. D. Neutrophil elastase: path clearer, pathogen killer, or just pathologic? *Am. J. Respir. Cell Mol. Biol.* **26,** 266–268 (2002).

271. Weiss, S. J. Tissue destruction by neutrophils. *N. Engl. J. Med.* **320,** 365–376 (1989).

272. Yoshimura, K., Nakagawa, S., Koyama, S., Kobayashi, T. & Homma, T. Roles of neutrophil elastase and superoxide anion in leukotriene B4-induced lung injury in rabbit. *J. Appl. Physiol. Bethesda Md 1985* **76,** 91–96 (1994).

273. Hoenderdos, K. & Condliffe, A. The neutrophil in chronic obstructive pulmonary disease. *Am. J. Respir. Cell Mol. Biol.* **48,** 531–539 (2013).

274. Voynow, J. A., Fischer, B. M. & Zheng, S. Proteases and cystic fibrosis. *Int. J. Biochem. Cell Biol.* **40,** 1238–1245 (2008).

275. Wiedow, O., Wiese, F., Streit, V., Kalm, C. & Christophers, E. Lesional elastase activity in psoriasis, contact dermatitis, and atopic dermatitis. *J. Invest. Dermatol.* **99,** 306–309 (1992).

276. Liu, Z. *et al.* A critical role for neutrophil elastase in experimental bullous pemphigoid. *J. Clin. Invest.* **105,** 113–123 (2000).

277. Korkmaz, B., Attucci, S., Jourdan, M.-L., Juliano, L. & Gauthier, F. Inhibition of neutrophil elastase by alpha1-protease inhibitor at the surface of human polymorphonuclear neutrophils. *J. Immunol. Baltim. Md 1950* **175,** 3329–3338 (2005).

278. Kessenbrock, K., Dau, T. & Jenne, D. E. Tailor-made inflammation: how neutrophil serine proteases modulate the inflammatory response. *J. Mol. Med. Berl. Ger.* **89,** 23–28 (2011).

279. Travis, J. & Salvesen, G. S. Human plasma proteinase inhibitors. *Annu. Rev. Biochem.* **52,** 655–709 (1983).

280. Ye, S. & Goldsmith, E. J. Serpins and other covalent protease inhibitors. *Curr. Opin. Struct. Biol.* **11,** 740–745 (2001).

281. Huntington, J. A., Read, R. J. & Carrell, R. W. Structure of a serpin-protease complex shows inhibition by deformation. *Nature* **407,** 923–926 (2000).

282. Carrell, R. W. alpha 1-Antitrypsin: molecular pathology, leukocytes, and tissue damage. *J. Clin. Invest.* **78,** 1427–1431 (1986).

283. Owen, C. A., Campbell, M. A., Sannes, P. L., Boukedes, S. S. & Campbell, E. J. Cell surface-bound elastase and cathepsin G on human neutrophils: a novel, non-oxidative mechanism by which neutrophils focus and preserve catalytic activity of serine proteinases. *J. Cell Biol.* **131,** 775–789 (1995).

284. Campbell, E. J., Campbell, M. A. & Owen, C. A. Bioactive proteinase 3 on the cell surface of human neutrophils: quantification, catalytic activity, and susceptibility to inhibition. *J. Immunol. Baltim. Md 1950* **165,** 3366–3374 (2000).

285. Owen, C. A. & Campbell, E. J. The cell biology of leukocyte-mediated proteolysis. *J. Leukoc. Biol.* **65,** 137–150 (1999).

286. Zemans, R. L., Colgan, S. P. & Downey, G. P. Transepithelial migration of neutrophils: mechanisms and implications for acute lung injury. *Am. J. Respir. Cell Mol. Biol.* **40,** 519–535 (2009).

287. Downey, G. P., Dong, Q., Kruger, J., Dedhar, S. & Cherapanov, V. Regulation of neutrophil activation in acute lung injury. *Chest* **116,** 46S–54S (1999).

288. Winn, R. K. *et al.* Role of protein synthesis and CD11/CD18 adhesion complex in neutrophil emigration into the lung. *Exp. Lung Res.* **19,** 221–235 (1993).

289. Campbell, E. J., Senior, R. M., McDonald, J. A. & Cox, D. L. Proteolysis by neutrophils. Relative importance of cell-substrate contact and oxidative inactivation of proteinase inhibitors in vitro. *J. Clin. Invest.* **70,** 845–852 (1982).

290. Campbell, E. J. & Owen, C. A. The sulfate groups of chondroitin sulfate- and heparan sulfate-containing proteoglycans in neutrophil plasma membranes are novel binding sites for human leukocyte elastase and cathepsin G. *J. Biol. Chem.* **282,** 14645–14654 (2007).

291. Cahalan, M. D. & Parker, I. Choreography of cell motility and interaction dynamics imaged by two-photon microscopy in lymphoid organs. *Annu. Rev. Immunol.* **26,** 585–626 (2008).

292. Coombes, J. L. & Robey, E. A. Dynamic imaging of host-pathogen interactions in vivo. *Nat. Rev. Immunol.* **10,** 353–364 (2010).

293. Germain, R. N., Miller, M. J., Dustin, M. L. & Nussenzweig, M. C. Dynamic imaging of the immune system: progress, pitfalls and promise. *Nat. Rev. Immunol.* **6,** 497–507 (2006).

294. Hickman, H. D., Bennink, J. R. & Yewdell, J. W. Caught in the act: intravital multiphoton microscopy of host-pathogen interactions. *Cell Host Microbe* **5,** 13–21 (2009).

295. Ng, L. G., Mrass, P., Kinjyo, I., Reiner, S. L. & Weninger, W. Two-photon imaging of effector T-cell behavior: lessons from a tumor model. *Immunol. Rev.* **221,** 147–162 (2008).

296. Roediger, B., Ng, L. G., Smith, A. L., Fazekas de St Groth, B. & Weninger, W. Visualizing dendritic cell migration within the skin. *Histochem. Cell Biol.* **130,** 1131–1146 (2008).

297. Frizzell, R. A. & Pilewski, J. M. Finally, mice with CF lung disease. *Nat. Med.* **10,** 452–454 (2004).

298. Kossodo, S. *et al.* Noninvasive in vivo quantification of neutrophil elastase activity in acute experimental mouse lung injury. *Int. J. Mol. Imaging* **2011,** 581406 (2011).

299. Mitra, S., Modi, K. D. & Foster, T. H. Enzyme-activatable imaging probe reveals enhanced neutrophil elastase activity in tumors following photodynamic therapy. *J. Biomed. Opt.* **18,** 101314 (2013).

300. Zhao, Z., Raftery, M. J., Niu, X. M., Daja, M. M. & Russell, P. J. Application of in-gel protease assay in a biological sample: characterization and identification of urokinase-type plasminogen activator (uPA) in secreted proteins from a prostate cancer cell line PC-3. *Electrophoresis* **25,** 1142–1148 (2004).

301. Lucas, S. D., Costa, E., Guedes, R. C. & Moreira, R. Targeting COPD: advances on low-molecular-weight inhibitors of human neutrophil elastase. *Med. Res. Rev.* **33 Suppl 1,** E73–101 (2013).

302. Chen, M., Kim, G. H., Prakash, L. & Woodley, D. T. Epidermolysis bullosa acquisita: autoimmunity to anchoring fibril collagen. *Autoimmunity* **45,** 91–101 (2012).

303. Grevers, L. C. *et al.* S100A8 enhances osteoclastic bone resorption in vitro through activation of Toll-like receptor 4: implications for bone destruction in murine antigen-induced arthritis. *Arthritis Rheum.* **63,** 1365–1375 (2011).

304. Hiratsuka, S., Watanabe, A., Aburatani, H. & Maru, Y. Tumour-mediated upregulation of chemoattractants and recruitment of myeloid cells predetermines lung metastasis. *Nat. Cell Biol.* **8,** 1369–1375 (2006).

305. Hoyaux, D. *et al.* S100 proteins in Corpora amylacea from normal human brain. *Brain Res.* **867,** 280–288 (2000).

306. Salama, I., Malone, P. S., Mihaimeed, F. & Jones, J. L. A review of the S100 proteins in cancer. *Eur. J. Surg. Oncol. J. Eur. Soc. Surg. Oncol. Br. Assoc. Surg. Oncol.* **34,** 357–364 (2008).

307. Zwadlo, G., Brüggen, J., Gerhards, G., Schlegel, R. & Sorg, C. Two calcium-binding proteins associated with specific stages of myeloid cell differentiation are expressed by subsets of macrophages in inflammatory tissues. *Clin. Exp. Immunol.* **72,** 510–515 (1988).

308. Foell, D. & Roth, J. Proinflammatory S100 proteins in arthritis and autoimmune disease. *Arthritis Rheum.* **50,** 3762–3771 (2004).

309. Foell, D. *et al.* Early recruitment of phagocytes contributes to the vascular inflammation of giant cell arteritis. *J. Pathol.* **204,** 311–316 (2004).

310. Foell, D. *et al.* Methotrexate treatment in juvenile idiopathic arthritis: when is the right time to stop? *Ann. Rheum. Dis.* **63,** 206–208 (2004).

311. Haga, H. J. *et al.* Calprotectin in patients with systemic lupus erythematosus: relation to clinical and laboratory parameters of disease activity. *Lupus* **2,** 47–50 (1993).

312. Rugtveit, J. *et al.* Cytokine profiles differ in newly recruited and resident subsets of mucosal macrophages from inflammatory bowel disease. *Gastroenterology* **112,** 1493–1505 (1997).

313. Lügering, N. *et al.* Immunohistochemical distribution and serum levels of the Ca(2+)-binding proteins MRP8, MRP14 and their heterodimeric form MRP8/14 in Crohn's disease. *Digestion* **56,** 406–414 (1995).

314. Gammon, W. R. & Briggaman, R. A. Functional heterogeneity of immune complexes in epidermolysis bullosa acquisita. *J. Invest. Dermatol.* **89,** 478–483 (1987).

315. Delabie, J., de Wolf-Peeters, C., van den Oord, J. J. & Desmet, V. J. Differential expression of the calcium-binding proteins MRP8 and MRP14 in granulomatous conditions: an immunohistochemical study. *Clin. Exp. Immunol.* **81,** 123–126 (1990).

316. Strupat, K., Rogniaux, H., Van Dorsselaer, A., Roth, J. & Vogl, T. Calcium-induced noncovalently linked tetramers of MRP8 and MRP14 are confirmed by electrospray ionization-mass analysis. *J. Am. Soc. Mass Spectrom.* **11,** 780–788 (2000).

317. Vogl, T., Roth, J., Sorg, C., Hillenkamp, F. & Strupat, K. Calcium-induced noncovalently linked tetramers of MRP8 and MRP14 detected by ultraviolet matrix-assisted laser desorption/ionization mass spectrometry. *J. Am. Soc. Mass Spectrom.* **10,** 1124–1130 (1999).

318. Donato, R. S100: a multigenic family of calcium-modulated proteins of the EF-hand type with intracellular and extracellular functional roles. *Int. J. Biochem. Cell Biol.* **33,** 637–668 (2001).

319. Leukert, N. *et al.* Calcium-dependent tetramer formation of S100A8 and S100A9 is essential for biological activity. *J. Mol. Biol.* **359,** 961–972 (2006).

320. Teigelkamp, S. *et al.* Calcium-dependent complex assembly of the myeloic differentiation proteins MRP-8 and MRP-14. *J. Biol. Chem.* **266,** 13462–13467 (1991).

321. Longbottom, D., Sallenave, J. M. & van Heyningen, V. Subunit structure of calgranulins A and B obtained from sputum, plasma, granulocytes and cultured epithelial cells. *Biochim. Biophys. Acta* **1120,** 215–222 (1992).

322. Passey, R. J. *et al.* A null mutation in the inflammation-associated S100 protein S100A8 causes early resorption of the mouse embryo. *J. Immunol. Baltim. Md 1950* **163,** 2209–2216 (1999).

323. Gebhardt, C., Németh, J., Angel, P. & Hess, J. S100A8 and S100A9 in inflammation and cancer. *Biochem. Pharmacol.* **72,** 1622–1631 (2006).

324. Lim, S. Y., Raftery, M. J., Goyette, J., Hsu, K. & Geczy, C. L. Oxidative modifications of S100 proteins: functional regulation by redox. *J. Leukoc. Biol.* **86,** 577–587 (2009).

325. Petersen, B. *et al.* The alarmin Mrp8/14 as regulator of the adaptive immune response during allergic contact dermatitis. *EMBO J.* **32,** 100–111 (2013).

326. Brun, J. G., Håland, G., Haga, H. J., Fagerhol, M. K. & Jonsson, R. Effects of calprotectin in avridine-induced arthritis. *APMIS Acta Pathol. Microbiol. Immunol. Scand.* **103,** 233–240 (1995).

327. Otsuka, K. *et al.* Suppression of inflammation in rat autoimmune myocarditis by S100A8/A9 through modulation of the proinflammatory cytokine network. *Eur. J. Heart Fail.* **11,** 229–237 (2009).

328. Ikemoto, M., Murayama, H., Itoh, H., Totani, M. & Fujita, M. Intrinsic function of S100A8/A9 complex as an anti-inflammatory protein in liver injury induced by lipopolysaccharide in rats. *Clin. Chim. Acta Int. J. Clin. Chem.* **376,** 197–204 (2007).

329. Wu, N. & Davidson, J. M. Migration inhibitory factor-related protein (MRP)8 and MRP14 are differentially expressed in free-electron laser and scalpel incisions. *Wound Repair Regen. Off. Publ. Wound Heal. Soc. Eur. Tissue Repair Soc.* **12,** 327–336 (2004).

330. Champaiboon, C., Sappington, K. J., Guenther, B. D., Ross, K. F. & Herzberg, M. C. Calprotectin S100A9 calcium-binding loops I and II are essential for keratinocyte resistance to bacterial invasion. *J. Biol. Chem.* **284,** 7078–7090 (2009).

331. Grimbaldeston, M. A., Geczy, C. L., Tedla, N., Finlay-Jones, J. J. & Hart, P. H. S100A8 induction in keratinocytes by ultraviolet A irradiation is dependent on reactive oxygen intermediates. *J. Invest. Dermatol.* **121,** 1168–1174 (2003).

332. Paccola, C. C. *et al.* Antinociceptive effect of the C-terminus of murine S100A9 protein on experimental neuropathic pain. *Peptides* **29,** 1806–1814 (2008).

333. Greenlee, K. J. *et al.* Proteomic identification of in vivo substrates for matrix metalloproteinases 2 and 9 reveals a mechanism for resolution of inflammation. *J. Immunol. Baltim. Md 1950* **177,** 7312–7321 (2006).

334. Foell, D. *et al.* Expression of the pro-inflammatory protein S100A12 (EN-RAGE) in rheumatoid and psoriatic arthritis. *Rheumatol. Oxf. Engl.* **42,** 1383–1389 (2003).

335. Stair, J. L., Watkinson, M. & Krause, S. Sensor materials for the detection of proteases. *Biosens. Bioelectron.* **24,** 2113–2118 (2009).

336. Liu, Z. *et al.* Gelatinase B-deficient mice are resistant to experimental bullous pemphigoid. *J. Exp. Med.* **188,** 475–482 (1998).

APPENDIX

Buffer and Media

Buffer	Composition
Anesthetic materials (short term anesthesia)	4.313 ml NaCl (0.9%) 625 µl Ketamin (10%) 62.5 µl Xylazin (2%)
Anesthetic materials (long term anesthesia, for in vivo microscopy)	3.5 ml NaCl (0.9%) 400 µl Fentanyl (0.1 mg/ml) 400 µl Midazolam (5 mg/ml) 200 µl Medetomidine (1 mg /ml)
Blotting buffer	25 mM Tris 150 mM Glycin Methanol 100% (20% v/v)
CL-Medium	RPMI 1640, modified (without Phenol Red)
Electrophoresis buffer	25 mM Tris 200 mM Glycin 3.5 mM SDS, in Aqua dest
FACS buffer	PBS-D without Ca^{2+} and Mg^{2+} 0.1% BSA
HBSS-Prep	HBSS without Ca^{2+} and Mg^{2+} 20 mM HEPES 0.5% FCS, in Aqua dest
Imaging medium (IM)	20 mM HEPES 1.2 mM $MgCl_2$ 1.2 mM K_2HPO_4 115 mM NaCl 1.2 mM $CaCl_2$ 2 g/L D-glucose, in Aqua dest
Lysis buffer (for erythrocytes, pH 7.2)	155 mM NH_4Cl 10 mM $KHCO_3$ 0.1 mM EDTA in, Aqua dest

Buffer	Composition
PBS (pH 7.2)	10 mM NaH_2PO4 0.15 M NaCl, in Aqua dest
PBS-Dulbecco (PBS-D, pH 7.2 - 7.3)	140 mM NaCl 2.7 mM KCl 10 mM Na_2HPO_4 1.5 mM KH_2PO_4, in Aqua dest
Trypan blue	0.9 % NaCl 0.5 % Trypan blue, in H_2O

Video legends

Video 1 Elastase-mediated cleavage of NEmo-2 FRET reporter on Jurkat T cells. Jurkat T cells were incubated with the reporter for 5 min and bound reporter was determined by confocal microscopy. NEmo-2 localized exclusively on the cell membrane. Donor fluorescence and sensitized acceptor emission was imaged and D/A ratio images were calculated. NE was added after 4 min of incubation. Representative confocal videos of donor (D) and acceptor (A) fluorescence intensities and the corresponding D/A ratios are shown in absence **(A-C)** and in presence **(D-F)** of neutrophil elastase. Video consists of 20 images collected every one second by photomultiplier tube (PMT) of confocal microscopy. Cleavage of reporter was observed is shown in D/A ratio video after addition of neutrophil elastase. Look up table (LUT): blue = low D/A ratio, intact NEmo-2; red = high D/A ratio, indicative for cleaved NEmo-2.

Video 2 Elastase enzyme activities on IC-activated neutrophils in presence of protease inhibitors. Neutrophils were preincubated with NEmo-2 in presence of A1AT and allowed to adhere to immobilized IC or irrelevant antibodies of the same isotype. Cells were analyzed by confocal microscopy and representative videos of fluorescence intensities of the donor and acceptor as well as the ratio of the intensities of D/A are shown. **(A-F)** Cells were able to spread on immobilized IC (but not unrelated antibodies) and as a consequence, cleavage of reporter was observed even in the presence of inhibitors which became visible after 5 min and significant after 10 min of incubation as compared to the controls. Video consists of 30 images collected every one second by photomultiplier tube (PMT) of confocal microscopy. LUT: blue = low D/A ratio, intact NEmo-2; red = high D/A ratio,

indicative of cleaved NEmo-2. Scale bars: 5 µm for IC-stimulated and 20 µm for unstimulated neutrophils.

Video 3 Migration of intrinsic neutrophils to the site of pathogenic antibodies. Local antibody transfer model of EBA was induced by a single dose injection of anti-mCOLVII labeled with DyLight 649 intradermally into the ventral ear skin of *lys-eGFP* mice. Neutrophil migration towards pathogenic antibody was monitored by two-photon microscopy. Results indicate the recruitment of neutrophils in close proximity of the antibody. Top video **(A)** as well as a side view generated by stack analysis demonstrate the close proximity of neutrophils to the pathogenic IgG **(B)**. EGFP appears as green color while deposition of anti-mCOLVII is shown in red. Results of one representative experiment are shown. Video is shown as a time-lapse over 15 min taken by multi-photon intravital microscopy.

Video 4 Response of adoptively transferred neutrophils to focal tissue damage. BM-derived neutrophils from Balb/c mice were labeled with cell tracker and injected intradermally into the ventral ear skin 2 h before laser-induced focal tissue damage was set. Neutrophil recruitment towards focal damage (white arrow; green spot) was recorded by multi-photon microscopy over a 30 min time-lapse **(A)**. Neutrophils (red dots) were identified and cell migration was followed by track analyses **(B)**. Tracks are indicated by colored lines. Migration areas of neutrophils are shown by direction lines which their color shifts from blue to red reflecting from the early step to the final area, respectively. Results of one representative experiment out of three experiments are shown. Video is shown as a time-lapse over 30 min taken by multi-photon intravital microscopy.

Video 5 Damage-induced neutrophil migrations in presence of IC. NEmo-2-labeled neutrophils (small bright dots) as well as anti-mCOLVII antibody conjugated to DyLight 649 (blue color) were simultaneously injected in presence of A1AT into the ear of wildtype Balb/c mice. After 2h, focal tissue injury was applied (arrow) and the dynamics of administrated neutrophils was subsequently monitored over 90 min. D/A ratio together with donor signal are shown. Results of one representative experiment out of three are shown. Video is shown as a time-lapse over 1 h and 38 min taken by multi-photon intravital microscopy.

Video 6 NE activities at the adhesion site of activated neutrophils *in vivo*. Local EBA was induced by single injection of anti-mCOLVII to the ventral side of ear. Thereafter, neutrophils were labeled with NEmo-2 reporter in presence of A1AT. Video represents NE activities on single neutrophil at different time-points over a 15 min time-lapse by multi-photon microscopy. D/A ratio (violet color) together with donor signal (green color) are shown.

PUBLICATIONS AND PRESENTATIONS

To be published manuscripts

2015 Xinhua Yu, **Reza Akbarzadeh**, Stefanie Gehrig, Carsten Schultz, Joseph T. Opferman, Detlef Zillikens, and Frank Petersen. Immune complex-induced neutrophil adhesion is indispensible for tissue damage in the experimental epidermolysis bullosa acquisita. *Submitted*

2015 **Reza Akbarzadeh**, Xinhua Yu, Thomas Vogl, Ralf J Ludwig, Detlef Zillikens, Frank Petersen. Myeloid-related proteins-8 and -14 are expressed but dispensable in the pathogenesis of experimental epidermolysis bullosa acquisita and bullous pemphigoid. *In preparation*

Oral presentation

2014 37th Symposium of the North German Immunologists, October 24, 2014, Borstel, Germany
Highly Sensitive Detection of Neutrophil Elastase Protease activity in Autoimmune Bullous Disease by Using FRET Reporter

2014 9th International Congress on Autoimmunity, March 26-30, 2014, Nice, France
Myeloid-related proteins-8 and -14 expression in experimental epidermolysis bullosa acquisita and bullous pemphigoid mouse model

2013 36th Symposium of the North German Immunologists, November 22, 2013, Borstel, Germany
Myeloid-related proteins-8 and -14 expression in experimental epidermolysis bullosa acquisita and bullous pemphigoid mouse model

2012 PhD-student Retreat for Borstel Biomedical Research School, August 15-16, 2012, Ahrensburg, Germany

2011-2014 PhD-student Retreat for GRK Graduate School, University of Lübeck, Germany

Poster presentation

2013 International Pre IID 2013 Meeting on Autoimmune Bullous Diseases, May 6-7, 2013, Lübeck, Germany
Myeloid-related protein-8 and -14 is not essential for disease expression in experimental epidermolysis bullosa acquisita mouse model

ACKNOWLEDGEMENTS

This work and writing my PhD dissertation was an extraordinary expedition and a monumental milestone in my academic life. I could have never step forward on this memorable journey, traveled this far, and successfully completed without continued support, patience, and guidance of supervisors, colleagues, friends and family.

I would like to express my profound sincere appreciation to my supervisor, Prof. Dr. Frank Petersen, who was the backbone of my professional life over the past three and half years. His outstanding supervision, creative suggestions, sustained enthusiasm, and exemplary motivation leads to converting my dreams and interests into reality and fundamentally important in the field of medicine and biology. Apart from the subject of research, he was also an understanding and encouraging friend who has stood by me in moments of difficulties.

I'm also deeply thankful to Dr. Xinhua Yu for his guidance, suggestions, valuable time, and comments throughout my thesis. I'm in particular thankful for his incorporation in the mouse experiments which has been very helpful for the study.

I offer my deep gratitude and intimate thanks to all members of the research group Biochemical Immunology in Research Center Borstel, Dr. Brigitte Kasper, Dr. Anika Kasprick, Junie Diane Tchudjin Magatsin, Carola Schneider, Cindy Hass, Gabrielle Huss, Diana Heinrich, Christine Engellenner, Marjan Ahmadi, Dr. Nestor Gonzalez Roldan, Dr. Sandra Minge, Hanno Ewers, and Xianoyang Yue for passing on their expertise and technical support in establishing and performing experiments and pleasant working environment. In particular, I would like to thank Gabrielle Huss and Carola Schneider for their help not only by technical assistance, but also by many social supports. Thank you also to Cindy Hass for her accompaniment of mouse experiments and spending a lot of time in animal facility.

I would like to record my gratitude again to Junie Diane Tchudjin Magatsin for being supportive throughout my time here and for offering her valuable support and sharing with me the difficulties of my moments.

I warmly thank my mentors Prof. Dr. Ralf Ludwig and Prof. Dr. Thomas Roeder for their interest in the progress of my research project and for interesting discussions, advice, and exchange opinions.

I wish to extend my thanks to GRK 1727/1 ‘Modulation of Autoimmunity’ from DFG for its financial support and for the opportunity of being a member of this research group. I also thank Department of Dermatology in University of Lübeck for providing some antibodies which I used during my experiments.

My sincere thanks also go to Dr. Peter König for providing the opportunity to work with multi-photon microscopy and Dr. Mario Pieper for technical support of *in vivo* microscopy, assistance to get excellent microscopy images, and analysis of the data.

I am grateful to Dr. Thomas Scholzen for helping me with confocal microscopy and fluorescence staining experiments.

I would like to thank Dr. Thomas Vogl for providing knockout animals and sharing his lab for performing some experiments in Münster.

My thanks also go to Prof. Dr. Carsten Schultz for giving me the opportunity of a visit in his laboratory in EMBL Heidelberg and also Dr. Stefanie Gehrig for technical support of first steps in the handling of FRET reporters.

Most importantly, these acknowledgments would not be complete without special gratitude to my family, to whom this dissertation is dedicated to:

To my parents whose three decades of love, encouragement, support, and inspiration have shaped my future and I definitely would not be where I am today if it wasn't for them.

To my loving wife, Pardis, whose love, kindness, fortitude, and underestanding have enriched my entire life and opened my heart to a new world I would never have imagined. I would like to express my deepest love and heart-felt thanks to her for supporting and encouraging me every day, sharing the housework, and taking care of our son during the most difficult time of writing the thesis.

To my little son, Adrian, who missed out on a lot of Daddy time while I was busy with the work.

CURRICULUM VITAE

REZA AKBARZADEH

Address: Parkallee 26, 23845 Borstel, Germany

Email: rz.akbarzadeh@gmail.com

Day/place of birth: 14.02.1982, Mashhad

Citizenship: Iranian

Higher education and professional carrier

2011-2015 PhD disputation
University of Kiel, dissertation completed at the Research Center Borstel in Research Group Biochemical immunology

Education

2006 **Master in Biology-Biochemistry**
Islamic Azad University, Science & Research Branch, Tehran, Iran

2004 **Bachelor in General Biology**
Islamic Azad University, Mashhad Branch, Mashhad, Iran

2000 **Diploma in Experimental Biology**
Imam Hossein High School, Mashhad, Iran

STATEMENT ON OATH

I hereby declare on oath that this dissertation is the product of my own work and has been provided by supervisor's guidance. No other expedients than those stated here were used. This work has not been submitted anywhere for any degree or examination. This dissertation has been prepared according to the 'Rules of Good Scientific Practice of the German Research Foundation' and subject to 'Application for Acceptance of Dissertation and Admission to the Disputation'.

Kiel, 2015

Reza Akbarzadeh